Dispersion Compensation for Reflection Holography

by

Arno Klein

B.S., Perception and Cognition Studies
University of Michigan in Ann Arbor, 1993

Submitted to the Program in Media Arts and Sciences,
School of Architecture and Planning
in partial fulfillment of the requirements for the degree of

Master of Science in Media Arts and Sciences
at the
Massachusetts Institute of Technology

September 1996

©1996 Massachusetts Institute of Technology
All rights reserved

Signature of Author _____
Program in Media Arts and Sciences
June 15, 1996

Certified by _____
Stephen A. Benton
Allen Professor of Media Arts and Sciences
Program in Media Arts and Sciences
Thesis Supervisor

Accepted by _____
Stephen A. Benton
Chair
Departmental Committee on Graduate Students
Program in Media Arts and Sciences

Dispersion Compensation for Reflection Holography

by
Arno Klein

Submitted to the Program in Media Arts and Sciences,
School of Architecture and Planning
on June 15, 1996 in partial fulfillment of the requirements for the
Degree of Master of Science in Media Arts and Sciences

ABSTRACT

The work outlined in this thesis is the exploration, application, and evaluation of the technique of dispersion compensation to reduce color blurring of reflection holograms. In particular, the technique of illuminating a hologram with a predispersing grating is applied to the development of full-color, full-parallax, reflection holographic stereograms in various display formats, from a large, open-air viewstation to a compact, light guide-mounted hologram. The effects of wave-front curvature are assessed for reducing the grating size for more compact displays.

A blur equation is derived and experimentally contrasted with Benton's blur equations with the use of spectrophotometer measurements of an experimental grating, and raytracing computer programs included in the appendices.

Finally, two approaches were developed that provide a consistent means of designing dispersion-compensation gratings tailored to realizable, desired geometries. Both approaches are effectively reverse-raytracing methods, beginning from the pupil and ending at the extended light source. Compensation is optimized for image points along a prescribed viewing axis, and depending on the geometry, along all lines of sight parallel to this axis. The first approach solves for a grating design where the grating is reconstructed with the same angles to which it was exposed. The second, more exact approach, is an optimization of a matrix expression containing the relevant angular and/or vertical focus equations, using the Moore-Penrose pseudoinverse function. This latter method will enable the reader to design a grating that will play out at the desired angles for component wavelengths at as close to the desired distances as possible.

Thesis Supervisor: Stephen A. Benton

Title: Allen Professor of Media Arts and Sciences

Dispersion Compensation for Reflection Holography

The following people served as readers for this thesis:

Certified by _____

Edward Adelson
Associate Professor of Vision Science

Certified by _____

Stephen D. Fantone
Senior Lecturer, Mechanical Engineering
President, Optikos Corp., Cambridge, MA

Certified by _____

Emmett N. Leith
Professor of Electrical Engineering
and Computer Science
University of Michigan, Ann Arbor



To my mother and father

Acknowledgments

This section is inevitably going to be woefully incomplete, so I will mention only the names of those who have had a direct impact on the production of this thesis.

First, I would like to thank **Steve Benton**, for the opportunity to work in the Media Laboratory, and for his extremely helpful e-mail correspondence.
Sincere thanks also goes to my other thesis readers for reviewing this document: Professor **Ted Adelson**, Professor **Stephen Fantone**, and Professor **Emmett Leith**.

The Spatial Imaging Group, as of spring, 1996:

Mike Klug, the other primary individual constituting the "we" that is used throughout the thesis. Mike shot the holograms illuminated by the gratings, and pulled together all elements to complete the viewstations for our sponsors. My reluctant lab mentor: "Don't you have a thesis to work on?"

Ravi Pappu, my colleague and cohort, for fielding my math questions, however far afield: "On what planet does sine of zero equal one?!" Thank you for bearing the innumerable intrusions!

Paul Christie, my 6th and longest-lasting officemate, for sharing my abode: "It would probably be safer if you'd sleep farther away from the door." Have a wonderful wedding!

Melissa Yoon, for countless administrative feats: "The package should have arrived in England this morning – Anything more you'd like to Fedex today?" Take care and good luck with your (near) future endeavors…

Wendy Plesniak, for inspirational work that adds touch to an otherwise ghostly medium.

Carlton Sparrell: "You didn't know? I'm leaving in two weeks."

Michael Halle

Our undergraduate researchers; in particular, **Adam Kropp** and **Benjie Chen**, for their computer graphics work instrumental to providing the subjects of our holograms.

John Sutter, our Japanese affiliate

Barrett Comiskey, director of darkroom #2, my friend, roommate, and fellow holographer: "Your thesis is my thesis."

Mitch Henrion, for edgelit enthusiasm.

Everyone in the **Physics and Media Group**, for providing me with a friendly place to work on my thesis round the clock.

Steve Mackara, **Kirk Steijn**, and **Bill Gambogi** of DuPont.
Steve Mackara was kind enough to shoot the master grating and some contact copies for the final viewstations of Chapter 5.
Kirk Steijn was very helpful in providing TK Solver information.

Our sponsors: **Honda R&D Co.**, **IBM**, and **NEC**, for their gratious support.

Sincere gratitude to those who have supported my work in the past:

My family
Jason Smith, my close friend and holography partner since high school,
for his shared vim, vigor, and vitality.
Kashiko Kodate and **Katsuma-sensei**, who made it possible for me to do independent holography work in Japan.
Professor **Emmett Leith** once again, for his generous offer to use his facilities during my stay at the University of Michigan: "Here comes the night shift."

Helpful discussions, distractions:

Professor **Seth Teller**, for discussions, not distractions.
Ranjana Mitra, my mutual distraction: "I know you've got a thesis, but do you want to scale some buildings tonight?"
David James, my personal D.J., for providing musical interludes from afar,
such as The Blur! They helped me to get focused…

Kory and **Ian –** Congratulations, and I wish you all the best for your future together

Text in this thesis was written on Microsoft Word for Windows 95, Version 7.0.
Mathematics segments were written with Microsoft Equation 2.0,
and for Chapter 2, Mathcad 5.0+ (MathSoft Inc.).
Figures were drawn with Microsoft PowerPoint for Windows 95, Version 7.0.
Graphs in Chapter 1 were made using Microsoft Excel for Windows 95, Version 7.0.
Computer programs were written in:
TK Solver+, Version 1.2 (Universal Technical Systems),
for the first program in Appendix 4.
Matlab (The Math Works, Inc.), for the programs of Appendices 5 and 6,
and the second program in Appendix 4.
Dictation was performed for parts of the thesis, using Dragon Dictate (Classic Edition) for Windows, Version 2.01 (Dragon Systems, Inc.).

Table of Contents

Page: 13 **Extended Table of Contents**

Page: 17 **List of Figures and Tables**

Page: 21 **Introduction**

Page: 23 **Dispersion compensation flowchart**

Page: 25 **1. Blur in holographic images**

Page: 49 **2. Trigonometric derivation of a single-plane blur equation**

Page: 65 **3. Introduction to dispersion compensation and a brief review of its application to holographic displays**

Page: 77 **4. Full-parallax reflection holographic stereograms**

Page: 85 **5. Example design of a dispersion-compensated, full-parallax holographic viewstation**

Page: 97 **6. Wave-front shapes, compact displays, and designing gratings**

Page: 125 **Conclusions and future work**

Page: 129 **A1. Single-plane trigonometric raytracing formulas**

Page: 133 **A2. Derivation of a vector blur equation and its reduction to the blur equation of Chapter 2**

Page: 141 **A3. TK Solver+ and Matlab programs applying the derived equations**

Page: 155 **A4. A Matlab program for the design of dispersion-compensation gratings (Chapter 6)**

Page: 159 **A5. A Matlab program attempting to solve for a pre- and post-dispersing grating set flush against a hologram (Chapter 6)**

Page: 161 **References**

Extended Table of Contents

Page: 17 **List of Figures and Tables**

Page: 21 **Introduction**

Page: 23 **Dispersion compensation flowchart**

Page: 25 **1. Blur in holographic images**
Page: 25 1.1 Blur in holographic images
Page: 26 1.2 Basic principles of holography
Page: 29 1.3 The Gabor zone plate
Page: 32 1.4 Longitudinal and lateral dispersion
Page: 35 1.5 Overlapping zone plates
Page: 35 1.6 Perception of color blur: acuity and stereoacuity
Page: 38 1.7 Resolution vs. detection / perceived vs. absolute color blur
Page: 40 1.8 Spectral intensity filter #1: The retina
Page: 41 1.9 Spectral intensity filter #2: Diffraction efficiency of the hologram(s)
Page: 42 1.10 Spectral intensity filter #3: The illuminant
Page: 44 1.11 Resolution of color-blurred reflection holographic images
Page: 47 1.12 Factor for perceived blur size

Page: 49 **2. Trigonometric derivation of a single-plane blur equation**
Page: 49 2.1 Derivation of a color blur equation
Page: 53 2.2 Inclusion of source-size blur into a final blur equation
Page: 55 2.3 Approximation to the final blur equation
Page: 55 2.4 Benton's color blur equation derivation
Page: 57 2.5 Benton's achromatic angle derivation
Page: 59 2.6 Benton's source-size blur equation derivation
Page: 60 2.7 Benton's final blur equation
Page: 61 2.8 Summary and comparison of the blur equations
Page: 62 2.9 Blur measurements using a spectrophotometer

Page: 65 **3. Introduction to dispersion compensation and a brief review of its application to holographic displays**
Page: 65 3.1 The first dispersion-compensation displays: single view angle transmission hologram / grating
Page: 70 3.2 Single viewpoint dispersion compensation: Burckhardt
Page: 71 3.3 Diffractive and refractive media
Page: 71 3.4 Compact single view angle displays: Burckhardt
Page: 72 3.5 Other transmission displays: Boj, et al., and Benton
Page: 73 3.6 Reflection displays: Bazargan, Kubota

Page: 77 **4. Full-parallax reflection holographic stereograms**
Page: 77 4.1 Making horizontal-parallax-only holographic stereograms
Page: 79 4.2 The transfer hologram
Page: 81 4.3 Full-parallax holographic stereograms

Page: 85 **5. Example design of a dispersion-compensated, full-parallax holographic viewstation**
Page: 86 5.1 The exposure wavelength
Page: 86 5.2 The holographic recording material
Page: 87 5.3 The exposure and reconstruction geometries
Page: 93 5.4 Selecting an illumination source
Page: 95 5.5 The resulting display

Page: 97 **6. Wave-front shapes, compact displays, and designing gratings**
Page: 97 6.1 Sources of blur in edgelit holograms
Page: 99 6.2 Pulling the grating and hologram closer together by using a light guide: the steep angle format
Page: 101 6.3 Compensation gratings with diverging wave fronts
Page: 102 6.4 Grating playout distances
Page: 104 6.5 Dispersion compensation and grating output wave-front shapes
Page: 105 6.6 The planar wave front case
Page: 107 6.7 The diverging wave front case (phase-conjugate)
Page: 108 6.8 The diverging wave front case (non-phase-conjugate)
Page: 110 6.9 Consistent method for designing gratings
Page: 110 6.10 Solving for optimized angles
Page: 112 6.11 Solving for optimized distances
Page: 112 6.12 Designing a diverging wave-front grating for a compact display
Page: 114 6.13 Designing a perfectly reconstructing diverging grating
Page: 116 6.14 Designing a diverging grating that plays out ideal angles and optimized distances
Page: 121 6.15 An attempt to design a pre- and post-dispersing compensation grating

Page: 125 **Conclusions and future work**

Page: 129 **A1. Single-plane trigonometric raytracing formulas**
A1.1 The X- and Z- raytracing equations
A1.2 The Welford and X-equations
A1.3 The Z-equation

Page: 130 A1.4 Spectrophotometer data
Page: 132 A1.5 The horizontal and vertical focus equations

Page: 145 **A2. Derivation of a vector blur equation and its reduction to the blur equation of Chapter 2**
Page: 133 A2.1 Color blur equation derivation
Page: 135 A2.2 Approximation proof
Page: 138 A2.3 Source-size blur derivation

Page: 141 **A3. TK Solver+ and Matlab programs applying the derived equations**
Page: 151 Alternative Matlab program
Page: 155 **A4. A Matlab program for the design of dispersion-compensation gratings (Chapter 6)**

Page: 159 **A5. A Matlab program attempting to solve for a pre- and post-dispersing grating set flush against a hologram (Chapter 6)**

Page: 161 **References**

List of Figures and Tables

Please note that in the figures, holographic images that seem to float outside of the solid angle subtended by the observer's eyes and the hologram are merely for illustrative purposes. Visible image points must lie along a line of sight from the eye to the hologram without the aid of smoke, mirrors, or re-emitting gases.

Figure 1.1: Successive wave fronts emanating from a point source of light
Figure 1.2: The Moire fringe pattern
Figure 1.3: The formation of a reflection hologram (after Jeong 1980)
Figure 1.4: The reconstruction of a reflection holographic image (Jeong 1980)
Figure 1.5: Interference pattern forming a Gabor zone plate
Figure 1.6: Spatial frequencies
Figure 1.7: Formation of a Gabor zone plate, with more closely spaced fringes toward its periphery (after Greivenkamp 1995)
Figure 1.8: Illumination of a Gabor zone plate with a single wavelength, with resulting virtual and real image points
Figure 1.9: Phase-conjugate illumination of a Gabor zone plate with a single wavelength
Figure 1.10: Illumination of a Gabor zone plate with two wavelengths, and the resulting longitudinal dispersion
Figure 1.11: The formation of an off-axis reflection hologram (after Jeong 1980)
Figure 1.12: Reconstruction of an off-axis reflection hologram
Figure 1.13: Dispersion in an off-axis reflection hologram: illumination by two wavelengths
Figure 1.14: Examples of different fringe patterns (Geisler and Banks, fig. 7.25.36-19)
Figure 1.15: Different acuity tests (Geisler and Banks, fig. 7.25.36-19)
Figure 1.16: Stereoacuity
Figure 1.17: Airy disk diffraction pattern (Riggs 1965, fig. 11.10)
Figure 1.18: Rayleigh's criterion for just resolvable points (Riggs 1965, fig. 11.11)
Figure 1.19: Two blurred points that are just resolvable
Figure 1.20: Photopic curve data from Wyszecki and Stiles (1967, table 4.2)
Figure 1.21: Illuminant A curve (Wyszecki and Stiles 1967; MIT 1936)
Table 1.1: Data from the spectral luminous efficiency (Wyszecki and Stiles 1936) and Illuminant A relative intensity (MIT 1936) curves
Figure 1.22: Intensity filters: the retina and illuminant
Figure 1.23: Just resolvable points defined by the diffraction efficiency curve
Figure 1.24: Perceived blur size factor

Figure 2.1: Spectral components from different points on the hologram contributing to blur
Figure 2.2: Dispersed focus at the pupil, perceived as color blur, from Appendix 2
Figure 2.3: Perceived color blur and source-size blur height
Figure 2.4: Dispersion for the cases of m = +1 or m = -1 order image points combined in one diagram
Figure 2.5: The achromatic angle for the cases of m = +1 or m = -1 order image points combined in one diagram
Figure 2.6: Wavelength-dependent focusing power of a hologram, and the achromatic angle (Saxby 1992)
Figure 2.7: The perceived blur angle according to Benton (1994)
Figure 2.8: (from Appendix 1)
Figure 2.9: Measurement 3 setup
Table 2.1: Blur length data for the vertical focus of 543.1 and 632.8 nm wavelengths

Figure 3.1: DeBitetto's original diagram discriminating the effects of diffraction orders on relative dispersion
Figure 3.2: Forward and reverse raytracing the spectral components through a transmission hologram
Figure 3.3: Raytracing the dispersed rays from the hologram through a transmission grating
Figure 3.4: A schematic representing the original geometry of the three researchers in reverse (Latta 1972)
Figure 3.5: Single view angle dispersion compensation This schematic represents the blurring of image points off of the local normal for a collimated reference /collimated illumination geometry.
Figure 3.6: Burckhardt's (1966) use of a louver film to block the zero order of the hologram in a single view angle dispersion-compensation display
Figure 3.7: Burckhardt's single viewpoint dispersion compensation technique (Collier, Burckhardt, and Lin 1971)
Figure 3.8: Example of the complexity of modern head-up displays incorporating dispersion-compensation gratings (Roberts, et al. 1995)
Figure 3.9: Bazargan's display, manufactured by Holoplex Systems, Ltd. (Syms 1990, fig. 10.5-2)
Figure 3.10: Benton's patent drawing of the white-light transmission hologram transfer step (1972)
Figure 3.11: Benton's patent drawing of the special achromatizing grating used in an exposure step (1985)
Figure 3.12: (a) Distortions of a square image across the visible spectrum (400-700 nm) (b) Single view angle dispersion compensation for reducing lateral chromatic aberration (Bazargan 1986, fig. 7.20)
Figure 3.13: Bazargan's suggested approach for making a full-color, dispersion-compensated display
Figure 3.14: Kubota's reflection /reflection dispersion-compensated display
Figure 3.15: Intensity profile of the reconstructed image points in Kubota's single view angle dispersion-compensation display

Figure 4.1: Sequential images are taken, and later projected to expose a hologram with an appropriately scaled geometry (Redman 1968).
Figure 4.2: DeBitetto's original drawing of the spatial multiplexing technique most commonly used in display holographic stereograms today (DeBitetto 1968)
Figure 4.3: A horizontal-parallax-only holographic stereogram (HPO HS, or H1)
Figure 4.4: The first (a) and last (b) vertical strip exposures of a holographic stereogram (top view)
Figure 4.5: Transfer setup
Figure 4.6: Phase-conjugate illumination of the HPO HS H2, and reconstruction of an orthoscopic, real image
Figure 4.7: Benton's pseudocolor technique for producing achromatic or full-color images (1983, 1988)
Figure 4.8: An example of different perspective views of a full-parallax hologram (image care of Michael Klug)

Figure 5.1: Uncompensated and compensated dispersion of a holographic image
Figure 5.2: Schematic of the final viewstation with tipped grating
Figure 5.3: Schematic of the exposure (225°) and illumination (45°) geometries of the dispersion-compensated H2 (from Chapter 4)
Figure 5.4: The desired grating playout (45°)
Figure 5.5: The required master grating exposure geometry (56.32° degrees), taking into account shrinkage of the photopolymer
Figure 5.6: The master grating exposure holographic table setup
Figure 5.7: The transfer grating exposure holographic table setup
Figure 5.8: filament orientation
Figure 5.9: Bulb with an ellipsoidal, dichroic reflector
Figure 5.10: Plane-wave grating dispersion-compensation display (photos care of Michael Klug)

Figure 6.1: Non-chromatic blurring of the edgelit hologram
Figure 6.2: Exposure of an edgelit hologram illuminated with the same source distance and folded beam path (Upatnieks 1992)
Figure 6.3: Reduction of chromatic and non-chromatic blurring of the edgelit hologram using a wave-front-shaping steep angle HOE
Figure 6.4: Upatnieks' achromatic edgelit hologram (1992)
Figure 6.5: A comparison of Birner's reflection HOE/transmission steep angle H2 with the author's reflection/reflection displays
Figure 6.6: Maximum acceptable perceived longitudinal blur length
Figure 6.7: Collimated, phase-conjugate, single view angle dispersion-compensated hologram with maximum depths (3 arc minutes of resolution):
Figure 6.8: Uncollimated, phase-conjugate, single view angle dispersion-compensated hologram with maximum forward compensated depths (1 arc minute of resolution)
Figure 6.9: Uncollimated, non-phase-conjugate, single view angle dispersion-compensated hologram with extreme field curvature (diverging/diverging geometry)
Figure 6.10: Ideal predispersed hologram illumination angles and distances should be equivalent to the ideal predispersed grating output angles.
Figure 6.11: Exposure of the transfer (H2) hologram with a diverging reference source
Figure 6.12: Reconstruction of the H2 with a diverging illumination source
Figure 6.13: The final table setup for the 750/750 diverging/diverging geometry
Figure 6.14: A graph of the exposure and illumination angles for a range of central output angles. This graph is the output from the Matlab 'plot' command in the program of Appendix 4.

Figure A1.1: Grating vector cloud (Goodman, 1996)
Figure A1.2: Dispersion measurements with an Oriel spectrophotometer
Table A1.1: Measurements of dispersion with an Oriel spectrophotometer
Figure A1.3: Diagram accompanying Benton's vertical focus equation derivation (Benton, 1994

Figure A2.1: Magnitudes and directions for the vector derivation of a blur equation
Figure A2.2: Trigonometric diagram
Figure A2.3: A dispersed focus at the pupil creating the perception of blur height

Introduction

"True observers of nature, however they may differ in opinion in other respects, will agree that all which presents itself as appearance, all that we meet with as phenomenon, must either indicate an original division which is capable of union, or an original unity which admits of division, and that the phenomenon will present itself accordingly. To divide the united, to unite the divided, is the life of nature; this is the eternal systole and diastole, the eternal collapsion and expansion, the inspiration and expiration of the world in which we live and move."

-- Goethe, Theory of Colours (1810, 293-4)

It is the sincere hope of the author that the following body of work, the result of a year of study, may serve as a helpful starting point for future researchers interested in the problems of image blur in holographic displays, and grating design. In order to expedite the reader's inquiry, this Introduction will serve as a brief outline of the contents of each chapter. The "Conclusions and future work" section will parallel this summary.

Chapter 1 consists of two parts: The first is an introduction to holography and dispersion, or color blur. In the second part, we will estimate the degree to which our perception of blur affects the resolution of a holographic image.

In **Chapter 2**, we derive and experimentally test a trigonometric blur equation for the absolute raytraced size of a blurred image. We then apply the perceived blur size factor from Chapter 1 to find the perceived size of this image. The author's blur equation is compared with Benton's blur equation.

In **Chapter 3**, we introduce dispersion compensation, a method to correct for color blur, and we give a brief history of the application of dispersion compensation to display holography.

Chapter 4 gives an introduction to full-parallax holographic stereograms, the particular type of hologram we will be illuminating in Chapter 5's display.

Chapter 5 is the culmination of the previous chapters' findings, applied to a plane-wave viewstation display. Laboratory techniques for forming a dispersion compensating grating are outlined here.

Chapter 6 compares the effectiveness of compact dispersion-compensation displays that do and do not use a plane-wave grating. Then, a consistent means for **designing dispersion-compensation gratings** is put forward in the chapter and in the accompanying computer programs of **Appendices 3** and **4**. It is shown that the method presented here (the use of the Moore-Penrose pseudoinverse) compares favorably with the perfect reconstruction geometries implemented in the viewstations of Chapters 5 and 6 and is well-suited to finding optimized angles, and also approximate distances, with less precision. It therefore is tailored to compensate for lateral and longitudinal dispersion as a function of eye position and orientation.

Dispersion compensation flowchart

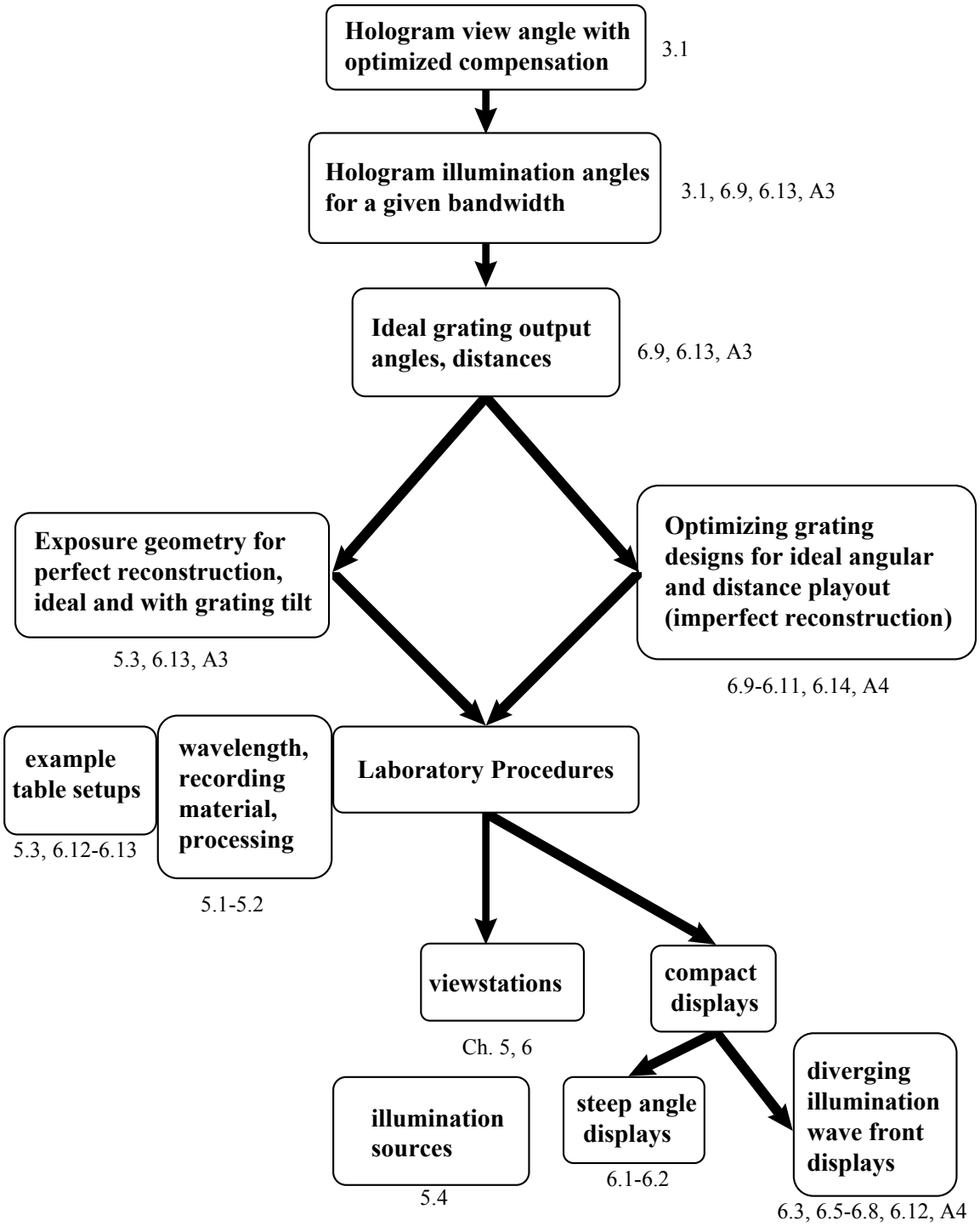

The numbers next to the boxes represent relevant sections.

Chapter 1
Blur in holographic images

1.1 Blur in holographic images

The primary sources of blur in holographic images are the spectral width and physical size of the illumination source, as well as non-ideal properties of the exposure medium and substrate. For full-parallax[1] holographic displays with controlled lighting conditions, the spectral width usually constitutes the greatest source of image blur, and as such will comprise the bulk of our discussions. As most optical aberrations have a chromatic component, we will refer to the blur due to polychromatic illumination simply as "color blur." In this first chapter, we will introduce blur as we cover basic principles of holography. Then we will determine how our perception of blur affects the resolution of a holographic image.

Because holograms rely on diffraction, and diffraction is wavelength dependent (that is, red wavelengths will deflect at greater angles through diffractive media than will blue wavelengths), a single holographically recorded object replays in a different location for each component wavelength of the illumination. This separation of component wavelengths, or dispersion, is analogous to the phenomenon of dispersion in refractive media, such as a prism. The extent of the spectral width of the source determines the extent to which light will disperse through a given medium, and therefore a broadband white light source can render an image an indistinguishable rainbow blur.

One trivial solution to the problem of color smearing of images is to illuminate the hologram instead with a very narrow spectral band source, such as a laser or an arc lamp with an interference filter. These are impractical for most viewing situations and, unless one sets up three such lamps, offer only monochromatic playback. Another solution is to produce better recording materials or to find better processing methods for producing more narrow band playout. In either case, whether a hologram is illuminated by a narrow spectral band source or a hologram with a narrow band playout is illuminated by an intense broad band source, much of the illumination light is wasted. To produce brighter, full-color, full-parallax holograms that are sharp and deep, correcting for color blur in white light illumination displays is vital.

[1] "Full-parallax" refers to the change in perspective vertically as well as horizontally. Synthetic full-parallax holograms are the subject of Chapter 5.

1.2 Basic principles of holography

To better understand color blur, we will take a brief look at some basic interference patterns, and then invoke the limiting case of the first type of hologram that was invented by Dennis Gabor in 1947 (Gabor 1948). If we have a source point acting as a harmonic oscillator, radiating waves in three dimensions, we can represent the instantaneous wave fronts emanating from the center as concentric spheres, whose radii are incremented by one-half of a wavelength (λ/2). The direction of travel for any point on the wave front is simply the direction of expansion, the local normal to the sphere (Figure 1.1). We will call the path the light's direction takes a ray, and tracing its path is called raytracing.

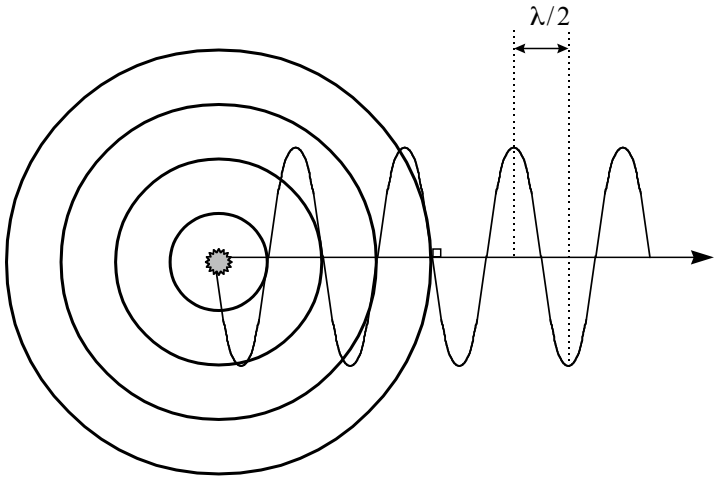

Figure 1.1: Successive wave fronts emanating from a point source of light

The superposition of two such wave fronts results in an interference pattern of hyperboloidal surfaces:

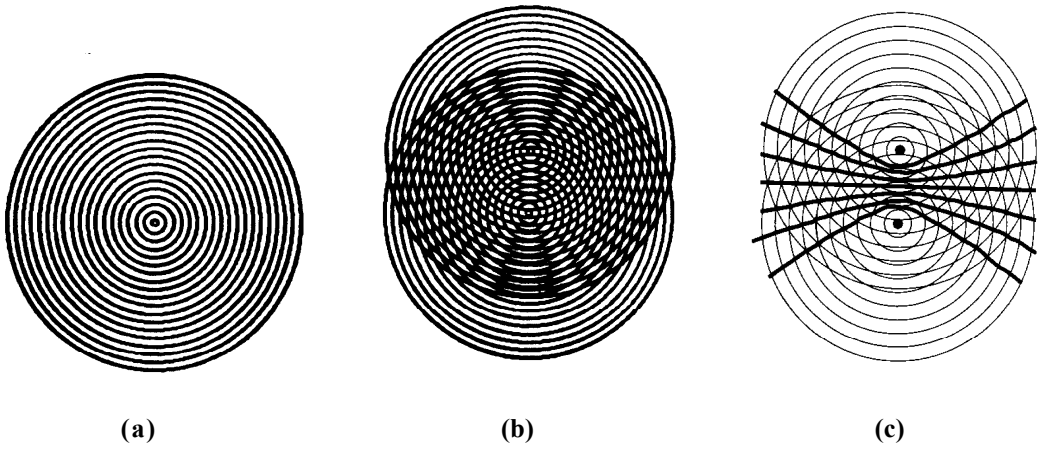

(a) **(b)** **(c)**

Figure 1.2: The Moire fringe pattern is a helpful visual aid to understanding interference effects[2]. Here we have the oscillating source above in isolation, and interfering with another source.
(a) The spherical wave fronts from a single light source
(b) The superposition of wave fronts from two light sources
(c) The interference pattern created by the two sources (Jeong 1980)

If the two sources are mutually coherent 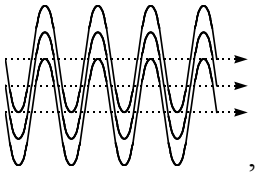, then this interference pattern will remain constant over time, a "standing wave." We may place a photosensitive recording material anywhere in the volume of space around or between these two sources to record the interference pattern. If placed between the two sources, the recording material will subsequently form partially reflective, hyperboloidal surfaces spaced through its volume:

[2] For and in-depth look into the analogy between moire fringe patterns and interference fringes, Abramson's book (1981) is an invaluable guide. A summary table may be found on page 9 of the book.

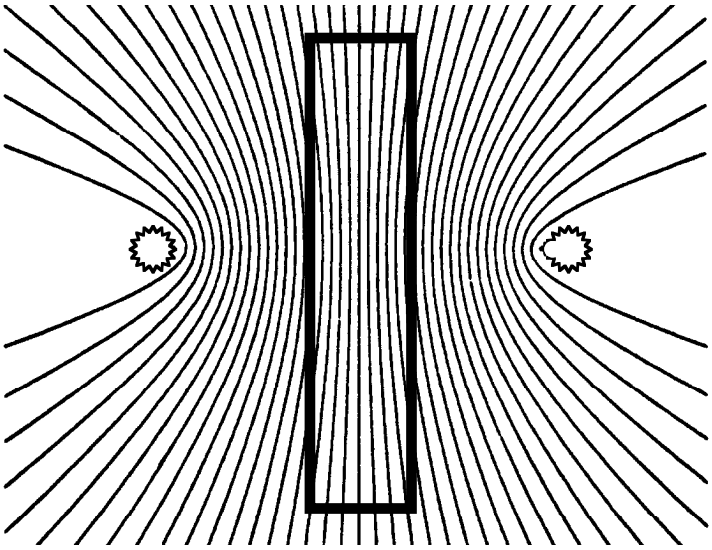

Figure 1.3: The formation of a reflection hologram (after Jeong 1980)

If the fringe pattern in this recording material retains its structural integrity and is then re-illuminated by a wave front from one of these two sources, this wave front will be partially reflected off each hyperboloidal surface and will interfere with itself. The interference determines the intensity of the light reflected off these surfaces in different directions. Light will be reinforced more in some directions than in other directions. Light traveling in directions corresponding to the directions light traveled from the other source during exposure are constructively interfered, and a reflection holographic image of the other source position will be formed (Figure 1.4).

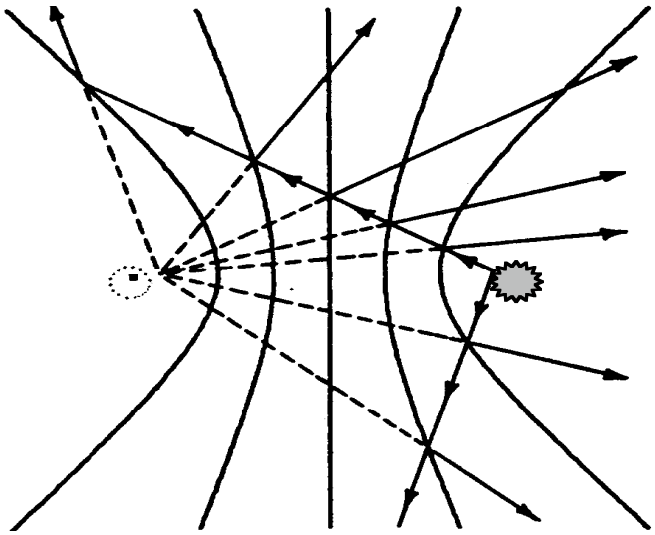

Figure 1.4: The reconstruction of a reflection holographic image (Jeong 1980)
The illumination source point is to the right, the reconstructed image to the left.

1.3 The Gabor zone plate

The particular interference pattern pictured in Figure 1.3, formed by source points on a line (the optical axis) intersecting the recording material, is called a "Gabor zone plate," or "in-line" hologram. If we had set the recording material along the optical axis, but not in between the two source points, a different form of Gabor zone plate would be formed, an in-line transmission hologram:

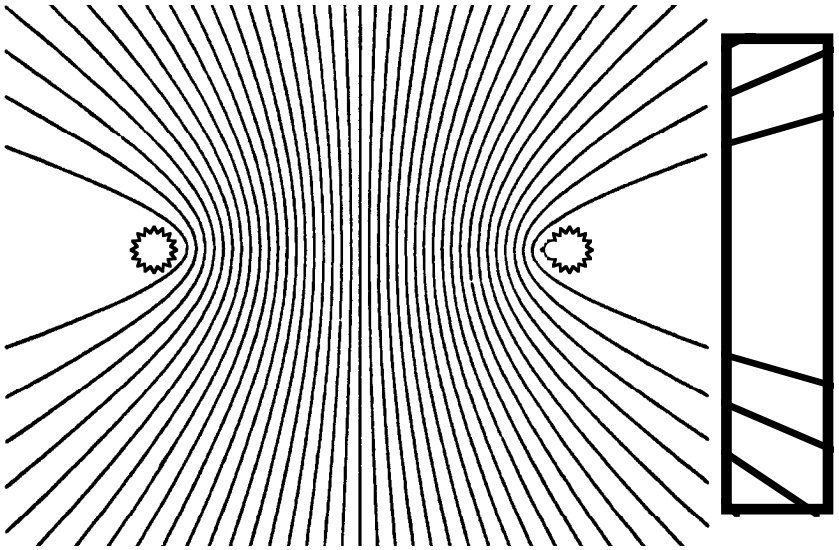

Figure 1.5: Interference pattern forming a Gabor zone plate

The interference pattern of the in-line transmission hologram is composed of concentric circles centered around the axis. Because the angle between the line containing the source points and the axis is zero, so too is the corresponding fringe density, or spatial frequency[3] of the interference pattern. The angle between these two points with respect to a point on the hologram off-axis increases toward the edges, and the corresponding spatial frequency increases (See Figures 1.6 and 1.7).

[3] Spatial frequency refers to the reciprocal of the distance between elements of a repeated pattern, such as holographic fringes: $f = \left| \frac{\sin(\theta_{ref}) - \sin(\theta_{ill})}{\lambda = wavelength} \right|$, in cycles/mm.

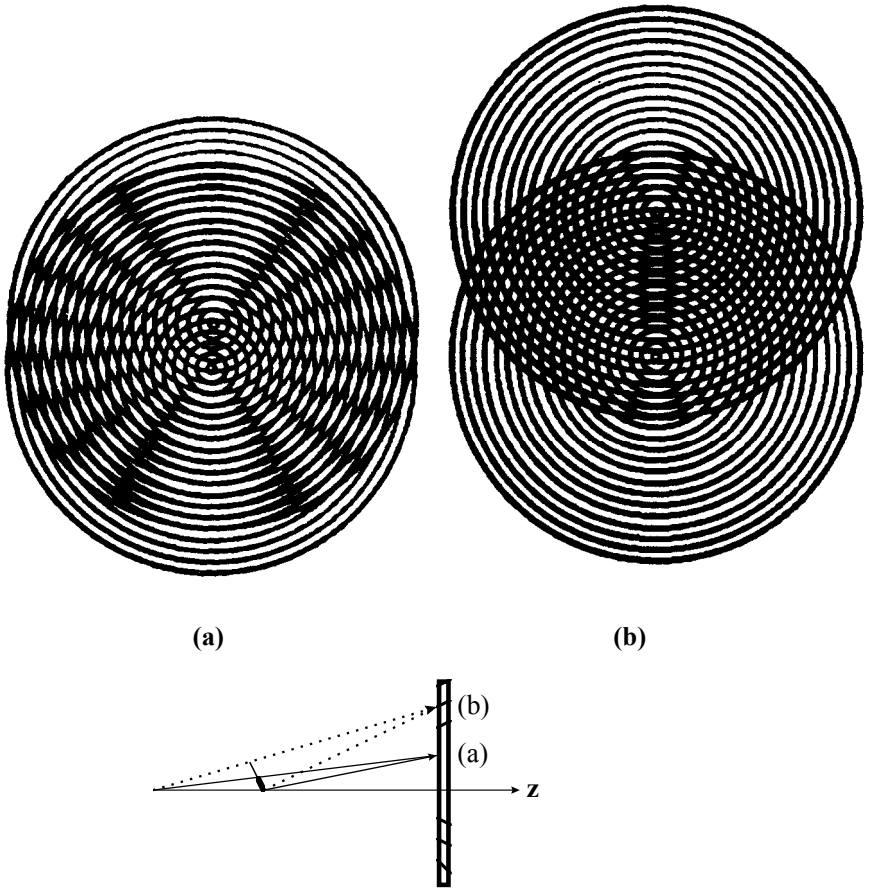

Figure 1.6: As the apparent distance between source points increases, so too does the spatial frequency of the fringes. In this figure, we are looking at the two sources from two different points on the recording material, one point close to the optical (**z**-) axis (a), another farther off-axis (b).

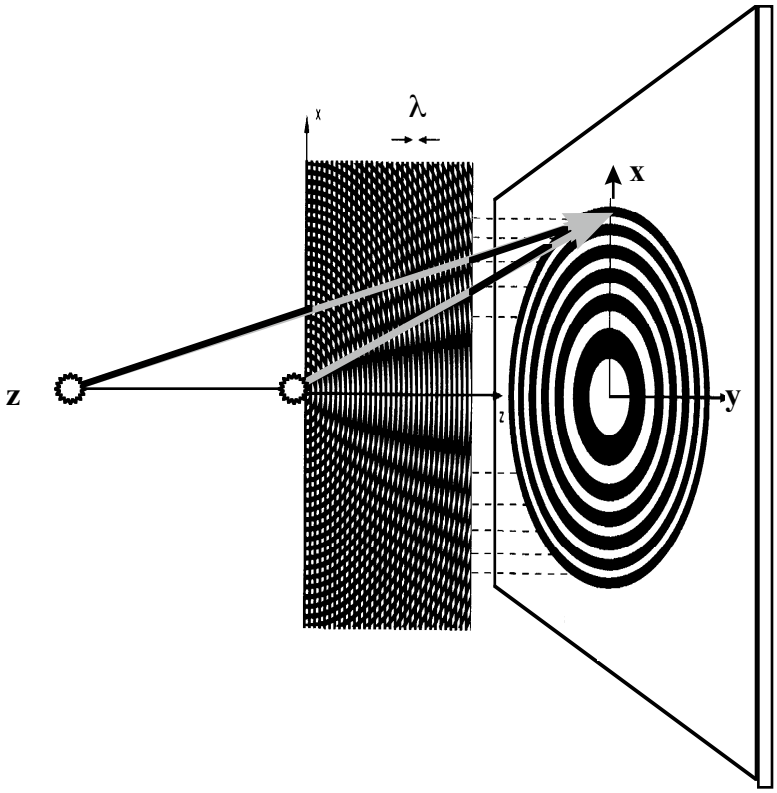

Figure 1.7: Formation of a Gabor zone plate, with more closely spaced fringes toward its periphery (after Greivenkamp 1995)

Because the center of the zone plate has zero spatial frequency[4], light illuminating the hologram on axis will pass through undiffracted. Diffractive, or focusing power increases with increasing spatial frequency, so the zone plate's edges deflect incident light the most, in the direction of the original wave front from the other source point, as well as toward a focused, real image point in front of the observer. This second image in line with the first, is sometimes referred to as a "twin image." In Figure 1.8, the twin image is a real, focused image.

[4] There may or may not be a fringe in the center of a transmission in-line hologram, depending on the relative phase of the two exposure beams. The reflection in-line hologram has fringes parallel with the surface. In either case, the center of the zone plate has no diffractive power for on-axis rays.

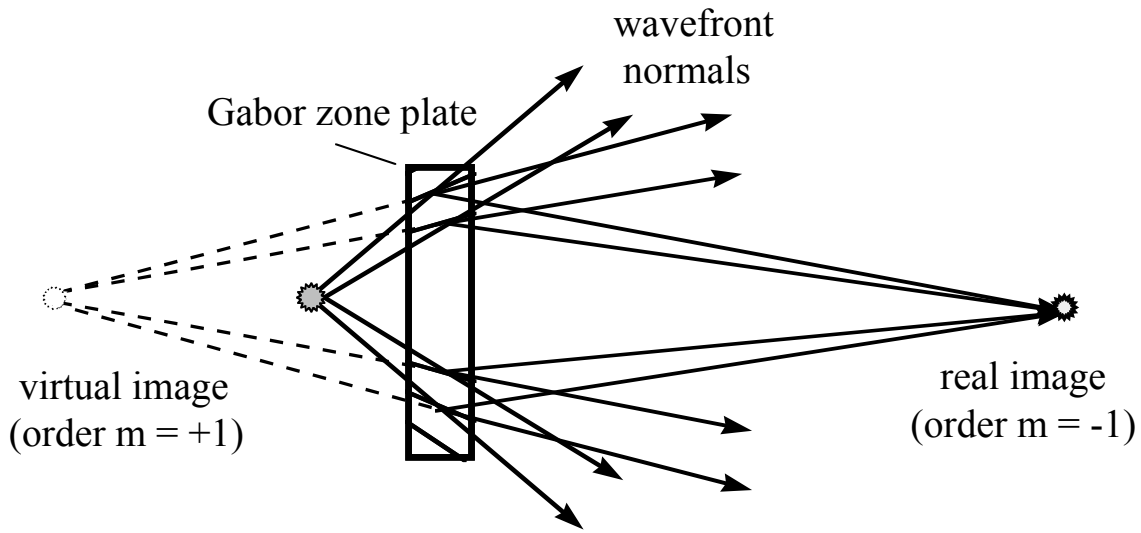

Figure 1.8: Illumination of a Gabor zone plate with a single wavelength, with resulting virtual and real image points

Phase-conjugate illumination is essentially a reversal of the directions of the rays that exposed the hologram. This "time-reversed" illumination results in a real image point projected where the original object point was located. Here, the twin image is a virtual image behind the hologram plane from the observer (Figure 1.9).

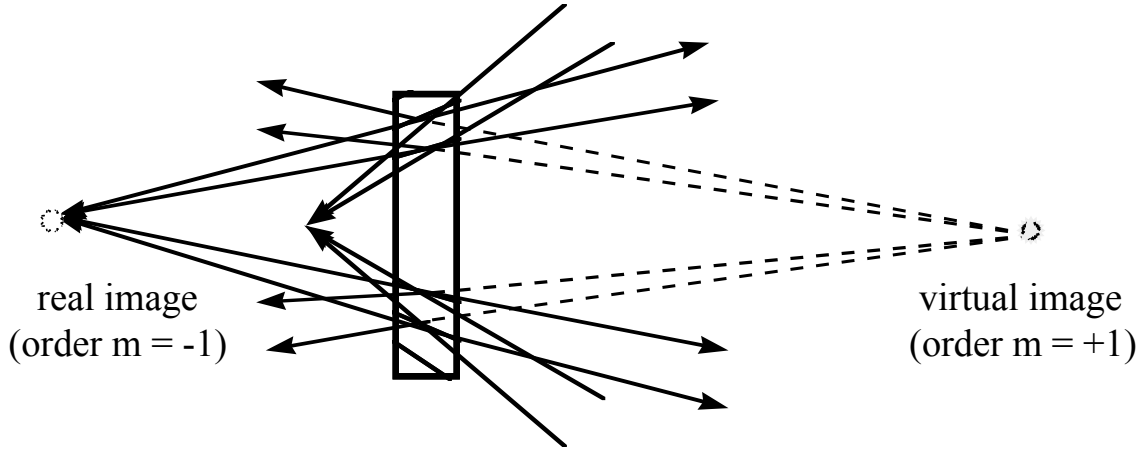

Figure 1.9: Phase-conjugate illumination of a Gabor zone plate with a single wavelength

1.4 Longitudinal and lateral dispersion

As the spacing of between the fringes determines what wavelengths will constructively interfere at different angles, it is possible to produce another image point at a different location by illumination with a different wavelength. The focusing power is therefore not only a function of spatial frequency, but also of wavelength, and therefore the wavelengths illuminating a Gabor zone plate focus to different points along the axis. The color blur of the longitudinally displaced images of the source points is termed longitudinal color blur and is not noticeable by an observer situated along this axis. If, however, the observer moves off the axis, the color blur becomes quite apparent.

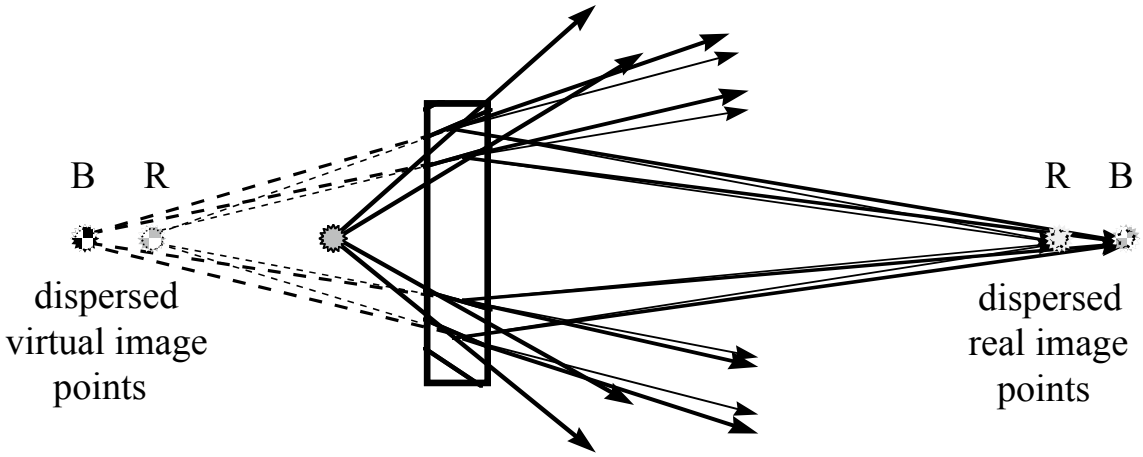

Figure 1.10: Illumination of a Gabor zone plate with two wavelengths, red (R) and blue (B), and the resulting longitudinal dispersion

Likewise, if we take a source point off-axis during recording of the hologram, white-light illumination of the hologram will result in lateral color blur. This off-axis hologram, invented by Leith and Upatnieks (1962), can eliminate the twin image so that the observer sees only one image.

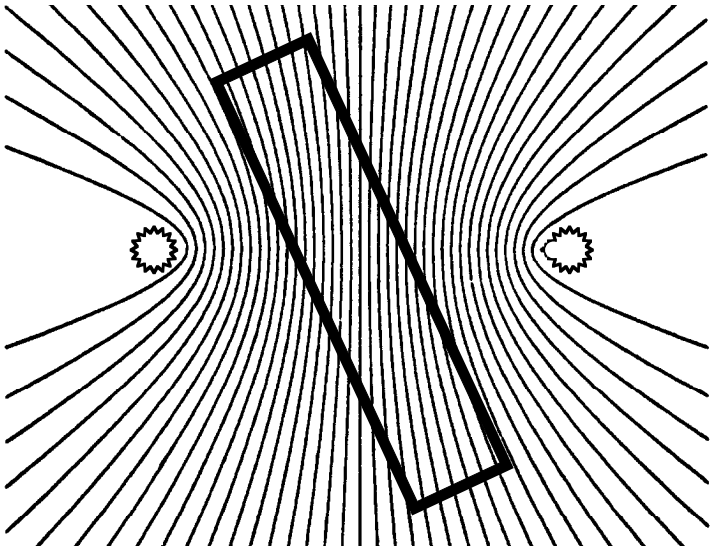

Figure 1.11: The formation of an off-axis reflection hologram (after Jeong 1980)

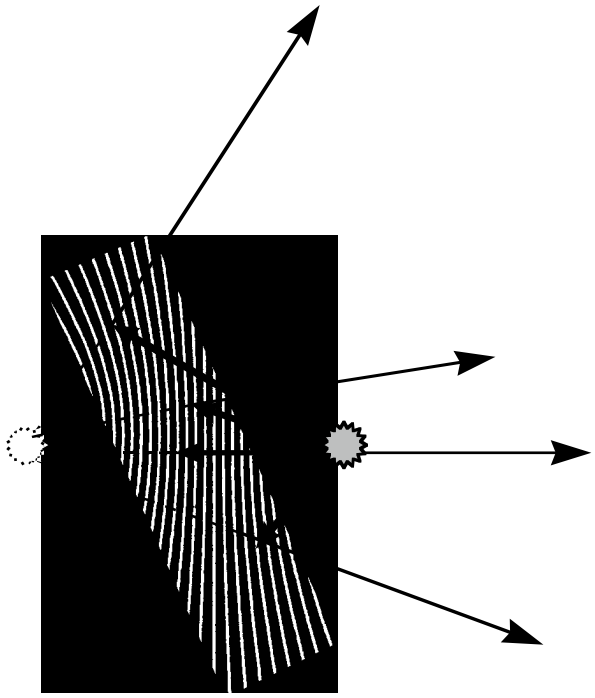

Figure 1.12: Reconstruction of an off-axis reflection hologram, where the twin image is eliminated. The illumination source point is to the right, and the virtual image is to the left.

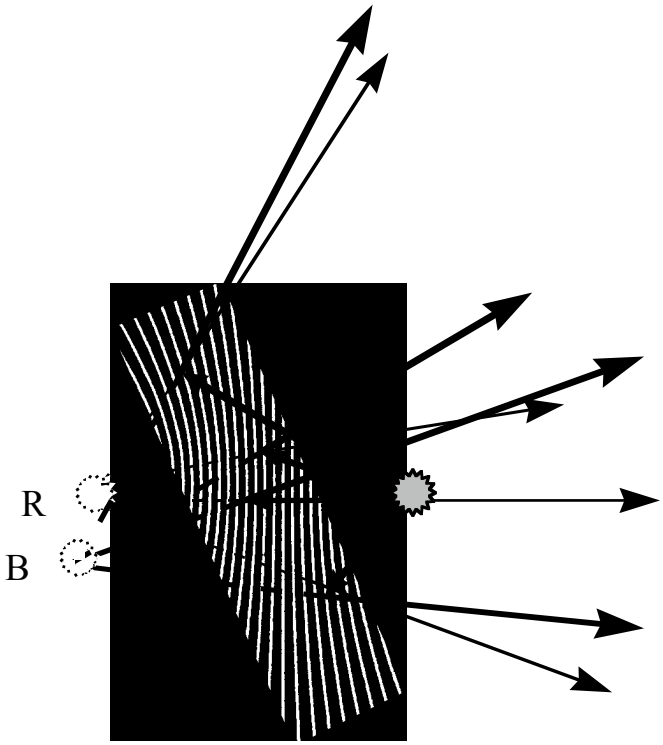

Figure 1.13: Dispersion in an off-axis reflection hologram: The broad band illumination source point to the right results in Red and Blue image points to the left.

The lateral color blur may be explained by the fact that the source points are laterally displaced, creating a different interference pattern, and therefore the off-axis white light illumination of the hologram will focus points of different colors so that they are laterally displaced, as well as longitudinally displaced (as in the in-line case). The resulting image not only suffers from spherical aberration, but also from coma, and most significantly from astigmatism (Latta December 1971).

1.5 Overlapping zone plates

An object illuminated by one of these sources may itself be considered a collection of a vast number of radiating sources, with spherical wave fronts emanating from each point location on its surface. We may therefore consider a hologram formed by an illuminated object to be a composite of a vast number of overlapping zone plates, or gratings. We will assume that diffraction by each of these gratings is independent of diffraction by the other gratings. As the points on the object's surface may be in disparate locations, the resulting fringes formed have different orientations and spacings. The more extreme the distances between these object points become, the closer their fringe patterns will resemble those of different hologram geometries (Figure 1.14).

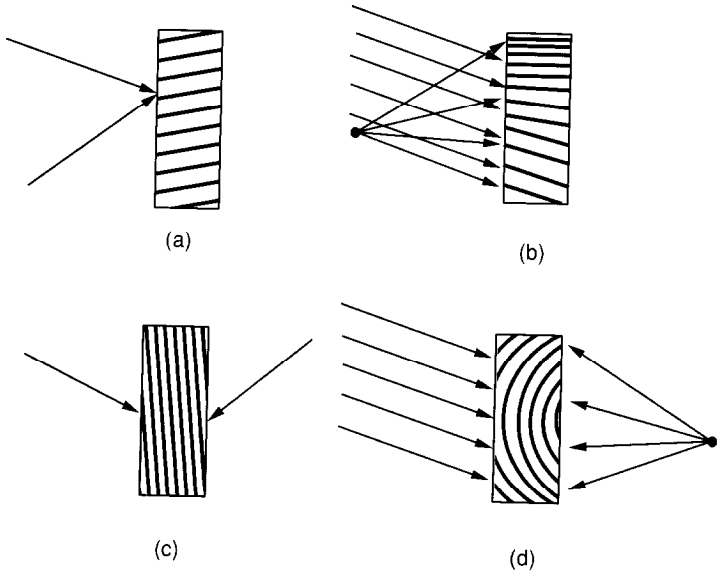

Figure 1.14: Examples of different fringe patterns (Goodman 1996):
(a) plane-wave transmission grating
(b) general transmission grating
(c) plane-wave reflection grating
(d) general reflection grating

1.6 Perception of color blur: acuity and stereoacuity

We will now attempt to quantify the amount of color blur we perceive when we look at a holographic image. George and McCrickerd (1969) derived the ultimate angular resolution of a hologram and of a holographic stereogram (to be described in Chapter 4)

according to depth-of-focus and diffraction blurring considerations, and found the former to be $\frac{\lambda}{L}$ (L = length of the hologram) and the latter to be $\frac{\lambda}{l}$ (l = length of the exposure aperture[5]). As we are concerned with blur of a considerably more insidious nature, due to a non-ideal illumination source, we will neglect George and McCrickerd's Gaussian beam analysis, and instead derive a filter factor that will determine the perceived image point size from an absolute raytraced size. The result of this analysis could have a significant effect on the raytraced blur equation derived in the following chapter.

For this analysis, it would be helpful to introduce some basic concepts and data from the psychophysics literature. In particular, data[6] on measurements of resolution, visual acuity and stereoacuity, will provide us with ideal quantities with which we may compare the resolution of dispersed holographic images. We will refer to visual acuity as a measurement of one eye's ability to just resolve two laterally spaced points, whereas stereoacuity will be a measurement of both eyes' ability to just resolve two longitudinally spaced points. Both measurements will be in terms of the reciprocal of the minimum angle of resolution, so a high visual acuity means that the minimum angle of resolution is small. The measurements will rely to some degree on parameters such as stimuli luminance and choice of stimuli (Figure 1.15).

In the case of acuity under ideal conditions, the average threshold for resolution in the grating task (resolving closely spaced lines) is considered to be about one arc minute[7] (1 arc minute = $\frac{1}{60}$ °), and under optimal conditions, the Landolt ring and letter acuity tasks result in an average threshold of about 30 arc seconds[8] (1 arc sec = $\frac{1}{60}$ arc minute). For high intensities of light (above 4000 meter-candles), acuity scores as low as 24 arc seconds have been measured. For vernier acuity, a hyperacuity task (where resolution of the image projected on the retina exceeds the intercone spacing), resolution can be as low as 2 arc seconds.

---

[5] The exposure aperture is an aperture in a mask through which a small area of a hologram may be exposed. The significance of the exposing small adjacent areas of a holographic recording material will become apparent in Chapter 4.

[6] Unless footnoted, the psychophysics data presented here is repeated from Riggs (1965)

[7] Grating task data is taken from Riggs (1965, 326)

64 arc sec (Lister)
50 arc sec (Hirschmann)
52 arc sec (Bergmann)
64 arc sec (Helmholtz)
56 arc sec (Uhtoff)
64 arc sec (Kobb)
35 to 40 arc sec (Shlaer (1937), Keesey (1960))

[8] Handbook of Optics, vol. I, pp. 25.36-7 (1995)

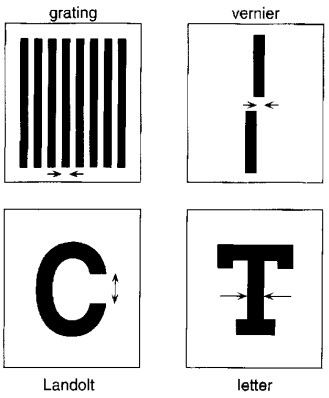

Figure 1.15: Different acuity tests
(Geisler and Banks, fig. 7.25.36-19)

Stereoacuity can vary depending on interpupillary and fixation distances. For an average interpupillary distance of 65 mm, the mean retinal disparity threshold has been found to be approximately 20 to 40 arc seconds for shorter distances (40 cm)[9], and 4 to 10 arc seconds for longer distances (65 to 130 cm).[10,11]

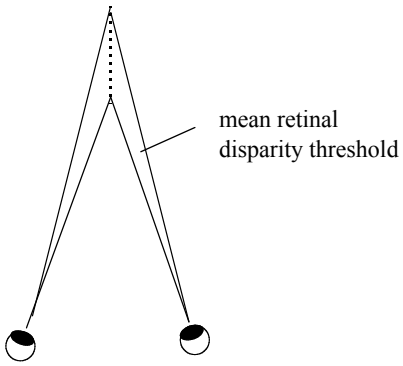

Figure 1.16: stereoacuity

As we will be calculating resolution of image points subjected to color blur primarily in the vertical direction due to a vertically offset illumination source, the value of one arc minute of lateral resolution will be sufficient for much of our work. Also important to note is that acuity depends on wavelength for low to moderate levels of illumination. Acuity is best for the middle of the visual spectrum (yellow-green) and degrades toward the longer (red), and is worst for the shorter (blue) wavelengths. Our prototype viewstation at the time of writing displays holograms exposed and reconstructed with a central wavelength of 514.5 nm. This wavelength is roughly in the central region of the visible spectrum, and therefore our ability to resolve image points for such an image should be better than for a full-color image in such a display.

1.7 Resolution vs. detection / perceived vs. absolute color blur

---

[9] G. Heron, et.al (1985), repeated in Charman (1995)

[10] McFadden paper: 2-12 arc sec range amongst his six subjects

[11] Repeated from Graham (Chapter 18, 1966) in Charman (1995)

To simply assess the perceived size of a single blurred image point by calculating the directions of the light rays that we can detect could prove inadequate. The reason for this is that our ability to detect a stimulus is dependent on many factors, including not only properties of the stimulus itself such as contrast and luminance, but also the state of the observer. The threshold for perceiving light ranges across a logarithmic scale depending on our level of light adaptation, and under optimal conditions, we can detect a light source when only a few photons impinge on our photoreceptor cells. Also, because the diffracted image of a point source is a set of concentric rings like those of the Gabor zone plate about an "Airy disk," very small stimuli (critical widths less than ten seconds of arc[12]) appear to be the same size.

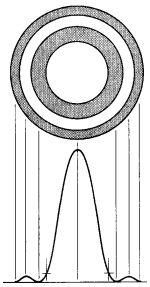

Figure 1.17: Airy disk diffraction pattern. The lines merely ascribe areas of the diffracted pattern to points on the corresponding intensity curve (Riggs 1965, fig. 11.10).

We will therefore rely not on absolute detectability or brightness discrimination of a single blurred image point to calculate its apparent size. Instead, we will calculate the resolvability of two closely situated points by defining a maximum overlap. One model to help us better understand resolvability is Rayleigh's criterion. Rayleigh's criterion states that the images of two points are considered just resolvable if the distance between them is at least the distance from the center of one Airy disk to its first minimum.

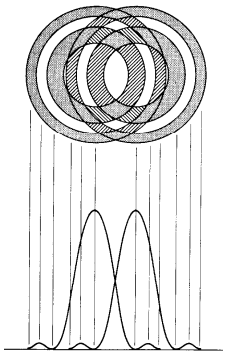

Figure 1.18: Rayleigh's criterion for just resolvable points. Here are two overlapping Airy disk patterns, the images of two closely spaced points. As in Figure 1.17, the lines merely ascribe areas of the diffracted pattern to points on corresponding intensity curves (Riggs 1965, fig. 11.11).

Equation (**1.1**): Rayleigh's criterion is given by the relation (Riggs 1965): $\omega = \frac{1.22\lambda}{d}$,

[12](Riggs 1965, 322)

where ω is equal to the minimum resolvable angular separation between the two centers, λ is the wavelength, and *d* is the diameter of the lens, in this case the pupil diameter. Although we could predict from this expression that an increase in pupil diameter should result in a corresponding linear decrease in the minimum angle of resolution, when the aperture size gets larger than 2 mm or so, resultant optical aberrations compromise the linear relation. Experimentally, the Dawe's Limit, $\omega = \frac{\lambda}{d}$, seems to be corroborated for pupil diameters of less than 1 mm. A maximum acuity is attained for pupil sizes of 2.5 to 4 mm, although the value does not increase dramatically from 2 to 5 mm. As we are interested in an average pupil size of 3 mm or so, it would be most appropriate to use Rayleigh's Limit with $d = 2.5$ mm.

We will apply the concept underlying Rayleigh's Limit equation not to Airy disks of concentric rings of diffracted maxima and minima, but instead to blurred points of decreasing intensity toward their peripheries. The minimum resolvable distance between two points will then be from the point's center of maximum intensity to its periphery of submaximal intensity, to be defined by a contrast specification below.

The primary confounding factor in defining resolution is, of course, noise in the image. We will assume a background noise that negligibly affects the relative intensity across blurred images, and is sufficient to preclude the possibility of "super resolution," where the resolving power exceeds Rayleigh's, Sparrow's (Smith 1990, 152), and Dawe's criteria. The holographic image contrast suffers from ambient illumination, scattering and dispersion of light in the recording material and substrate, intermodulation noise ("cross-talk" between component gratings), and other artifacts that compromise the observer's ability to discriminate intensity differences in an image.

If were interested in radiometric image brightness (Caulfield 1979, 235-6), then we would need to include factors such as the relative size of the image to the object, or in the case of the stereogram (Chapter 4), the magnification of the viewzone, as this will affect how spread out the light from the hologram becomes[13]. However, as we have ruled out the consideration of absolute intensity thresholds of the eye for blur size determination, we will instead make a photometric estimation of relative intensities based on the three wavelength-dependent intensity filters

---

[13] In actuality, the image size is dependent on wavelength, and the viewzone will be magnified for longer wavelengths. We will assume that this has a negligible effect on the relative intensities for different wavelengths of the blurred image. The topic of a hologram's viewzone will be taken up in Chapter 3 ("Full-parallax reflection holographic stereograms") and in Chapter 6 ("Wavefront shapes and compact displays"). It will prematurely be stated that this magnification is equal to the ratio of the area of the viewzone to the area of the master hologram. For the collimated grating in the viewstation of Chapter 5 ("Design of a full-parallax holographic viewstation"), this magnification is unity. For a diverging illumination geometry, this value drops below one as the image of the master hologram, and therefore the viewzone, becomes magnified.

The perceived intensity dropoff determining the boundaries of the blurred images will be calculated using three filters: (1) the spectral luminous efficiency curve of the eye, (2) the diffraction efficiency curve of the hologram, and (3) the relative intensity curve for the illumination source.

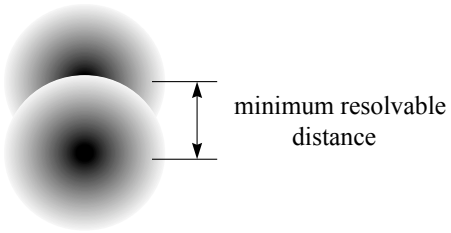

Figure 1.19: Two blurred points that are just resolvable

1.8 Spectral intensity filter #1: The retina

The ultimate filter for these color-blurred images will be the eye, so it would be appropriate to first outline the sensitivity of the eye to different wavelengths. The CIE graph usually used to demonstrate the relative response of the eye is termed the spectral luminous efficiency curve. There are actually two curves, one for the light-adapted eye, the "photopic curve," and one for the dark-adapted eye, the "scotopic curve." The photopic curve peaks at about 550 nm, attributable to the yellow-green sensitivity of the cone photoreceptors, whereas the scotopic curve peaks at 507 nm, the "Purkinje shift" toward the blue, attributable to the blue-sensitive rods. We will use the data from the photopic curve, as it is our aim to produce displays that are viewable in even brightly lit surrounds.

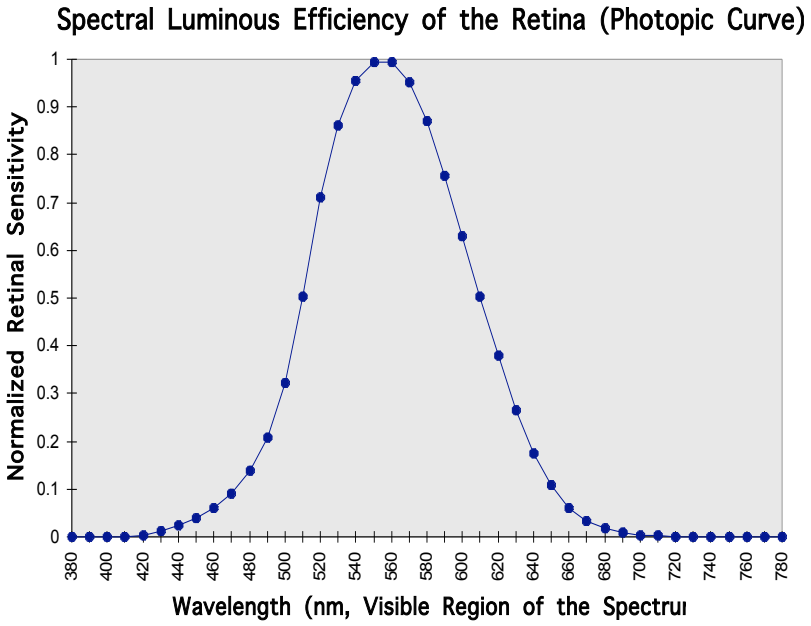

Figure 1.20: Photopic curve data from Wyszecki and Stiles (1967, table 4.2)

1.9 Spectral intensity filter #2: Diffraction efficiency of the hologram(s)

The eye will only receive the wavelengths at the intensities the hologram can deliver to it, so the next filter we will apply will be that of the hologram as an interference filter. The filter limits the diffraction efficiency of different output wavelengths, and may be calculated using Kogelnik's coupled wave equations (Kogelnik 1967, 1969).

For our analysis, we will assume that the diffraction efficiency distribution of the spectral components, and therefore the intensity distribution of a blurred image point composed of these spectral components, is gaussian and centered at the playout wavelength of maximum diffraction efficiency. The intensity distribution of a gaussian beam is described by

Equation (**1.2**) (Smith 1990, 155-6): $$I(r) = I_o e^{\frac{-2r^2}{w^2}},$$

where I_o is the intensity on axis (the playout angle at the central wavelength), e is 2.17…, r is the radial distance (distance from the center of the blurred image), and w is the beam width. Beam width is defined as the radial distance at which the intensity is $\frac{I_o}{e^2}$ (13.5% of the central value). If the intensity distribution is then normalized, with the peak intensity equaling one, then fractional values would be ascribed to the relative visibility along r in Equation (1.2). This fractional value would need to be raised to the power of the number of holograms in the system, assuming there is no wasted light and each hologram reconstructs with the same bandwidth.

1.10 Spectral intensity filter #3: The illuminant

There is one final factor affecting the relative intensity of different wavelengths in our consideration. Just as we needed to know what light intensities the hologram imparted to the retina, we need to specify the relative intensities of the different wavelengths illuminating the hologram. For an example of such data, we will use the International Commission on Illumination's choice source for a colorimetry standard: "Illuminant A," a tungsten lamp at a temperature of 2848K (MIT 1936). The choice of a tungsten filament is appropriate, as one of the viewstations of Chapter 5 is illuminated by one. However, the modern standard color temperature for quartz-halogen lamps, including those of Chapter 5, is either 3200 or 3400K. If we were to choose a higher color temperature, we will find that this choice further substantiates the final filter factor we are deriving.

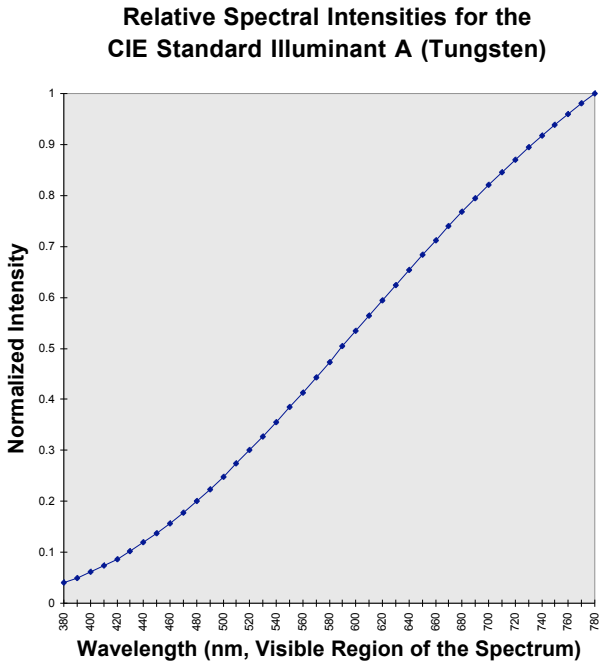

Figure 1.21 (Wyszecki and Stiles 1967; MIT 1936)

The relative intensities of the wavelengths have been normalized in Table 1.1 below. Each Illuminant A normalized value may be multiplied by the values for the corresponding wavelengths from the spectral luminous efficiency and diffraction efficiency curves. The resulting product of the corresponding Illuminant A and retinal efficiency data are listed in the rightmost column and represent what fraction of the light of that wavelength is delivered from the tungsten source to the hologram, and from the hologram to the eye, neglecting diffraction efficiencies.

	Retinal efficiency, normalized	Illuminant A (CIE tungsten, normalized)	Product of the retinal efficiency & Illuminant A
380	0	0.04051	0
390	0.0001	0.050027	5E-06
400	0.0004	0.060868	2.43E-05
410	0.0012	0.073158	8.78E-05
420	0.004	0.086895	0.000348
430	0.0116	0.102081	0.001184
440	0.023	0.118757	0.002731
450	0.038	0.136922	0.005203
460	0.06	0.156494	0.00939
470	0.091	0.177391	0.016143
480	0.139	0.199652	0.027752
490	0.208	0.223073	0.046399
500	0.323	0.247693	0.080005
510	0.503	0.273348	0.137494
520	0.71	0.299996	0.212997
530	0.862	0.32743	0.282245
540	0.954	0.35565	0.33929
550	0.995	0.38445	0.382528
560	0.995	0.413787	0.411718
570	0.952	0.443497	0.422209
580	0.87	0.473538	0.411978
590	0.757	0.503703	0.381303
600	0.631	0.533951	0.336923
610	0.503	0.564158	0.283771
620	0.381	0.594281	0.226421
630	0.265	0.624116	0.165391
640	0.175	0.653701	0.114398
650	0.107	0.682873	0.073067
660	0.061	0.711549	0.043404
670	0.032	0.739728	0.023671
680	0.017	0.767286	0.013044
690	0.0082	0.794182	0.006512
700	0.0041	0.820375	0.003364
710	0.0021	0.845823	0.001776
720	0.001	0.870443	0.00087
730	0.0005	0.894277	0.000447
740	0.0003	0.917201	0.000275
750	0.0001	0.939297	9.39E-05
760	0.0001	0.960442	9.6E-05
770	0	0.980718	0
780	0	1	0

Table 1.1: Data from the spectral luminous efficiency (Wyszecki and Stiles 1936) and Illuminant A relative intensity (MIT 1936) curves, and their corresponding products

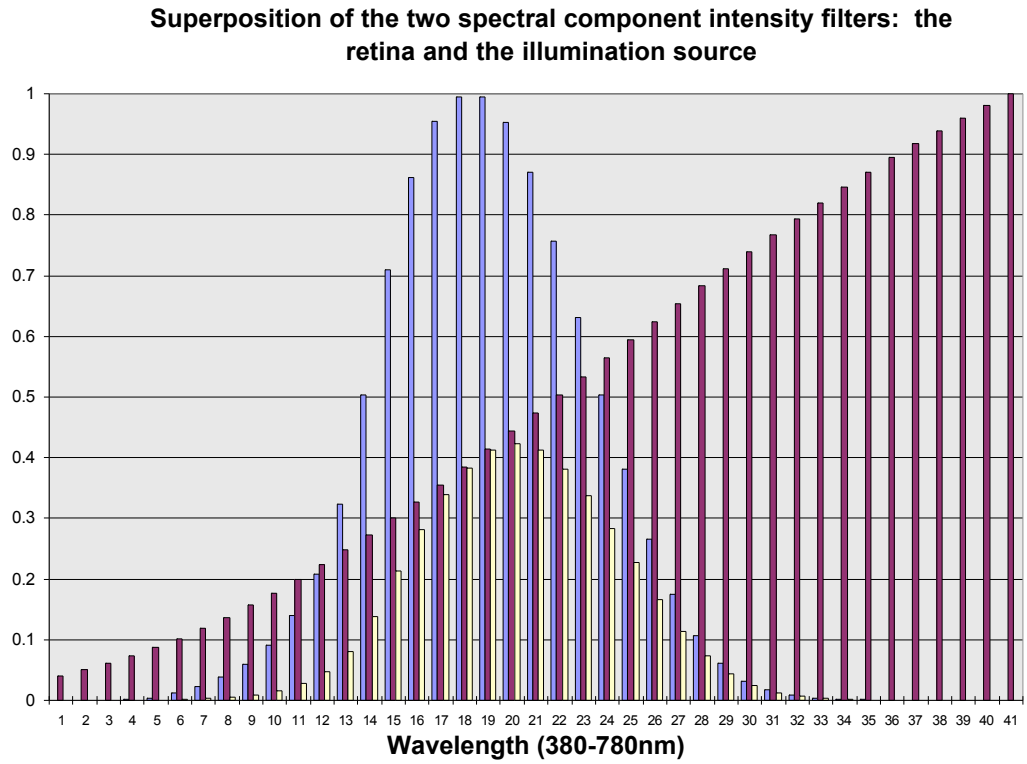

Figure 1.22: Intensity filters: the retina and illuminant

1.11 Resolution of color-blurred reflection holographic images

The data used to make Figure 1.22 could have been multiplied by their corresponding diffraction efficiency values for a complete determination of the relative intensities of the spectral components. However, the above analysis is only reasonable for application to transmission holograms with a wide spectral bandwidth (on the order of 200 to 300 nm), and is more extensive than it needs to be for thicker, reflection holograms having a narrow spectral band (of about 20 to 30 nm).

For a narrow segment of the visual spectrum, the spectral luminous efficiency and relative illumination intensity curves are approximately linear and of small slope for the illumination source that was chosen. The diffraction efficiency curve, on the other hand, is very narrow about the central wavelength, and therefore of very steep slope. We will therefore consider the retinal and illuminant distributions to have a negligible effect on the perceived size of blurred image points. Instead, we will consider the perceived size to be wholly dependent on the diffraction efficiency distribution. First, we will define the resolvability of two blurred images, and then we will define the perceived size of a single blurred image point.

To define the resolvability of two blurred images, we will overlap the intensity distributions of two very closely situated images (as in section 1.7). A correspondence exists between distance from the center of a blurred image and playout wavelength, so the spectral intensity distribution will enable us to determine the size of the image above a specified cutoff intensity. The distance from the center to the "boundary" of a blurred image is simply the length along the blur from the focused wavelength of highest diffraction efficiency to the focused wavelengths of some cutoff diffraction efficiency. We will define the minimum resolvable distance between two images as half of the distribution width at 50 percent intensity, the point on the Gaussian profile without curvature (Figure 1.23). We will further define the absolute bandwidth, $\Delta\lambda$, as those wavelengths contributing 95 percent of the intensity, from Equation (1.2):

Equation (**1.3**): $\frac{I(r_{\Delta\lambda})}{I_o} = \frac{1}{e^3} \cong 0.95,$ with $r_{\Delta\lambda}$ equal to half the absolute image size

For a 50 percent spectral intensity cutoff, the minimum resolvable distance may be calculated from the absolute size of the blurred image, using the total calculated bandwidth.

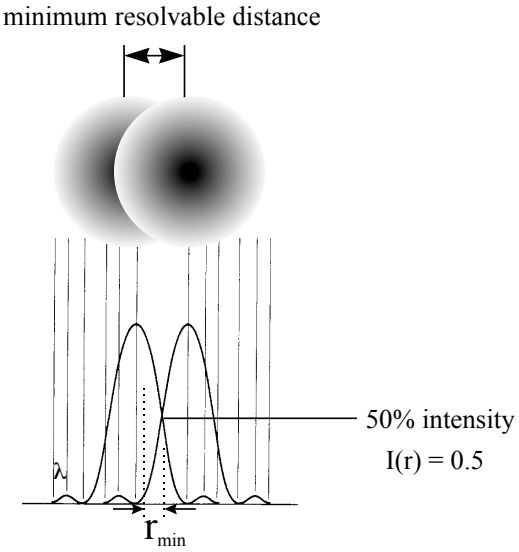

Figure 1.23: Just resolvable points defined by the diffraction efficiency curve. Here are two overlapping blurred images. As in Figure 1.18, the lines merely ascribe areas of the blurred image to points on corresponding intensity curves.

First, the bandwidth of the hologram may be defined using Equation (**1.4**) (Syms1990, 7)[14]:

[14] Leith (1992) uses a completely different method for deriving the bandwidth, and defines the bandwidth to equal the illumination wavelength divided by the number of fringes, N:
$\Delta\lambda \approx \frac{\lambda}{N}$, Ths is equivalent to Sym's $\frac{\Lambda \cdot \lambda}{t_2}$ for the conformal (untilted) fringe case with θill = 45 degrees.

$\Delta\lambda = \frac{\Lambda \cdot \lambda}{t_2}\cot(\theta ill)$, where Λ is the fringe spacing, λ is the illumination wavelength, t_2 is the thickness of the grating, and θill is the illumination angle.

For most of the thesis, we will use a geometry with θill = 45°, and λ = 514.5 nm. For t2 = 10μm:

From Benton (1994, 1996), we have Equation (**1.5**): $\Lambda = \frac{\lambda}{2 \cdot \sin\left(\frac{\theta out - \theta ill}{2}\right)}$

Therefore, Δλ = 34.59 nm.

The extreme wavelengths of this bandwidth may then be used in the calculations of Chapter 2 as the extreme raytracing wavelengths. For consistency, however, we will assume from this point forward a bandwidth of 20 nm for the different recording mediums we will be using.

Now we will calculate a "resolution factor," *R,* to determine the minimum resolvable distance between two points from the absolute blurred image height, h_{blur} (Chapter 2):

Mimimum resolvable distance = absolute image size × resolution factor (*R*),

Equation (**1.6**): $R = \frac{r_{50\%}}{r_{\Delta\lambda}}$

From Equation (1.2): $r_{50\%} = \sqrt{\frac{-w^2 \ln(0.5)}{2}} = 0.5887w$,

and beam width $w = \sqrt{\frac{-2r_{\Delta\lambda}^2}{\ln\left(\frac{1}{e^3}\right)}} = 0.8165r_{\Delta\lambda}$

Therefore, *R* = 0.4807

An ideal quantity to which resulting minimum resolvable distance calculations may be compared may be obtained from Equation (1.2), Rayleigh's criterion: $\omega = \frac{1.22\lambda}{d}$. With a pupil diameter *d*=2.5mm and wavelength λ=514.5 nm, the ideal theoretical resolution is then 2.51×10^{-4} radians, about 5.2 arc seconds.

With a mimimum resolvable angle of $2.51 \times 10^{-4} = \frac{h_{blurmin} \times 0.4807}{D_{eye}}$, the minimum absolute blur height, $h_{blurmin}$, is equal to 0.261 mm at a viewing distance of 500 mm, or about 1.8 arc minutes.

For the rest of the thesis, we will be concerned primarily with determining the extent of the blur in holographic images, not with their resolution. Therefore, we need to perform a similar calculation as Equation (1.6) to find the perceived blur size.

1.12 Factor for perceived blur size

The perceived size of a blurred image is the absolute blurred image size, h_{blur} (Chapter 2), multiplied by some perceived blur size factor, B. We will estimate this perceived blur size factor to be the ratio of the perceived height, $h_{perceivedblur}$ to the total height, h_{blur}. Just as the total width of the gaussian distribution was marked by a cutoff intensity $\left(\frac{1}{e^3}\right)$ that also determined the boundary of the blurred image point, the distance from the center to the *perceived* boundary of a blurred image is the radial distance from the center to a perceived cutoff intensity. As the beam width, defined above in section 1.9, contains 86.5 percent of the beam power, we will define our perceived bandwidth as the wavelengths playing out within the beam width. Now we are prepared to define a the perceived blur factor, B:

Perceived image size = absolute image size × perceived blur factor (B),

Equation (**1.7**): $R = \frac{w}{r_{\Delta\lambda}}$

From Equation (1.2), beam width $w = \sqrt{\frac{-2r_{\Delta\lambda}^2}{\ln\left(\frac{1}{e^3}\right)}} = 0.8165 r_{\Delta\lambda}$

Therefore, $B = 0.8165$

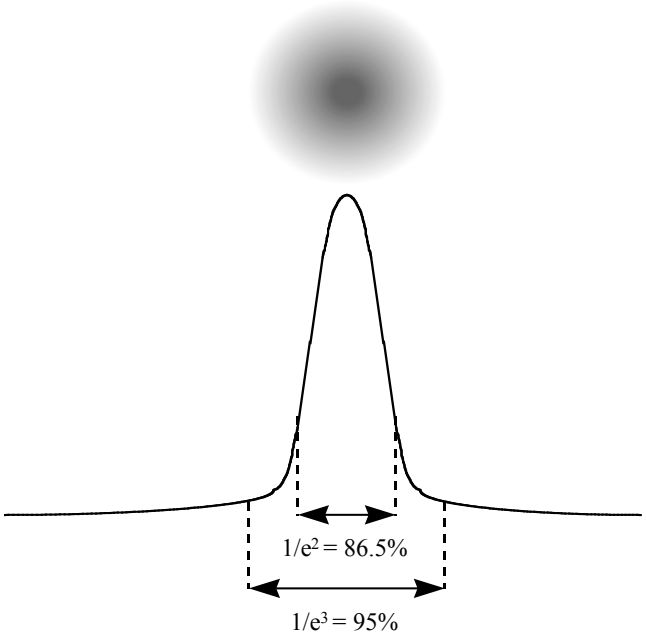

Figure 1.24: Perceived blur factor, *B*=0.8165

This perceived blur factor should be a reasonable approximation, considering the multiple sources of contrast degradation and noise mentioned above in section 1.7. In the next chapter, we will derive the absolute blur extent in terms of height, as well as angle subtended from the eye. The perceived blur factor may be applied to this absolute blur extent as an estimate of the perceived extent of a blurred image.

Chapter 2
Trigonometric derivation of a single-plane blur equation

In the previous chapter, we first looked at color blur from a qualitative standpoint, and applied successive intensity filters to determine the apparent size of a blurred image point as perceived by an observer. We found that we could define the extent of the perceived blur as well as resolution of blurred image points by simply approximating the diffraction efficiency of the recording material as a normal distribution about a mean wavelength, and defining the wavelengths at two standard deviations as the cutoff perceived wavelengths. In this chapter, we will take a more mathematical approach to define the absolute extent of this blur. We will then experimentally test the results with spectrophotometer measurements. Finally, we will apply last chapter's perceived blur factor to the forthcoming derived blur equation.

The trigonometric derivation below gives us a formula for determining hologram color and source-size blur. We will compare the resulting formula with Benton's blur equations. A vector blur equation is derived in Appendix 2, and reduces to the trigonometric form developed here.

2.1 Derivation of a color blur equation

Figure 2.1 will provide us with the physical model we will be using in the derivation and future discussions. Spectral components of the illuminant reconstructing displaced images produce the blur. These components diffract at the hologram and create a "dispersed focus" at the pupil of the eye:

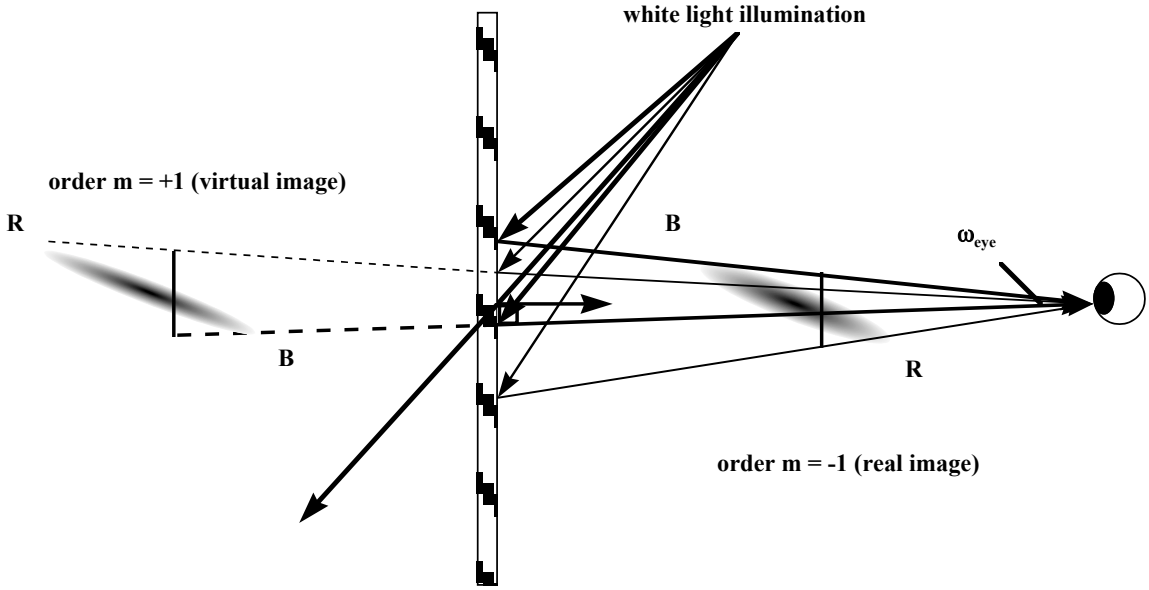

Figure 2.1: Spectral components from different points on the hologram contributing to blur

We will start our derivation with the "X-equation" of Appendix 1. The X-equation is a raytracing equation that describes the relationship between the exposure and reconstruction geometries at some position (1) on the hologram.

The method we will use for the derivation of a blur equation is to substitute unknown angles at some position (2) with known position (1) angles. Position (1) is the point on the hologram in direct line of sight of the viewer and reconstructs at the central ("green") wavelength. Position (2) is another point on the hologram that will reconstruct at another wavelength. In the following figures, this is a longer ("red") wavelength. The key to this technique is that position (1) variables are in terms of the central wavelength, denoted by "λ_2," whereas position (2) variables are in terms of an extreme wavelength for a given spectral bandwidth illuminating the hologram. Although these extreme wavelengths will be denoted by "λ_{2red}" and "λ_{2blue}," the color names merely describe their wavelengths relative to the central wavelength. For reflection holograms with very narrow spectral bandwidths, these wavelengths may all appear, for example, to be red or blue.

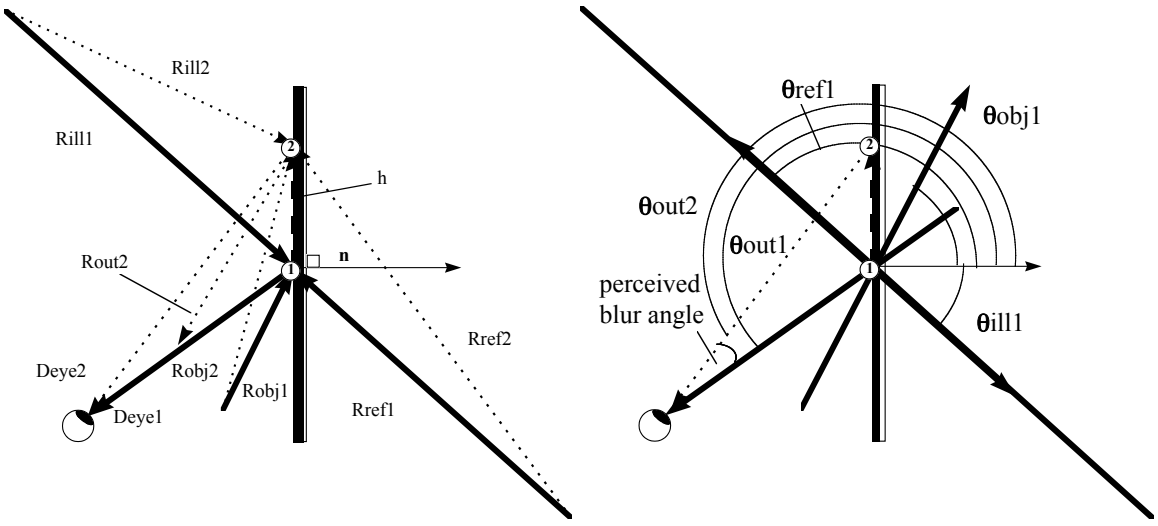

Figure 2.2: Dispersed focus at the pupil, perceived as color blur, from Appendix 2
The angles in the text are denoted with the same subscripts as the vector magnitudes. For example, Robj2 corresponds to an object distance of Robj2 exposing the holographic recording material at the angle θobj2. For clarity, only θout 2 of the longer playout wavelength is included in the right diagram.

Equation **(2.1)**: $\sin\{\theta out_2\} := m \cdot \frac{\lambda_2}{\lambda_1} \cdot \{\sin\{\theta obj_2\} - \sin\{\theta ref_2\}\} + \sin\{\theta ill_2\}$

For small h, R_1 is approximately R_2: Equation **(2.2)**: $\sin\{\theta_2\} := \frac{R_1 \cdot \sin\{\theta_1\} + h}{R_1}$

For a proof of the validity of the above approximations, please refer to Appendix 2. The resulting sine values to be substituted into the above equation follow.

Equation **(2.3)**: $$\sin\left\{\theta obj_2\right\} := \frac{Robj_1 \cdot \sin\left\{\theta obj_1\right\} + h}{Robj_1}$$

Equation **(2.4):** $$\sin\left\{\theta ref_2\right\} := \frac{Rref_1 \cdot \sin\left\{\theta ref_1\right\} + h}{Rref_1}$$

Equation **(2.5):** $$\sin\left\{\theta ill_2\right\} := \frac{Rill_1 \cdot \sin\left\{\theta ill_1\right\} + h}{Rill_1}$$

Regardless of the reconstruction geometry (reflection or transmission, order m = ± 1), the difference between the sines of the output angles from the viewer's eye to positions (1) and (2) on the hologram ($\sin(\theta out_1)$-$\sin(\theta out_2)$) is opposite that of the difference between the sines of the other angles from their respective source positions to the same two positions on the hologram. In other words, notice that h is not added with the other term in the numerator, as is the case in the other sine variables listed above.

Equation **(2.6)**: $$\sin\left\{\theta out_2\right\} := \frac{D_{eye1} \cdot \sin\left\{\theta out_1\right\} - h}{D_{eye1}}$$

When we substitute the four sine equations into the modified X-equation, we obtain a value for h, the length of the hologram contributing to color blur for a particular eye position and spectral bandwidth:

Equation **(2.7):** $$h = \left| \left\{\frac{\Delta\lambda_2}{\lambda_1}\right\} \cdot \frac{\sin\left\{\theta obj_1\right\} - \sin\left\{\theta ref_1\right\}}{\left\{\frac{\lambda_2}{\lambda 1} \cdot m\right\} \cdot \left\{\frac{1}{Robj_1} - \frac{1}{Rref_1}\right\} + \frac{1}{Rill_1} + \frac{1}{D_{eye1}}} \right|$$

This may be simplified to the following expression, with either a long (red) or short (blue) peripheral λ_2 resulting in either a red or blue horizontal focus (denoted by the subscript "HORIZ") and associated height h_{red} or h_{blue} along the hologram in question:

Equation **(2.8)**: $$h_{red} := \left\{\frac{\lambda_{2red} - \lambda_{2green}}{\lambda_1}\right\} \cdot \frac{\sin\left\{\theta obj_1\right\} - \sin\left\{\theta ref_1\right\}}{\frac{1}{Rout_{1redHORIZ}} + \frac{1}{D_{eye1}}}$$

The final color blur height, as seen by a viewer at a given distance D_{eye} along the θ_{out} angle, is then scaled by the distance of the blurred point from the hologram (D_{eye}+$Rout_{greenVERT}$, where D_{eye} is taken to be positive and the latter term is the vertical focus at the central wavelength) and by the output angle from position (1):

Equation **(2.9)**: $$h_{colorblur} := \frac{D_{eye1} + Rout_{1greenVERT}}{D_{eye1}} \cdot \cos\left\{\theta out_1\right\} \cdot \left(h_{red} + h_{blue}\right)$$

When expanded, the final expression for color blur is the sum of the following with its blue counterpart (or simply twice the following as an approximation):
Equation (**2.10**):

$$\left\{\frac{D_{eye1} + Rout_{1greenVERT}}{D_{eye1} + Rout_{1redHORZ}}\right\} \cdot Rout_{1redHORZ} \cdot \cos\left\{\theta out_1\right\} \cdot \left[\left\{\frac{\lambda_{2red} - \lambda_{2green}}{\lambda_1}\right\} \cdot \left\{\sin\left\{\theta obj_1\right\} - \sin\left\{\theta ref_1\right\}\right\}\right]$$

From this form, it is more apparent that for this perceived blur function there is a nonlinear effect for small viewer distances. There is also a discontinuity when the chromatically dispersed focus D_{eye} coincides with either $Rout_{redHORIZ}$ or $Rout_{blueHORIZ}$, that is, when the pupil is situated at one of the horizontal foci. This discontinuity makes physical sense, as a pupil situated at these foci will have light filling the retina; the image should appear to be very large.

2.2 Inclusion of source-size blur into a final blur equation

To include the effect of source size on the vertical blur of an image point, a new h_{red} and h_{blue} are found from the effective translation of the illumination source by half of the height of the source, Φ_{ill}, in opposite directions for the two extreme wavelengths. The longer, "red" wavelength determines the maximum h_{red}, and the shorter, "blue" wavelength determines the maximum h_{blue}. The final blur equation follows the inclusion of the change in illumination angle from the extreme ends of the source into the original equation. The central illumination angle, θill_1, is that from the center of the source to position (1) on the hologram.

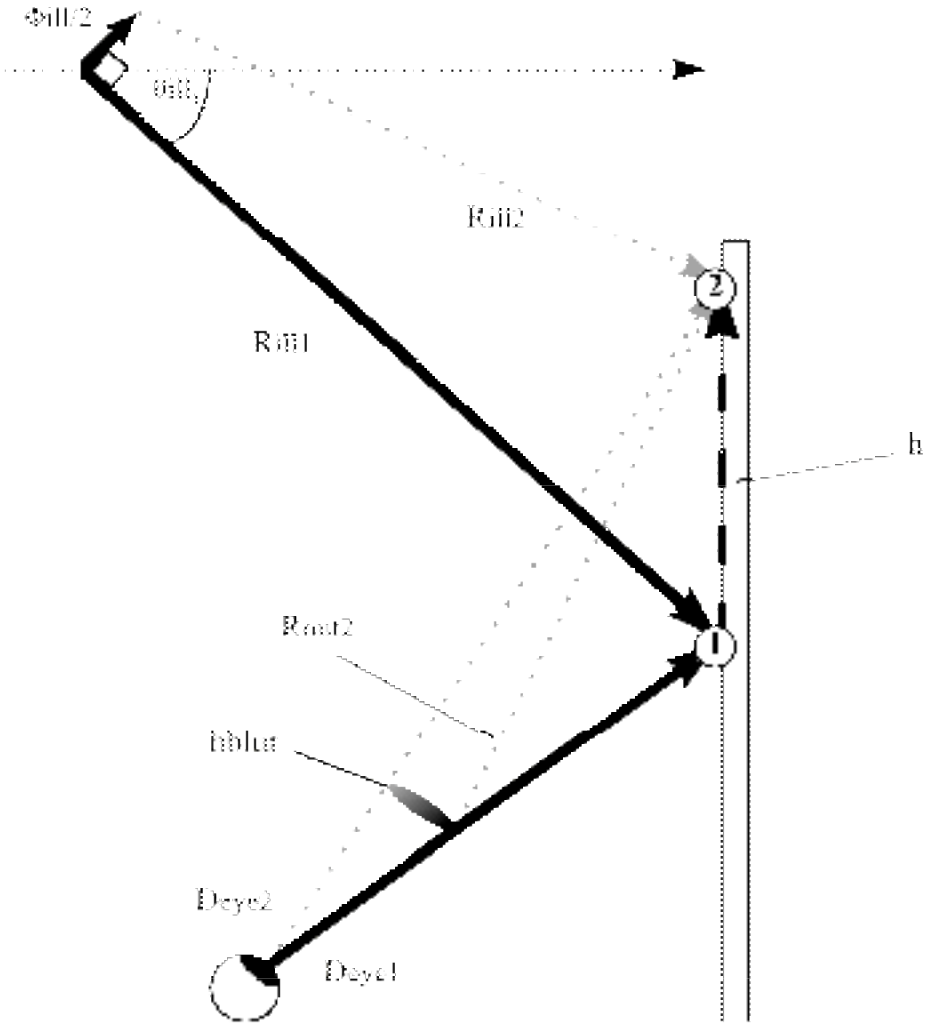

Figure 2.3: Perceived color blur and source-size blur height

Equation (**2.11**):

$$\sin\left\{\theta ill_2\right\} := \frac{Rill_1 \cdot \sin\left\{\theta ill_1\right\} + h + \frac{\Phi_{ill}}{2} \cdot \cos\left\{\theta ill_1\right\}}{\sqrt{\left\{Rill_1 \cdot \cos\left\{\theta ill_1\right\} + \frac{\Phi_{ill}}{2} \cdot \sin\left\{\theta ill_1\right\}\right\}^2 + \left\{Rill_1 \cdot \sin\left\{\theta ill_1\right\} + h - \frac{\Phi_{ill}}{2} \cdot \cos\left\{\theta ill_1\right\}\right\}^2}}$$

$$= \frac{Rill_1 \cdot \sin\left\{\theta ill_1\right\} + h + \frac{\Phi_{ill}}{2} \cdot \cos\left\{\theta ill_1\right\}}{\sqrt{\left(Rill_1 + h\right)^2 + \frac{\Phi_{ill}^2}{4} - h \cdot \Phi_{ill} \cdot \cos\left\{\theta ill_1\right\}}}$$

For illumination angles that are not too obtuse, the new $Rill_1$ (the denominator in the above expression) is assumed to remain unchanged (Again, please refer to the proof of the validity of this assumption in A2.2).

Equation **(2.12)**:

$$\sin\left\{\theta ill_2\right\} := \frac{Rill_1 \cdot \sin\left\{\theta ill_1\right\} + h + \frac{\Phi_{ill}}{2} \cdot \cos\left\{\theta ill_1\right\}}{Rill_1}$$

The final blur equation is composed of two components: the color blur term and the source-size term. Here we have the height of the hologram contributing to blur with the portion of the spectrum from the central wavelength to the longest wavelength ("red"): Equation (**2.13**):

$$h_{red} := \left| Rout_{redHORIZ} \cdot D_{eye1} \cdot \frac{\left\{\frac{\lambda_{2red} - \lambda_{2green}}{\lambda_1}\right\} \cdot \left\{\sin\left\{\theta obj_1\right\} - \sin\left\{\theta ref_1\right\}\right\} + \frac{\Phi_{ill} \cdot \cos\left\{\theta ill_1\right\}}{2 \cdot Rill_1}}{Rout_{redHORIZ} + D_{eye1}} \right|$$

$$h_{blur} := \frac{D_{eye1} + Rout_{1greenVERT}}{D_{eye1}} \cdot \cos\left\{\theta out_1\right\} \cdot \left(h_{red} + h_{blue}\right)$$

The perceived blur angle, ω_{eye}, is simply the angle subtended by the blur height from the pupil:

Equation **(2.14)**:

$$\omega_{eye} = \frac{h_{blur}}{D_{eye1} + Rout_{1greenVERT}} = \frac{\cos\left\{\theta out_1\right\} \cdot \left(h_{red} + h_{blue}\right)}{D_{eye1}}$$

2.3 Approximation to the final blur equation

Assuming a uniform spectral bandwidth about central wavelength λ_{2green}, and that this central wavelength's playout distance is the average playout distance, a reasonable approximation of the above equations follows, with $R_{red} = Rout1_{redHORIZ}$ and $R_{blue} = Rout1_{blueHORIZ}$: Equation (**2.15**):

$$h_{red} + h_{blue} =$$

$$2 \cdot \left| \left[\frac{\Delta\lambda}{2 \cdot \lambda 1} \cdot (\sin(\theta obj) - \sin(\theta ref)) + \frac{\Phi_{ill} \cdot \cos\left(\theta ill_1\right)}{2 \cdot Rill_1} \right] \cdot \frac{D_{eye1}^{2} \cdot \left(R_{blue} + R_{red}\right) + 2 \cdot R_{red} \cdot R_{blue} \cdot D_{eye1}}{R_{red} \cdot R_{blue} + D_{eye1} \cdot \left(R_{red} + R_{blue} + D_{eye1}\right)} \right|$$

$$= \left| \left[\frac{\Delta\lambda}{\lambda 1} \cdot (\sin(\theta obj) - \sin(\theta ref)) + \frac{\Phi_{ill} \cdot \cos\left(\theta ill_1\right)}{Rill_1} \right] \cdot \frac{D_{eye1}^{2} \cdot 2 \cdot R_{green} + 2 \cdot R_{green}^{2} \cdot D_{eye1}}{R_{green}^{2} + D_{eye1} \cdot \left(2 \cdot R_{green} + D_{eye1}\right)} \right|$$

$$= \left| \left[\frac{\Delta\lambda}{\lambda 1} \cdot (\sin(\theta obj) - \sin(\theta ref)) + \frac{\Phi_{ill} \cdot \cos\left(\theta ill_1\right)}{Rill_1} \right] \cdot \frac{R_{green} \cdot D_{eye1}}{R_{green} + D_{eye1}} \right|$$

Resuming our extended subscripts, we have the blur length, Equation (**2.16**):

$$h_{blur} = \left\{ \frac{D_{eye1} + Rout_{1greenVERT}}{D_{eye1} + Rout_{1greenHORIZ}} \right\} \cdot \left| Rout_{1greenHORIZ} \cdot \cos\left(\theta out_1\right) \cdot \left[\frac{\Delta\lambda}{\lambda 1} \cdot \left\{ \sin\left(\theta obj_1\right) - \sin\left(\theta ref_1\right) \right\} + \frac{\Phi_{ill} \cdot \cos\left(\theta ill_1\right)}{Rill_1} \right] \right|$$

Above, it was mentioned that there is a nonlinear effect in perceived blur for small viewer distances. In this approximated form of the blur equation, it may now be seen that this nonlinearity is controlled by astigmatic aberration, reflected in the vertical and horizontal focus distances of the first factor.

2.4 Benton's color blur equation derivation

In order to compare these equations with Benton's, I will follow his derivations, without making on-axis object and image assumptions. The following derivations assume that, for a given spectral bandwidth, the cone of light dispersed from a single point on the hologam, position(1) (Figure 2.4 below), subtends the same solid angle as the cone of light composed of wavelengths dispersed from different points of the hologram and entering the pupil (Figure 2.1).

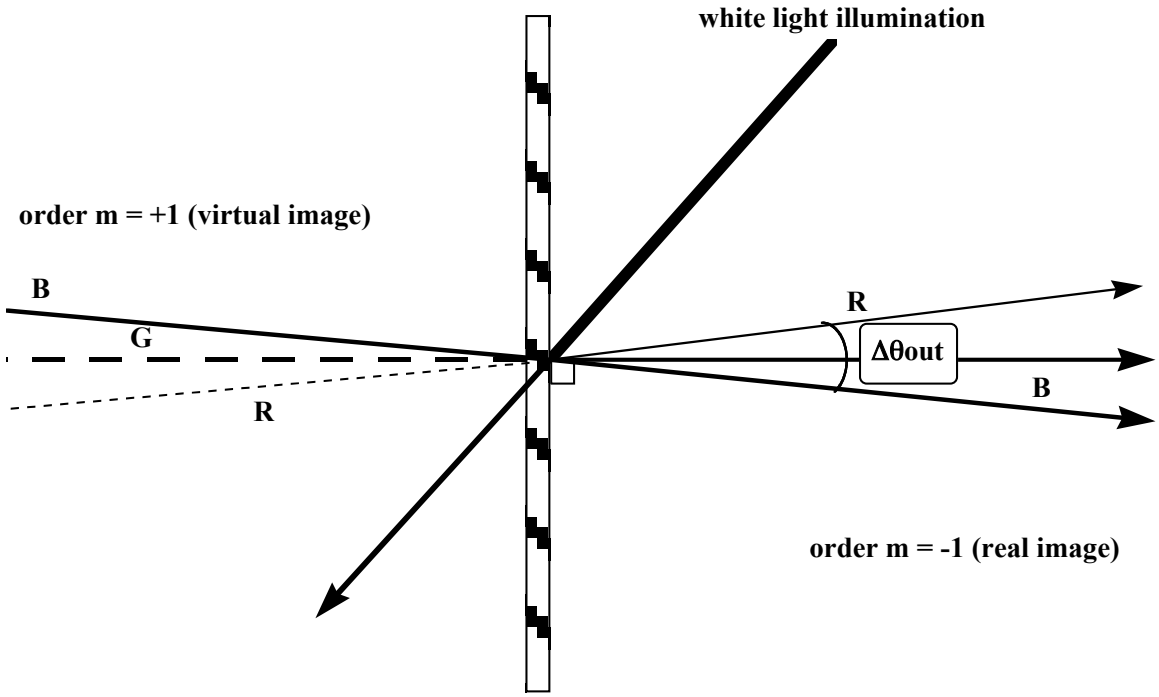

Figure 2.4: Dispersion for the cases of m = +1 or m = -1 order image points combined in one diagram. (The hologram would in reality have to be rotated 180° about the normal to the page to see the opposite order.)

Benton's color blur derivation:

Equation **(2.17)**:
$$\sin\left(\theta out\right) := m\cdot\frac{\lambda_2}{\lambda_1}\cdot(\sin(\theta obj) - \sin(\theta ref)) + \sin(\theta ill)$$

Equation **(2.18)**:
$$\frac{d}{d\lambda_2}\sin(\theta out) := \cos(\theta out)\cdot\left(\frac{d}{d\lambda_2}\theta out\right) = m\cdot\frac{\lambda_2}{\lambda_1}\cdot(\sin(\theta obj) - \sin(\theta ref))$$

Equation **(2.19)**:
$$\Delta\theta out_{color} := \frac{\Delta\lambda_2\cdot(\sin(\theta out) - \sin(\theta ill))}{\lambda_{2green}\cdot\cos(\theta out)}$$

Equation **(2.20)**:
$$h_{Bentoncolorblur} := Rout_{greenVERT}\cdot\Delta\theta out_{color}$$
$$= Rout_{greenVERT}\cdot\frac{\Delta\lambda_2\cdot(\sin(\theta out) - \sin(\theta ill))}{\lambda_{2green}\cdot\cos(\theta out)}$$

2.5 Benton's achromatic angle derivation

Before we follow with Benton's source-size blur derivation, and his resulting blur equation, we will include Benton's derivation of the "achromatic angle," as this will play an important role in our discussions of Chapter 6 ("Wave-front shapes and compact displays"). This angle is the space along which image points reconstructed in different wavelengths will focus.

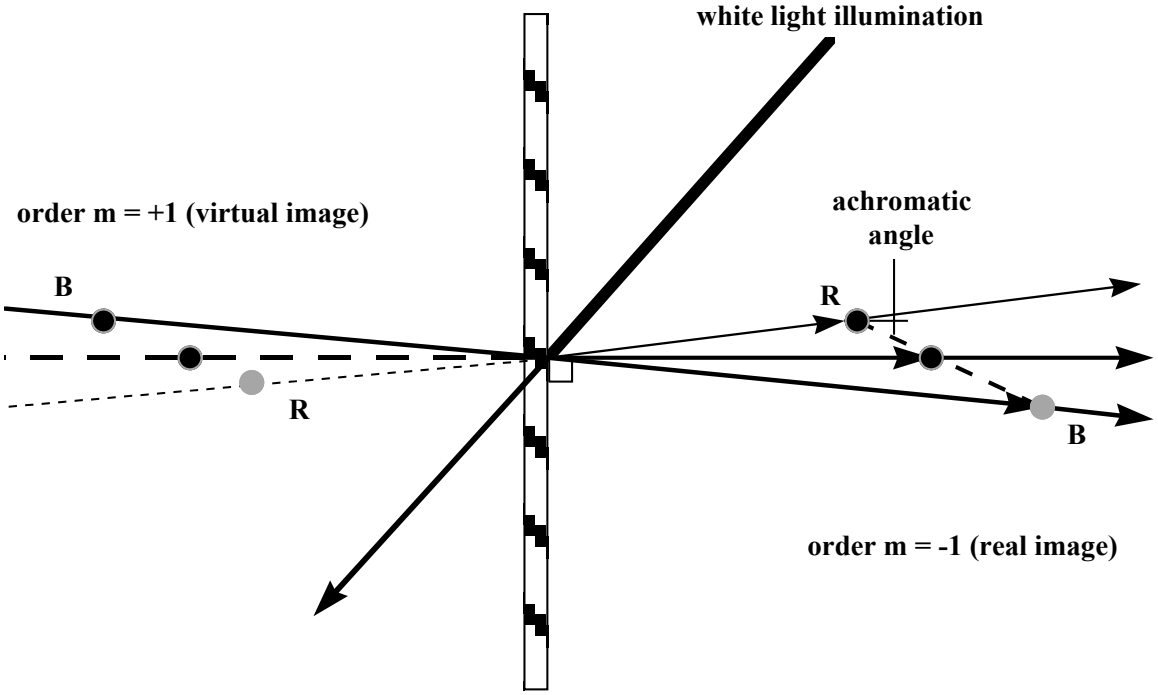

Figure 2.5: The achromatic angle for the cases of m = +1 or m = -1 order image points combined in one diagram. (The hologram would in reality have to be rotated 180° about the normal to the page to see the opposite order.)

The angle, α, is given by Equation (**2.21**):

$$\tan\alpha = \frac{\text{Rout}\cdot\Delta\theta\text{out}}{\Delta\text{Rout}}$$

Rout is the vertical focus of the central wavelength, $\Delta\theta$out is the angular spread of the output wavelengths from above, and ΔRout is the difference in focus lengths for the two extreme wavelengths.

ΔRout may be found by taking the derivative of the vertical focus equation:

Equation **(2.22)**:

$$\frac{d}{d\lambda_2}\left\{\frac{1}{Rout}\right\} := \frac{1}{Rout^2}\cdot\left[\frac{d}{d\lambda_2}(Rout)\right] = m\cdot\frac{1}{\lambda_1\cdot(\cos(\theta out))^2}\cdot\left[\frac{\left\{\cos\left\{\theta obj\right\}\right\}^2}{Robj} - \frac{\left\{\cos\left\{\theta ref\right\}\right\}^2}{Rref}\right]$$

$$\frac{d}{d\lambda_2}(Rout) = -m\cdot\frac{Rout^2}{\lambda_2\cdot(\cos(\theta out))^2}\cdot\left[\frac{\left\{\cos\left\{\theta out\right\}\right\}^2}{Rout} - \frac{\left\{\cos\left\{\theta ill\right\}\right\}^2}{Rill}\right]$$

Equation **(2.23)**:
$$\Delta Rout = -m\cdot\frac{\Delta\lambda_2\cdot Rout^2}{\lambda_2\cdot(\cos(\theta out))^2}\cdot\left[\frac{\left\{\cos\left\{\theta out\right\}\right\}^2}{Rout} - \frac{(\cos(\theta ill))^2}{Rill}\right]$$

Equation **(2.24)**:
$$\tan\alpha = \frac{Rout\cdot\left[\frac{\Delta\lambda_2\cdot m\cdot\left\{\sin\left\{\theta out\right\} - \sin\left\{\theta ill\right\}\right\}}{\lambda_2\cdot\cos(\theta out)}\right]}{-m\cdot\frac{\Delta\lambda_2\cdot Rout^2}{\lambda_2\cdot(\cos(\theta out))^2}\cdot\left[\frac{\left\{\cos\left\{\theta out\right\}\right\}^2}{Rout} - \frac{(\cos(\theta ill))^2}{Rill}\right]}$$

The final form of Benton's achromatic angle can be expressed as

Equation **(2.25)**:
$$\tan\alpha = \frac{\sin(\theta out) - \sin(\theta ill)}{\cos(\theta out) - \frac{Rout}{\cos\left\{\theta out\right\}}\cdot\frac{(\cos(\theta ill))^2}{Rill}}$$

Or, for paraxial object and output angles,

Equation **(2.26)**: $\tan\alpha = \sin(\theta ill)$

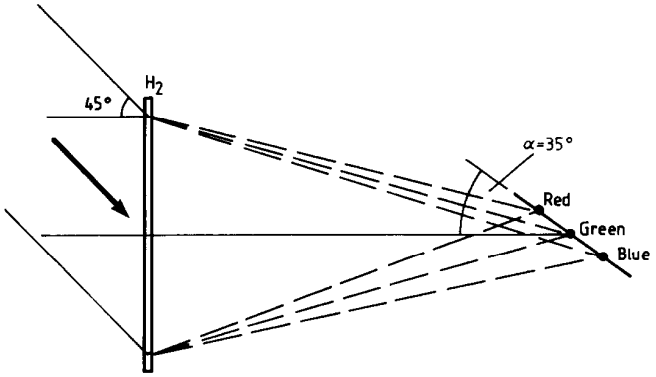

Figure 2.6: Wavelength-dependent focusing power of a hologram, and the achromatic angle (Saxby 1992)

2.6 Benton's source-size blur equation derivation

Benton's derivation of source-size blur:

$$\frac{d}{d\theta ill}\left\{\frac{1}{Rout_{greenVERT}}\right\} := -\frac{1}{Rout_{greenVERT}^{2}}\cdot\left\{\frac{d}{d\theta ill}Rout_{greenVERT}\right\}$$

$$= \frac{1}{Rill\cdot(\cos(\theta out))^{2}}\cdot\left[\frac{d}{d\theta ill}(\cos(\theta ill))^{2}\right]$$

Equation **(2.27)**: $$\Delta Rout_{greenVERT} := \frac{Rout_{greenVERT}^{2}}{Rill\cdot(\cos(\theta out))^{2}}\cdot\sin(2\cdot\theta ill)\cdot\Delta\theta ill$$

Benton also considers this change in the vertical focus to be negligible. (Please refer to the proof in A2.2). Therefore:

$$\frac{d}{d\theta ill}\sin(\theta out) := \cos(\theta out)\cdot\frac{d}{d\theta ill}\theta out = \frac{d}{d\theta ill}\sin(\theta ill) = \cos(\theta ill)$$

Equation **(2.28)**: $$\Delta\theta out_{source} = \frac{\cos(\theta ill)}{\cos(\theta out)}\cdot\Delta\theta ill$$

$$h_{Bentonsourcesizeblur} := Rout_{greenVERT}\cdot\Delta\theta out_{source}$$

Equation **(2.29)**: $$= Rout_{greenVERT}\cdot\frac{\cos(\theta ill)}{\cos(\theta out)}\cdot\frac{\Phi_{ill}}{Rill}$$

As the primary assumption made in these trigonometric derivations is that all of the angles comprising the exposure and reconstruction geometry are all coplanar, there was no horizontal component to the color blur. There is a non-negligible source width effect, however, that is simply the same as the effect of the height without the vertical slant angle factor:

Equation **(2.30)**: $$w_{Bentonsourcesizeblur} := Rout_{greenVERT}\cdot\frac{\Phi_{ill}}{Rill}$$

2.7 Benton's final blur equation

In the author's derivations, the source size was explicitly incorporated in the reformulation of color blur, as it determined the two new distances from position (1), h_{red} and h_{blue}, that would contribute the extreme wavelengths of a given spectral band to the perceived blur angle. From the Chapter 1's final discussion, there is a perceived blur factor (= 0.8165) that would be applied to the final blur equation to give a perceived blur size of an image.

In Benton's final equation, on the other hand, the color blur and source-size components are considered independent, and are therefore treated as two different distributions. Assuming that these distributions do not deviate significantly from Gaussian distributions, the convolution of one by the other results in a Gaussian distribution as well. The sum of the two distributions' variances therefore equals the variance of the convolved distribution, and likewise, the sum of the square of the two blur terms closely approximates the square of the final blur term:

Equation **(2.31)**: $\theta^2_{Bentonblur} = \theta^2_{Bentoncolorblur} + \theta^2_{Bentonsourcesizeblur}$

Equation **(2.32)**: $$\theta^2_{Bentonblur} = \frac{1}{\cos(\theta out)} \cdot \left[\left[\frac{\Delta\lambda_2 \cdot (\sin(\theta out) - \sin(\theta ill))}{\lambda_{2green}} \right]^2 + \left\{ \cos(\theta ill) \cdot \frac{\Phi ill}{Rill} \right\}^2 \right]$$

The perceived blur angle is therefore:

Equation **(2.33)**: $\omega_{eye,\ Bentonblur} =$

$$\frac{Rout_{greenVERT}}{D_{eye} + Rout_{greenVERT}} \cdot \frac{1}{\cos(\theta out)} \cdot \sqrt{\left[\frac{\Delta\lambda_2 \cdot (\sin(\theta out) - \sin(\theta ill))}{\lambda_{2green}} \right]^2 + \left\{ \cos(\theta ill) \cdot \frac{\Phi ill}{Rill} \right\}^2}$$

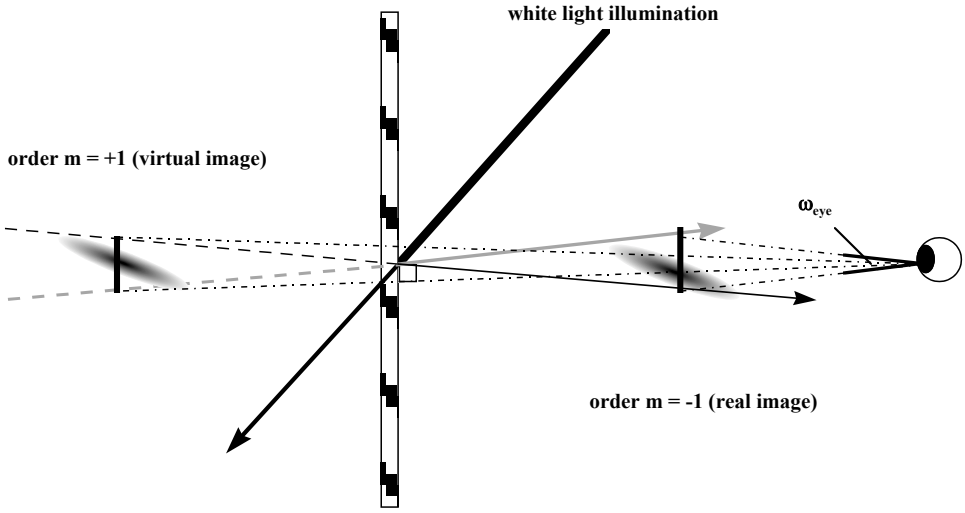

Figure 2.7: The perceived blur angle according to Benton (1994)

2.8 Summary and comparison of the blur equations

To summarize, the final angular blur equations are as follows (angles are in radians). To obtain the height of the blurred image point, simply multiply the angle by the output distance (RoutGvert).

The unapproximated form of the author's equation, from Equations (2.13) and (2.14):

$$\omega_{eye} = \frac{h_{blur}}{D_{eye} + Rout_{greenVERT}} = \frac{\cos(\theta out)\cdot\left(h_{red} + h_{blue}\right)}{D_{eye}}, \quad \text{where } h_{red} + h_{blue} =$$

$$\left| Rout_{redHORIZ}\cdot D_{eye}\cdot\frac{\left\{\frac{\lambda_{2red} - \lambda_{2green}}{\lambda_1}\right\}\cdot(\sin(\theta obj) - \sin(\theta ref)) + \frac{\Phi_{ill}\cdot\cos\left\{\theta ill_1\right\}}{2\cdot Rill_1}}{Rout_{redHORIZ} + D_{eye}}\right|$$

$$+ \left| Rout_{blueHORIZ}\cdot D_{eye}\cdot\frac{\left\{\frac{\lambda_{2blue} - \lambda_{2green}}{\lambda_1}\right\}\cdot(\sin(\theta obj) - \sin(\theta ref)) + \frac{\Phi_{ill}\cdot\cos\left\{\theta ill_1\right\}}{2\cdot Rill_1}}{Rout_{blueHORIZ} + D_{eye}}\right|$$

An approximation of the author's equation, after some cosmetic steps to better compare it with Benton's equation, takes the following form (Equation (2.16)). For perceived, as opposed to absolute blur extent, the author's equations would be multiplied by Chapter 1's blur factor of 0.8165:

$$\omega_{eye} = \frac{Rout_{greenHORIZ}}{D_{eye} + Rout_{greenHORIZ}}\cdot\cos(\theta out)\cdot.8165\cdot\left[\frac{\Delta\lambda_2\cdot(\sin(\theta out) - \sin(\theta ill))}{\lambda 2green} + \cos(\theta ill)\cdot\frac{\Phi ill}{Rill}\right]$$

Benton's equation differs slightly, Equation (2.33):

$$\omega_{Bentoneye} = \frac{Rout_{greenVERT}}{D_{eye} + Rout_{greenVERT}}\cdot\frac{1}{\cos(\theta out)}\cdot\sqrt{\left[\frac{\Delta\lambda_2\cdot(\sin(\theta out) - \sin(\theta ill))}{\lambda_{2green}}\right]^2 + \left\{\cos(\theta ill)\cdot\frac{\Phi ill}{Rill}\right\}^2}$$

If we discount the different methods that Benton and the author choose to combine the effects of color blur and source-size blur (convolution versus filtering), there is still one subtle difference between the two, dependent on astigmatism.

2.9 Blur measurements using a spectrophotometer

To experimentally compare the blur height with calculations using the author's and Benton's equations, a grating was exposed to an on-axis object source (Robj = 125 mm) and a reference source at 225° (Rref = 1200 mm) with a Krypton-ion laser (647 nm). It was then illuminated with an imperfect phase-conjugate white-light source at 45° at a distance of 600 mm. The author then took three types of blur measurements:

- **Measurement 1:** A measurement of the distance along the achromatic angle between the vertical focus points at two spectral lines, that of a Helium-Neon laser (632.8 nm) and a Gre-Ne laser (543.1 nm);
- **Measurement 2:** An interpolated distance along the achromatic angle corresponding to the above bandwidth from the broadband data of Appendix 1 (Figure 2.8), and
- **Measurement 3:** A similar setup as that of Appendix 1, with the spectrophotometer rotating 300 mm in front of the 591.1 nm focus[15], and the exposed fiber tip on the axis of rotation (Figure 2.9). This final setup was an attempt to mimic the field of view through the pupil.

Measurement 1

For all of the measurements, an opaque mask with a vertical aperture was affixed to the grating so that astigmatism would not confound the data. A diffuser was placed at the illumination distance of 600 mm. The resulting distance was measured to be **32 mm**.

Measurement 2

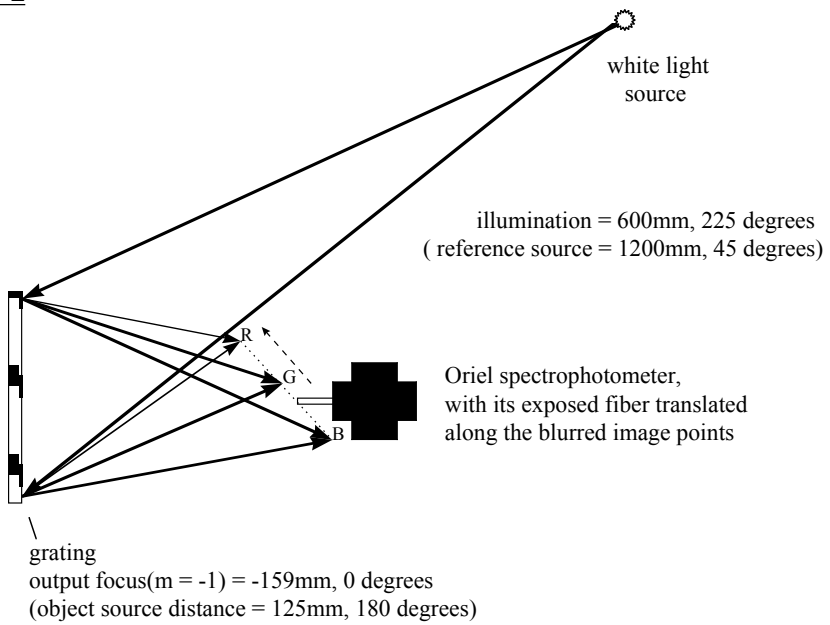

[15] The grating played out at 591.1 nm, 159mm along the normal to the hologram.

Figure 2.8 (from Appendix 1)

When illuminated with a white-light source (with and without a diffuser at the focused source distance), the resulting spectrally dispersed image points were indeed found to lie on the calculated achromatic angle, 31°. An Oriel spectrophotometer was mounted on a translator such that its exposed fiber end would ride along this angle of vertically focused spectral points, oriented orthogonal to the hologram surface. Interpolated from Table A1.1 of Appendix 1, the 543.1 to 632.8 distance was found to be **30.5 mm**.

Measurement 3

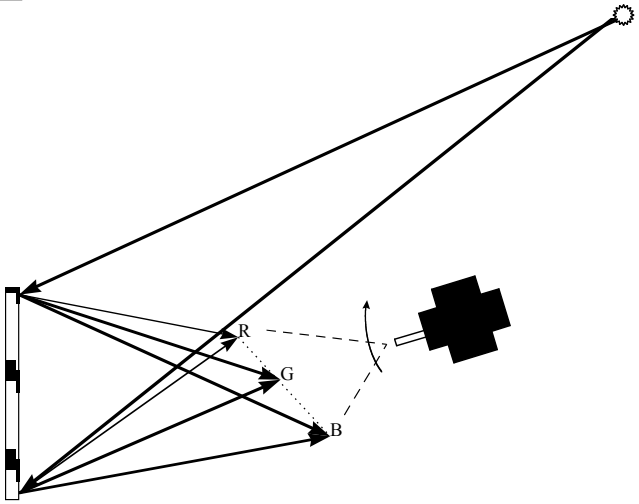

Figure 2.9: Measurement 3 setup

As the spectrophotometer fiber tip was rotated to couple light of different wavelengths, protractor readings were taken at the wavelength intervals of Table A1.1. These readings could not be made with the same degree of precision as were those taken with the translating stage of the previous run. The interpolated distance was found to be **27.4 mm**[16]. The corresponding calculations are included in Table 2.1:

Measurement 1	32 mm
Measurement 2	30.5 mm
Measurement 3	27.4 mm (Oriel = 300 mm; See footnote)
The author's equation	27.2 mm (Deye = 300 mm)
Benton's blur equation	17.5 mm

Table 2.1: Blur length data for the vertical focus of 543.1 and 632.8 nm wavelengths in the geometry described in the text

[16] In a private communication with Professor Fantone, the author was informed that the intensity profile of an optical fiber is angle- and wavelength-dependent. For the limited range of acceptance angles here, this should not pose a significant problem.

Although the author's equation gives a blur length very close to the measured quantities, we must realize that this value is a function of the distance of the pupil to the hologram, unlike in Benton's equation. If the pupil is situated at one of the dispersed foci, the blur height is infinitely large. For all practical distances greater than the nearpoint of the human eye, 250 mm[17], however, this value levels off.

The results of the author's derivations have been used in Matlab[18] programs to compare their output with that of the corresponding equations derived by Benton, given input data representing different exposure and reconstruction scenarios. A list of the equations used for these calculations have been converted from Matlab to the TK Solver+ program[19] of Appendix 3. For ordinary scenarios close to perfect reconstruction (where the illumination geometry equals exposure geometry) or perfect phase-conjugation and no shrinkage, the author's blur equation outputs data almost identical to Benton's blur equation. However, as the geometry/illumination source changes significantly, the two equations give different answers. Although the above grating shrank and was illuminated with different wavelengths, it was exposed and illuminated with the most common geometry (on-axis image and 45° illumination). Still, the results are different in the different blur calculations. It is hoped that further measurements may be taken with different gratings and geometries to probe the degree of deviation between the two formulas.

The author's blur equation matched spectrophotometer measurements taken in the above experiments closely enough that it seems to characterize the physical nature of blur rather well. The perceived blur factor of Chapter 1 would then be included to estimate the perceived extent of the blur.

Now that we have characterized and quantified the extent of perceived blur, it is time for us to review the different techniques that have been implemented to compensate for this blur. The subject of the next chapter is to introduce the concept of dispersion compensation and to recount a brief history of the application of dispersion compensation to display holograms.

---

[17] The nearpoint is the closest an object can approach one's pupil and still be in focus. This distance increases with age, and is about 250 mm for normal individuals in their early 20's.
[18] Matlab®, The Math Works, Inc., Natick, MA
[19] Universal Technical Systems, Inc., Rockford, IL;
Universal Technical Software (UK) Ltd., Witham, Essex

Chapter 3
Introduction to dispersion compensation and a brief review of its application to holographic displays

3.1 The first dispersion-compensation displays: single view angle transmission hologram / grating

The theoretical notion of applying dispersion-compensation methods in holography is almost as old as holography itself[20] (Leith 1956). In 1966, however, three researchers, Paques, Burckhardt (Burckhardt 1966), and DeBitetto (DeBitetto 1966) independently published papers outlining an approach in which a post-compensating grating is placed after a transmission hologram to minimize color blur of the holographic image.

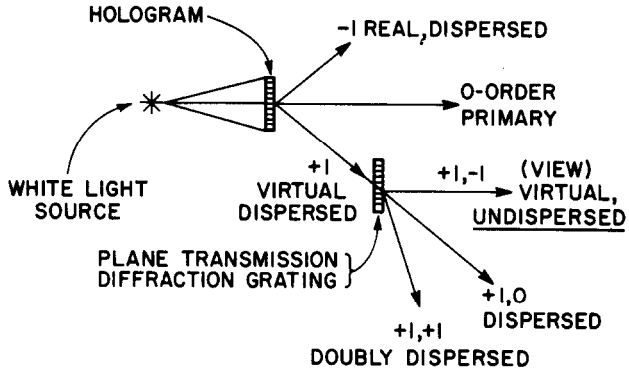

Figure 3.1: DeBitetto's original diagram discriminating the effects of diffraction orders on relative dispersion

Although all three of these displays feature a broadband transmission hologram illuminating a plane-wave grating, the following discussion applies to the case of reflection holograms as well. In fact, DeBitetto also used a blazed reflective grating in essentially the same setup. The angles for an "equivalent"[21] reflection hologram are also the same (Appendix 1).

In the above diagrams, the hologram illuminating the grating disperses the light from an illumination source, producing a color-blurred image off axis. Longer ("red") component wavelengths are diffracted at more oblique angles than the shorter ("blue") wavelengths, so for a hologram with a wide spectral band, blurred virtual image points appear behind the hologram (order m = +1), with a red edge lying toward the illumination source and a blue edge lying at the farther periphery (See Figure 2.5). For the case when the hologram is illuminated from the opposite side as the reference source (order m = -1),

[20] In a memorandum written by Leith in 1956 while at Willow Run Laboratories, he describes a theoretical basis for dispersion compensation of a point imaged through a lens on and off axis.
[21] An equivalent reflection hologram is exposed with its reference source on the opposite side of, and symmetric about, the recording material.

real image points are focused in front of the hologram, so the colors are reversed with respect to the viewer.

If we reverse raytrace the red and blue light from the dispersed image to the hologram, these rays impinge on a point of the hologram and leave the grating superimposed, as undispersed light.

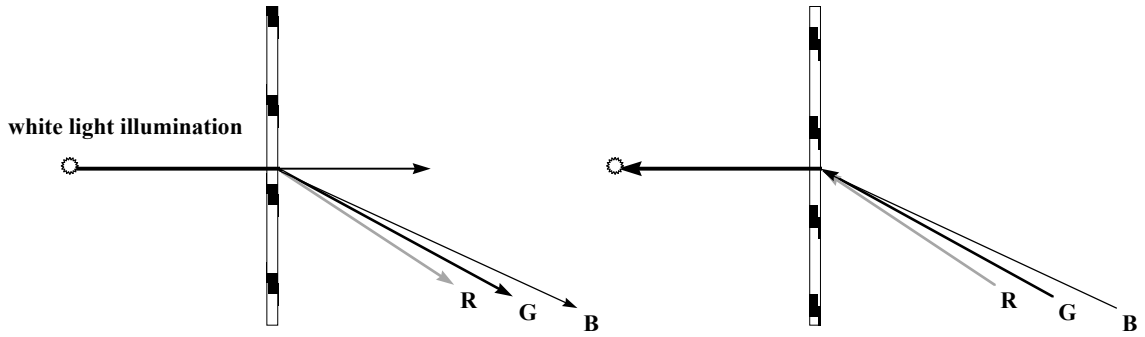

Figure 3.2: Forward and reverse raytracing the spectral components through a transmission hologram

The grating of the above scenario post-compensates for dispersion by performing effectively this reverse raytrace. If we forward raytrace the dispersed light from the hologram through the grating, the grating deflects light in the opposite direction as the hologram. That is, red light diffracted from the normal to the hologram at an oblique angle is taken in by the grating at an oblique angle. The grating structure then diffracts the red toward its normal. Blue is diffracted less by both diffractive structures, so the spectral components all play out superimposed, in a single direction.

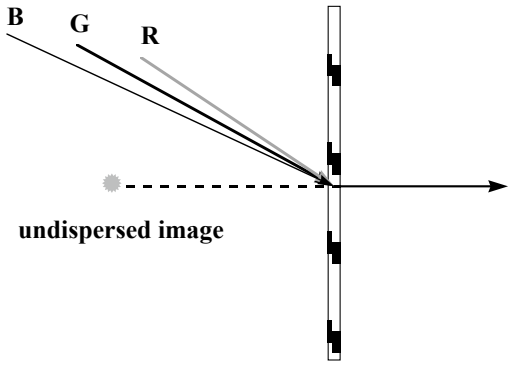

Figure 3.3: Raytracing the dispersed rays from the hologram through a transmission grating

At least this is superposition is the ideal case where the image wave front from the hologram corresponds to the reference wave front that exposed the grating. In reality, each object point during exposure of the hologram subtends a different angle as any other (noncollinear) object point to every point on the hologram. Therefore, a representative object point must be chosen to design the grating so that its compensating power matches the average dispersing power of the hologram. As focusing or dispersing power in a diffractive medium is directly proportional to the spatial frequency of its constituent

diffracting elements (Chapter 1), researchers have universally chosen to match the average spatial frequencies of the hologram and grating, and usually to simply orient one parallel to the other. For matched spatial frequencies, the dispersed angles illuminating the grating are considered the primary concern, not the distances between the focused image points and the grating. The grating illumination distance is therefore taken to be infinity, that is, the reference and illumination beams are collimated.[22] This universally accepted approach is suitable for ideal reconstruction[23] of both the hologram and grating, but is inadequate for some compact display geometries to be discussed in Chapter 6.

The grating is made by exposing the recording material to two sources (from the same laser): the reference and object sources. The reference beam is collimated, and is set at the angle the grating will be illuminated from, that is, the average playout angle of the hologram. If the hologram and grating exposure setups are identical for average source point positions, then both the grating and the hologram have equal average spatial frequencies. This again means that they both are of equal power and disperse white light to an equal degree. However, the grating is flipped with respect to the hologram, as in Figure 3.3, so that it disperses light in the opposite direction as the hologram (so long as the exposure and reconstruction angles are coplanar). The dispersed beam from the white-light reconstructed hologram (order m = ±1) serves as the grating's illumination beam (m = 0 order). The grating then reconstructs the dispersion compensated image in front of the viewer (Figure 3.1).

[22] A collimated wave front is a planar wavefront, usually created by a collimating lens placed its focal distance from a beam expander in an optical setup.

[23] Perfect reconstruction is the case such that the fringe spacing is the same when illuminated as when recorded, and the central wavelength and position of the illumination source/focus is equal to that of the reference source when recorded.

Alternatively, the hologram and grating positions may be switched, and a predispersing grating may compensate for a hologram that receives its m = +1 order beam for a geometry analogous to the one above:

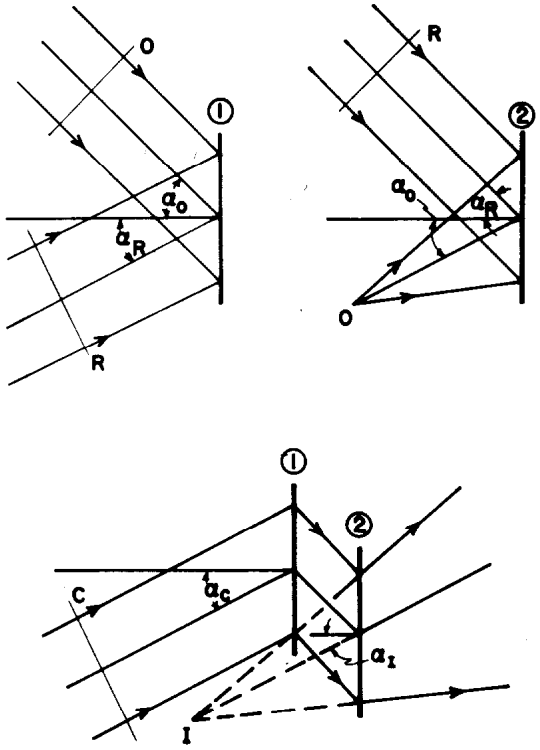

Figure 3.4: A schematic representing the original geometry of the three researchers in reverse (Latta 1972)
(1) is an off-axis plane-wave grating, and
(2) is a hologram to be illuminated at the output angle of (1).

For the present discussion, we will refer to the hologram and grating as "diffracting structures," and will be more specific when referring to a particular geometry. We will find below that all subsequent work has the grating as the first diffracting structure and the hologram as the second diffracting structure. Consequently, all further discussions will assume this arrangement, unless specific reference is made to the three researchers' work.

The diffracting structures are set at some distance from one another so that the illumination beam for the first does not also strike the second. As stated above, the second diffracting structure's reference source is at the same angle but not necessarily at the same distance it is to be illuminated from (the average focus of the first diffracting structure's image), so the resulting image is not dispersion-compensated for that particular point, but instead for a point at infinity, that is, for the viewing angle matching the average exposure angle (See Figures 3.5, 3.12, and 3.15 in particular).

For example, if a hologram's average object point lay on the normal, then the corresponding grating will match that exposure geometry so that it compensates for dispersion along the normal. A viewer looking along the normal to the hologram will see no color blur for all the image points exposed along that axis, but will see color blur exhibited to an increasing degree for image points farther off of the viewing axis and toward the periphery of the field of view. Image points on the axis will also appear blurred when the viewer moves off axis.

If the reference and illumination beams of the second diffractive structure are collimated, then this compensation holds for all local normals. We will refer to this technique as "**single view angle dispersion compensation**." As it is usually preferable to allow a reasonable field of view of sharp image points in depth as opposed to dispersion-compensating for one image points position, almost all of the literature cited and research work done use the single view angle dispersion-compensation method.

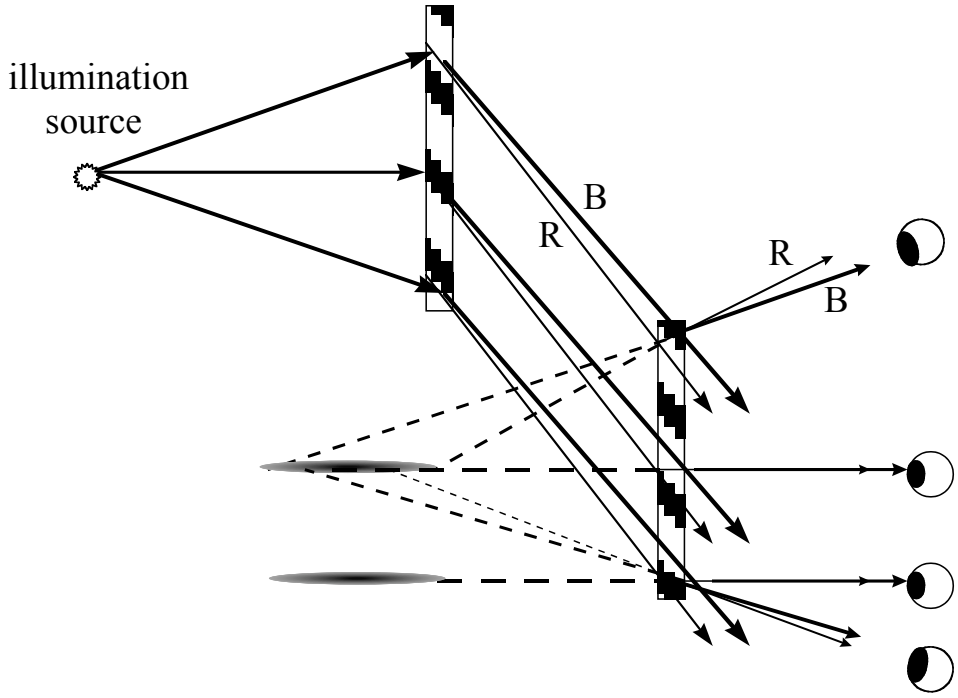

Figure 3.5: Single view angle dispersion compensation
This schematic represents the blurring of red (R) and blue (B) image points off of the local normal for a collimated reference /collimated illumination geometry.

Burckhardt also includes a diagram (Figure 3.6) picturing the grating and the transmission hologram sandwiched together, again with the transmission hologram illuminating the transmission grating. It is possible to make such a compact display and avoid having to look into the zero order illumination beam of the hologram if a venetian blind type structure (louver film)[24] is placed between the hologram and grating.

[24] "Light control film" is produced by 3M.

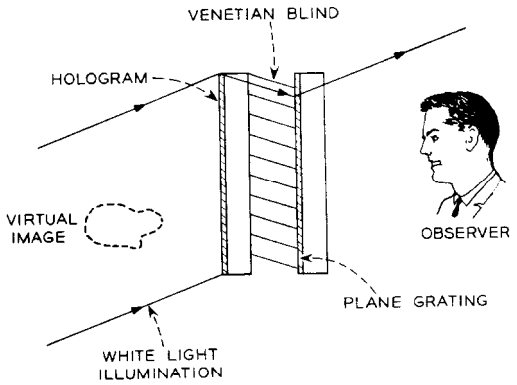

Figure 3.6: Burckhardt's (1966) use of a louver film to block the zero order of the hologram in a single view angle dispersion-compensation display

3.2 Single viewpoint dispersion compensation: Burckhardt

In one special variant of Burckhardt's approach, the hologram's illumination beam blocked by the louver film would otherwise converge behind the viewer's eye, to where the original reference source lay (Figure 3.7). Because the convergence of the illumination source corresponds to the divergence of the original reference source, the viewer near that focus is in effect looking through the centers of "in-line" zone plates toward the illumination source, thus eliminating color blur of all image points, as in the case of the Gabor in-line hologram (Chapter 1). Burckhardt refers to this point as the "quasi-achromatic" (QA) point. Assuming complete zero order absorption, and no diffraction by the louver film, all of the image points should appear perfectly sharp to the viewer near the QA point, and blur as the viewer deviates from this position. We will refer to this technique as "single viewpoint dispersion compensation".

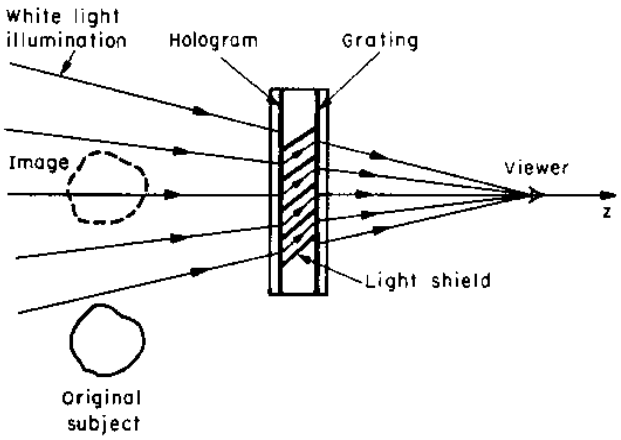

Figure 3.7: Burckhardt's **single viewpoint dispersion compensation** technique (Collier, Burckhardt, and Lin 1971)

3.3 Diffractive and refractive media

In his paper, DeBitetto also describes the use of prisms for dispersion compensation, opening up from the outset the possibility of combining diffractive and refractive media to produce the complementary effects. Three years later, Katyl (1972) outlined three dispersion-compensation geometries (two in-line, and one slightly off-axis) that involve multiple refractive and/or diffractive lenses, one of the components of which is placed at the QA point in Burckhardt's geometry. An appropriately dispersing element placed at the QA point can compensate for longitudinal dispersion and magnification variation. In the same year, the problem of longitudinal dispersion compensation for in-line geometries was also addressed by Latta (1972). In this paper, Latta simultaneously evaluates lateral and longitudinal dispersion in addition to aberrations for in-line and off-axis holograms, and is only able to compensate for longitudinal dispersion in off-axis holograms by placing them in in-line reconstruction geometries. The topic of achromatic imaging in broad band light is later addressed by Faklis and Morris (1988) and is the subject of many patents, particularly for head-up displays.

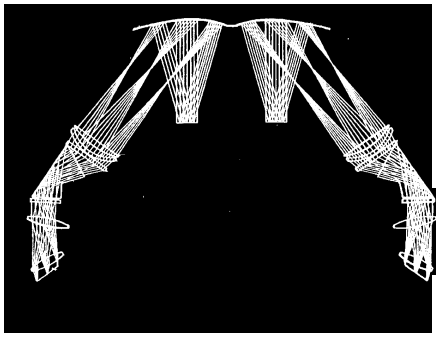

Figure 3.8: Example of the complexity of modern head-up displays incorporating dispersion compensation gratings (Roberts, et al. 1995)

3.4 Compact single view angle displays: Burckhardt

In 1985, Bazargan (1986) described how there is greater color smearing of a holographic image that is in turn imaged through a post-compensating grating than there would be if the hologram were illuminated by a predispersing, precompensating grating (See Figures 3.4 and 3.5 above). However, his analysis is based on the on-axis illumination of the grating by a dispersed holographic image, and he compares this with the off-axis illumination of a hologram. For thin diffractive elements, the difference between the two off-axis arrangements (grating, then a hologram, and vice versa) is simply the effect of Bragg selectivity on the achromaticity of the resulting image. For instance, in Burckhardt's geometry, the grating is illuminated by all of the image points from the hologram at many different angles, most of which are off of the Bragg angle. These off-Bragg angles are diffracted with less intensity. Bazargan's grating, on the other hand, introduces a single illumination angle to the hologram. Otherwise, the order of the two diffractive structures should not have a significant effect on image quality.

Bazargan chose in the early 1980's to switch the position of the two diffracting structures in Burckhardt's single viewpoint dispersion-compensation display, and to have the grating illuminate the hologram with a predispersed, collimated beam through louver film (See Figure 3.9). This approach suggested by Bazargan allows for an even more compact display than Burckhardt's single viewpoint dispersion compensation, as the illumination geometry of the grating is quite flexible compared with the strictly converging illumination of the Burckhardt hologram. However, Bazargan's single view angle dispersion-compensation display does not take advantage of Burckhardt's "in-line" viewing. Bazargan showed a prototype display at the SPIE Conference in Geneva in 1983, and the display has been manufactured by Icon Holographics, Ltd., England.

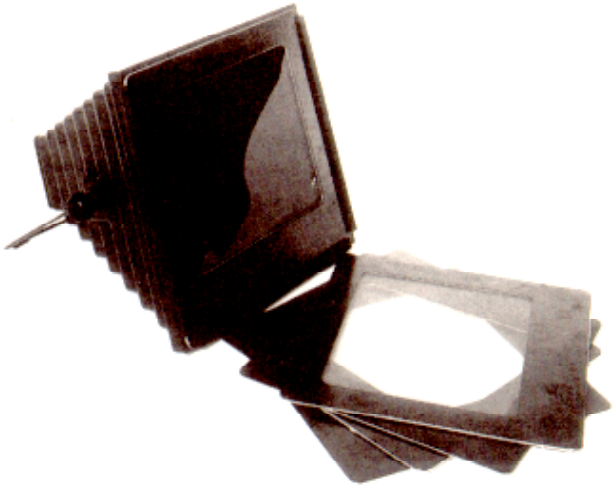

Figure 3.9: Bazargan's display (Syms 1990, fig. 10.5-2)

3.5 Other transmission displays: Boj, et al., and Benton

Boj, Pardo, and Quintana (1986) were able to achieve a 30 cm image depth for a dispersion compensated transmission hologram in 1986, limited primarily by the size of their illumination source. Their grating is a cylindrical holographic optical element (HOE) that disperses in only one direction. By changing the illumination distance to the grating, they show that it is possible to alter its precompensating ability to suit holograms of different average spatial frequencies and orientations.

Benton (1985) furthered attempts to produce an achromatic white-light transmission hologram not through dispersion compensation in its illumination, but by exposing the transfer hologram (Chapter 4) with a special grating exposed to multiple reference sources set along a calculated achromatic angle (Chapter 2). The resulting effect simulates the effect of illuminating the transfer hologram with a linear white light source oriented along the same angle: a superposition of the spectral components of the source in the center of the viewing zone.

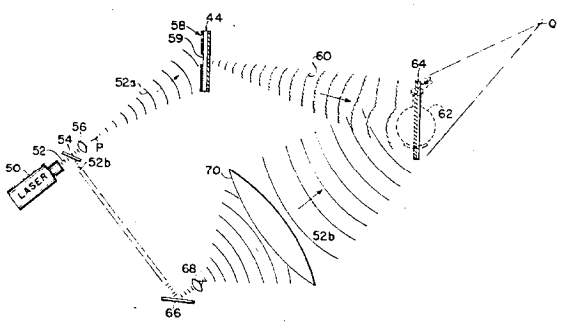

Figure 3.10: Benton's patent drawing of the white-light transmission hologram transfer step (1972)

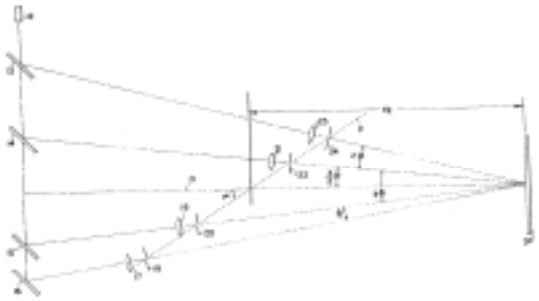

Figure 3.11: Benton's patent drawing of the special achromatizing grating used in an exposure step (1985)

3.6 Reflection displays: Bazargan, Kubota

For the remaining portion of our brief history, we will review work that has been done to dispersion compensate reflection holograms. Bazargan was the first person (as far as the author is aware) to publish anything regarding the theoretical use of a predispersing reflection grating for the dispersion compensation of a reflection hologram (Bazargan 1986). Bazargan used a vector approach with Ewald sphere diagrams[25] to ascertain the viability of generalized setup geometries, and suggested dispersion compensation as a means of reducing residual chromatic blurring in reflection holograms.

[25] For a clear introduction to Ewald sphere diagrams representing reflection hologram reconstruction, see Benton (1988)



Figure 3.12: (a) Distortions of a square image across the visible spectrum (400-700 nm)
(b) Single view angle dispersion compensation for reducing lateral chromatic aberration (Bazargan 1986, fig. 7.20)

Bazargan also suggested the use of dispersion compensation in multicolor reflection holograms by superimposing several monochromatic holograms (Figure 3.13).

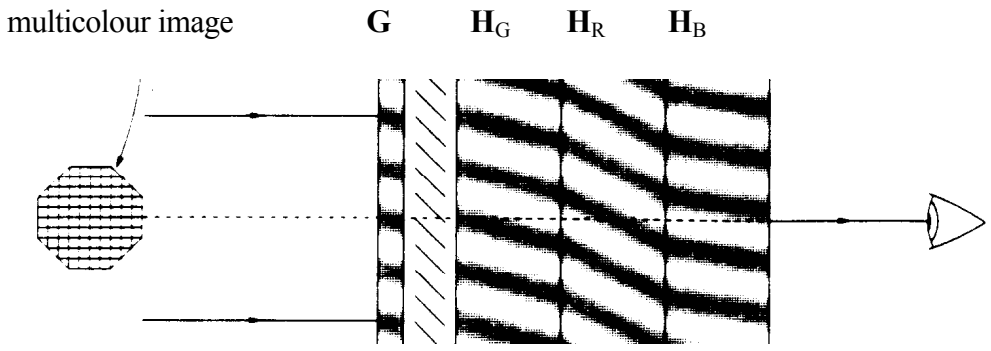

Figure 3.13: Bazargan's suggested approach for making a full-color, dispersion-compensated display

At this time, Ward, et al. (1985, 1986) published two rather comprehensive articles on the subject of image blurring in display holograms. It is Ward's diagram portraying the focus of multiple wavelengths from a small area of hologram to a viewer's eye that is the basis for the derivations in the previous chapter. However, his equations ignore the effect of astigmatism that plays a vital role in the author's blur equation derivations.

In 1989, Kubota published a paper on an experimental reflection grating/reflection hologram display, the first actual construction of such a display known to the author. In the tradition of the work of his predecessors, Kubota uses a plane-wave grating, and does not consider the effect of astigmatic aberration in his analysis. However, Kubota uses Ward's approach for portraying the manner in which we see color blur (Ward, Newell, and Solymar 1985). We will describe in detail the building of a similar reflection/reflection plane-wave grating display when we outline the design considerations of Chapter 5's viewstation.

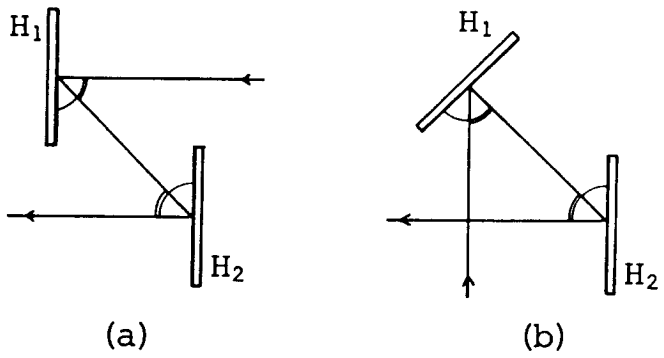

Figure 3.14: Kubota's reflection /reflection dispersion-compensated display

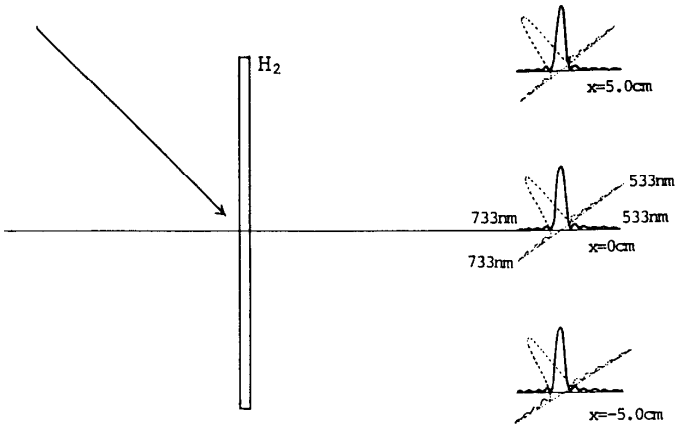

Figure 3.15: Intensity profile of the reconstructed image points in Kubota's single view angle dispersion-compensation display

Birner's (1989) dispersion-compensation steep angle display is effectively the equivalent of Kubota's, except that the reflection grating and hologram facing each other are sandwiched about an optical light guide for a much more compact display. Upatnieks uses basically the same approach, but also includes folding geometries with optics such as a reflective collimator. Upatnieks' and Birner's displays will be described in the final chapter: "Compact dispersion-compensation displays."

It is in this historical context that we are able to better understand where dispersion compensated displays are headed, and what improvements need to be made. Many of the references made in the latter half of this section include a mention of the prospect of having full-color, dispersion compensated displays. What seems to have been left unmentioned is the adverse effect of dispersion on vertical parallax, a potential barrier to using this technique for very deep, full-parallax displays. Also not dealt with explicitly is the effect of exposure and illumination wave-front curvatures on dispersion compensation. The viewstation of Chapter 5 addresses the former concern, and the compact displays described in Chapter 6 address the latter.

Chapter 4
Full-parallax
reflection holographic stereograms

So that we may appreciate the benefits of the application of dispersion compensation in displays such as the full-parallax viewstation of the next chapter, we will first describe the procedure for making a **horizontal-parallax-only holographic stereogram** (**HPO HS**). The case of the **full-parallax holographic stereogram** will arise naturally from our description. Then we will consider the particular merits of predispersed illumination for this type of stereogram.

4.1 Making horizontal-parallax-only holographic stereograms

An HPO HS is a hologram composed of multiple images of a scene taken from different angles. The images can be captured by a regular camera translated in front of the scene, or by the equivalent in computer graphics: a "synthetic camera." Each image represents a different perspective view of the same scene. There are various ways we can record multiple images in a hologram. We can record the images at different wavelengths, different angles, or in different positions on the recording material. Figure 4.1 has two of Redman's original drawings introducing an angular multiplexing technique:

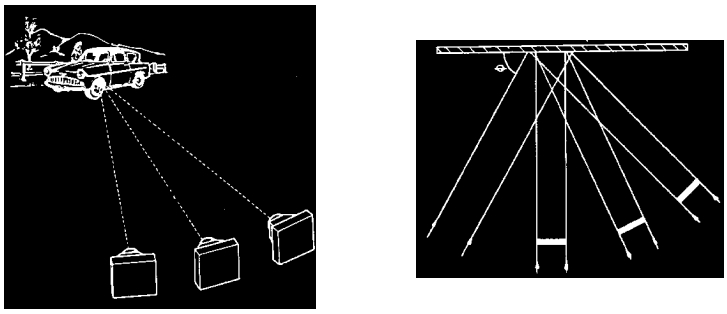

Figure 4.1: Sequential images are taken, and later projected to expose a hologram with an appropriately scaled geometry (Redman 1968).

The method for storing images of highest diffraction efficiency is to spatially multiplex them, that is, to record them in adjacent regions. Each region then acts as a window through which we can view one of the images. This method was introduced by McCrickerd and George in 1968 and took the form still commonly used today in DeBitetto's process (DeBitetto 1968).

In the actual recording setup of a DeBitetto HPO HS, a mask with a vertical slit the width of a pupil is translated across a master hologram (**H1**)(Figures 4.2, 4.4). Successive adjacent vertical strips of the H1 are exposed to different horizontal perspective views of the image projected in front of the hologram. As these are usually exposed with the holographic recording film held flat, a "toe-in" geometry like that pictured above in Figure 4.1 results in distortion of the image (Ferwerda 1982).

Therefore, the capture geometry must be one of strictly orthogonal orientation with respect to a straight translation of the camera.

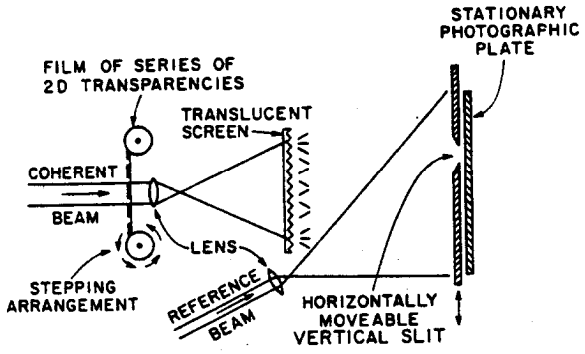

Figure 4.2: DeBitetto's original drawing of the spatial multiplexing technique most commonly used in display holographic stereograms today (DeBitetto 1968)

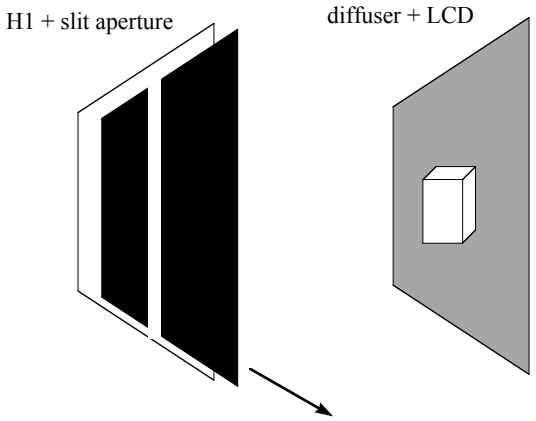

Figure 4.3: A horizontal-parallax-only holographic stereogram (HPO HS, or H1) is exposed to sequential perspective views taken from a translating camera and projected in front the H1. Here, the slit is translated in front of a stationary H1.

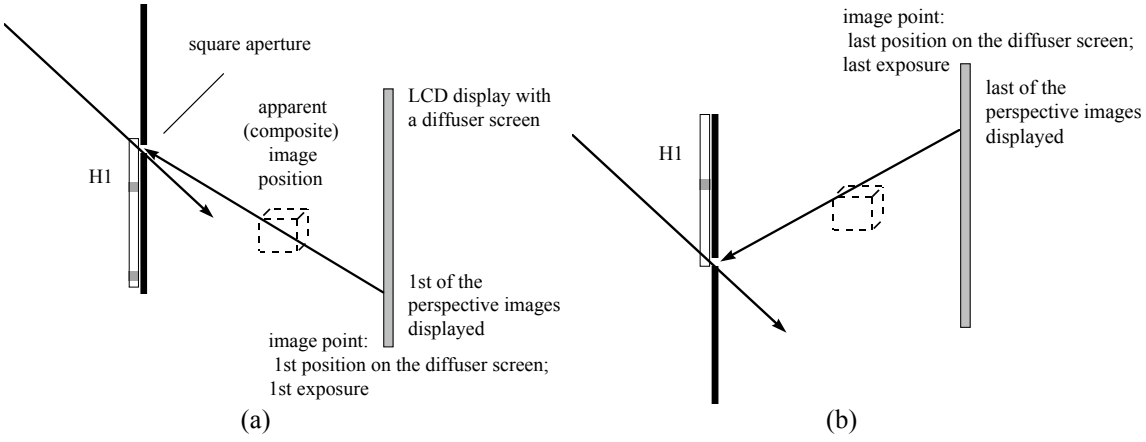

Figure 4.4: The first (a) and last (b) vertical strip exposures of a holographic stereogram (top view)

If we were to look through this illuminated H1, we would see an image of each of the projected views through different exposed strips. If the exposure geometry is scaled appropriately from the camera capture geometry, then with both of our eyes looking through the H1, each eye through a different strip, we should see a stereoscopic pair of images, giving us the illusion of perceiving the static scene in three dimensions. As we move in front of the H1, we should then see different stereoscopic pairs of images, as if we were moving in front of the original scene.

4.2 The transfer hologram

However, we do not want to have to place our face against the H1 in order to look through the vertical strips, so a second hologram, the transfer hologram (H2), is placed in the position where the original images were projected, and the H1 is illuminated in a phase-conjugate fashion (King, Noll, Berry 1970). As described in Chapter 1, phase-conjugate illumination is essentially a reversal of the directions of the rays that exposed the hologram. This "time-reversed" illumination results in a real image projected where the original object was. The H2, if placed in this position, is exposed to all of the H1's images simultaneously from their respective strip exposures. The images are therefore vertically focused on the H2 plane, as is the case with the white light transmission, or "rainbow" hologram.

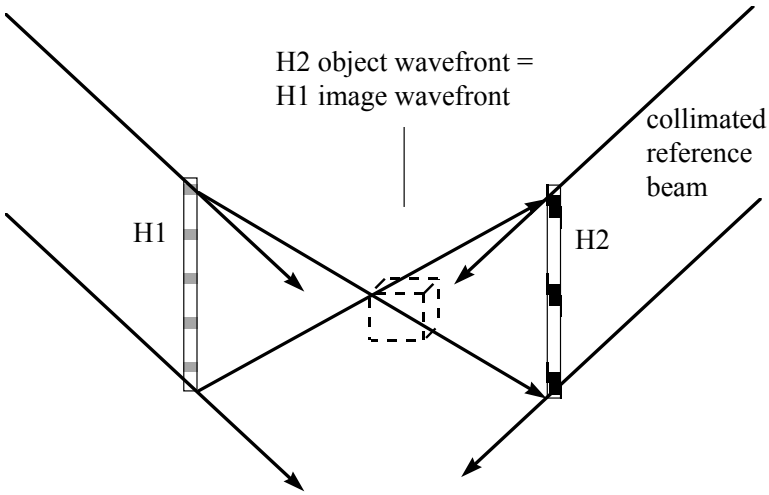

Figure 4.5: Transfer setup: The H1 is illuminated with a phase-conjugate beam, reconstructing a pseudoscopic image (inverted depth), whose wave front exposes the H2.

When the H2 is now illuminated in a phase-conjugate manner, the image of the H1 is projected to its original position with respect to the H2. When we approach the final H2 to view the image that usually straddles the plane, we are actually looking through the real images of the H1's vertical windows. The size of the projected H1 image is therefore the viewzone at the front of the viewing frustum.

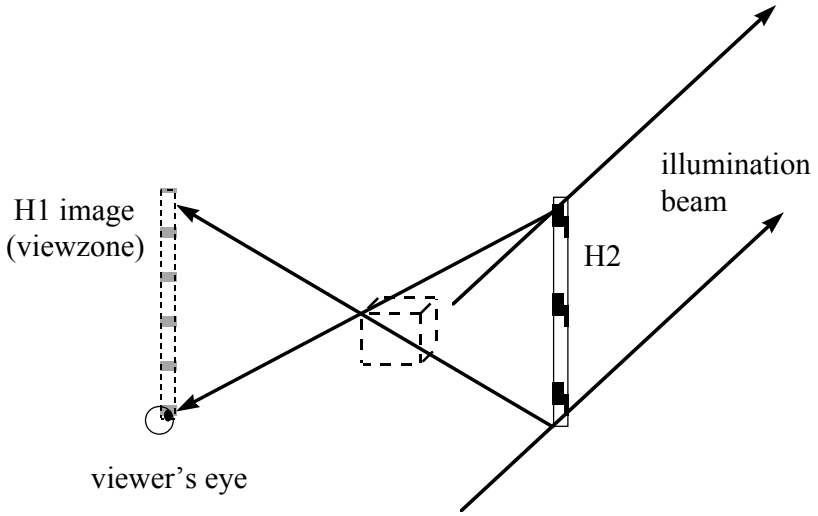

Figure 4.6: Phase-conjugate illumination of the HPO HS H2, and reconstruction of an orthoscopic, real image

As holograms are usually illuminated by a vertically displaced light source, dispersion will fan out red, green, and blue components vertically. The image of the H1 is then spectrally spread just as the image points are. Anticipating this dispersion, if we tip the H1 at the achromatic angle (Chapter 2) during exposure and transfer stages, then we may be able to reduce color blurring on playback. This technique can be used to produce less saturated, nearly achromatic images (Benton 1983, 1985, 1988). Or, if three strip holograms are made of three sets of perspective views, each set constituting one color separation, then a full-color image may be realized, in transmission or reflection format.

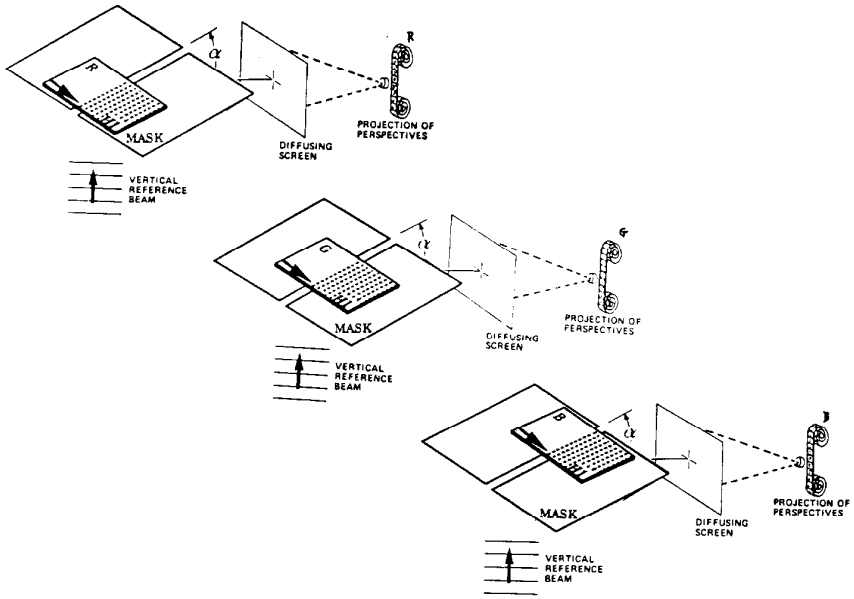

Figure 4.7: Benton's pseudocolor technique for producing achromatic or full-color images (1983, 1988) Three successive exposures are made at the same wavelength at different positions, so that they will all play out superimposed.

When we view the H2 from some distance not equal to the H1 image distance, however, the lines of sight from our eyes are no longer directed through the vertical view windows they were intended to look through. Instead, we see perspective views that are taken from lateral displacements that do not properly scale with the viewing geometry, so the image may have reduced depth (hypostereoscopic case) or exaggerated depth (hyperstereoscopic case). As there is perspective sampling information only in the horizontal direction (the original images were taken with a translating camera), the astigmatism we see manifests itself in an apparent vertical lengthening of images as we step backwards from the HPO HS, and a horizontal expansion of images as we step too close[26].

4.3 Full-parallax holographic stereograms

The full-parallax holographic stereogram (Nicholas George and J.T. McCrickerd 1969) is made in precisely the same way as the HPO HS except that, instead of a mask with a vertical slit translating in front of the H1, there is a small square aperture translating vertically as well as horizontally. The phase-conjugate illuminated transfer image projects a grid of real-image square windows, enabling us to see a parallax shift in the vertical as well as the horizontal direction. Unlike in the above HPO case, where the vertical focus is restricted to the image plane while the horizontal foci extend off the plane, in a full-parallax system, the vertical and horizontal foci may both lie off the plane. Therefore, the astigmatism inherent in the HPO case may be reduced or eliminated in the full-parallax case. What this means is that the hologram is viewer distance independent. The viewer's pupils do not have to be restricted to movement along the H1 image of pupil-width windows for undistorted views of the 2-D images, but instead can look through the square aperture windows from any distance.

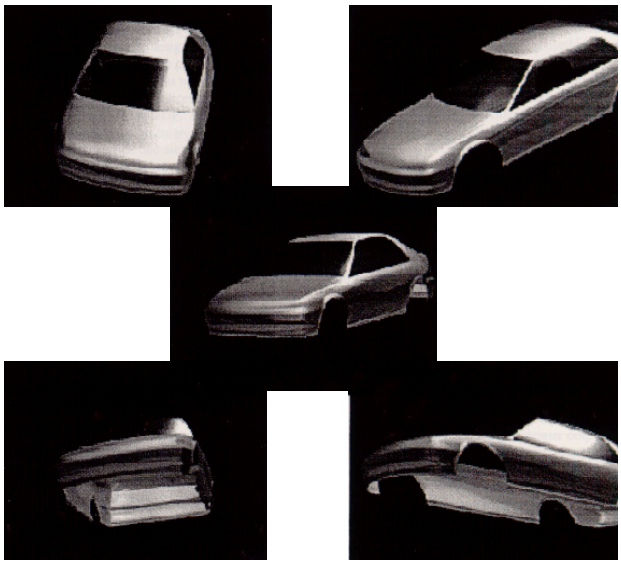

Figure 4.8: An example of different perspective views of a full-parallax hologram (image care of Michael Klug)

[26] For an excellent description of astigmatism in HPO HS's, please refer to Halle (1991).

The difficulty that then arises in the construction of such an HS is the number of exposures necessary to provide an acceptable level of resolution of image points at a range of distances about the H2 plane (Halle 1991). In addition, the number of perspective views increases to an almost unwieldy level as the H1 size (and the viewzone size) increases, although deviance from the phase-conjugate illumination geometry can magnify this viewzone and reduce the number of necessary exposures (Chapter 6).

A couple of examples[27] should help us better understand what kind of (non-resolution) sampling issues arise when making a full-parallax HS. One of the full-parallax H2's used in Chapter 5's viewstation projects an image of its H1 consisting of about 6,600 3 mm by 8 mm exposures arranged in 133 columns by 50 rows. Because the viewzone is discretized differently in the horizontal and vertical directions, and is more coarsely sampled in the latter, the resulting laser-illuminated image exhibits relatively smooth motion parallax for a viewer moving to the side, but less continuous motion parallax when the viewer's head bobs up and down, like looking at a jerky animation.

This H2 was soon replaced with one exposed to an H1 composed of 3 mm^2 apertures. The result is significantly improved over that of the previous rectangular aperture trial. As another experiment, the H1 was exposed through square apertures in its central region, and with vertical strip apertures in the regions above and below. The resulting H2 exhibits a full-parallax image in the central portion of the viewzone, and the same image with only horizontal parallax when the viewer looks through the upper or lower portions of the viewzone. When the viewer moves vertically across the viewzone, the transition from HPO to full-parallax is quite interesting: the image suddenly appears to move as one would expect, and it becomes noticeably brighter, as the light is focused through the pupil-sized apertures in the vertical as well as horizontal directions.

Although the first chapter was dedicated to issues of characterizing and measuring the extent of color blur in terms of resolution, our aim in using dispersion compensation is not merely to sharpen image points for increased resolution at greater depths. If this were the case, we might just as well have turned to the white light transmission format (Benton 1977) that sacrifices vertical parallax and consequently does not suffer significantly from color blur. The primary reason why we are applying dispersion compensation to holographic stereograms is to improve the quality of full-parallax images. The need for color correction for full-parallax images may be more easily understood if we contrast the effect of dispersion in a full-parallax HS with an HPO HS.

We noted earlier that for the HPO HS case, the vertical focus is in the plane of the H2. Therefore, any dispersion in the vertical direction will merely result in a color change of the focused images as the viewer height changes. Even in the case of a full-color HPO HS above, dispersion in the vertical direction merely displaces the images of the H1 color

[27] The full-parallax stereograms were all shot by Research Specialist Michael Klug.

separations. A full-color (or achromatic) image is still visible over some range of viewer heights.

With a full-parallax display, on the other hand, dispersion in the vertical direction will blur the vertically-sampled perspective views, just as it would for a full-aperture hologram of a real object. Each illuminating wavelength will reconstruct a different vertical perspective of the image, and together, the band of wavelengths will reconstruct many staggered images that we perceive as a blurry image. The author's work is aimed at reducing this blurring of vertical perspectives.

Another focus of this thesis is the application of dispersion compensation to reflection holograms. Although dispersion compensation has been successfully applied to transmission type holograms, little work has been done to improve the image quality and depth of reflection holograms with predispersing gratings. The primary reason why dispersion compensation has been relegated to one display format and not commonly extended to the other is one of relative necessity. Transmission holograms transmit effectively all the component wavelengths of the illumination source, each of which reconstructs an image displaced from the others along the achromatic angle. The holographer relies on reflection holograms to act like interference filters, on the other hand, taking in white light and returning to the viewer a very narrow band of the visible spectrum, essentially one color that produces a single, sharp image, seemingly obviating the need for color blur correction.

If reflection holograms were to truly reconstruct with a very narrow spectral band, the resulting images would be very dim indeed. The spectral band for most materials is actually rather wide -- about 20 nm for silver halide and photopolymer materials used for the work described in the following chapters. Such a spectral bandwidth is sufficient to produce a noticeable discrepancy between the points focused off of the hologram plane by the short and long wavelengths of that band. As the distance of the image point from the hologram plane increases, this discrepancy also increases. Therefore, the depth of a white light illuminated holographic image is severely restricted by a "spreading focus" of points distant from the hologram.

To demonstrate the distinct advantage of dispersion compensation to aid in the blur correction of full parallax, reflection holographic stereograms, comparisons will be made between the resolutions of points at different depths in uncompensated and compensated displays in the final chapter. In the next chapter, the plane-wave grating display will be detailed. The final chapter deals in part with different reference and illumination wave-front shapes and their effects on dispersion.

Chapter 5
Example design of a full-parallax holographic viewstation

In this chapter, we will take what we have learned from all of the preceding chapters to design a dispersion-compensated, full-parallax, reflection holographic viewstation of the single view angle (plane-wave grating) type. We will approach the design of the grating in this chapter from a practical, laboratory setup and display oriented perspective.

The chapters have been organized so that we may follow from general discussions about dispersion in a hologram to its specific exploitation in the displays of the present and succeeding chapter. In Chapter 4, we outlined how a full-parallax holographic stereogram is made, and discussed the desirability of dispersion compensation for the illumination of such a hologram. We contrasted different dispersion-compensation techniques, such as single view angle and single viewpoint dispersion compensation in Chapter 3. We derived a blur equation in Chapter 2 so that we can calculate the blur required of the predispersing grating to precompensate for the calculated blur of the uncompensated hologram. Finally, we defined resolvability for a blurred holographic image in Chapter 1, so that we may evaluate the effectiveness of the technique.

The purpose of the viewstation is to present a large (at least 210 mm by 300 mm), full-parallax reflection holographic stereogram with appreciable image depth and minimal color blur. The making of the hologram and grating involve a choice of exposure wavelength, holographic recording material, determination of a suitable exposure and reconstruction geometry, and appropriate selection of illumination source. We will address each of these points in the above order through the course of this chapter. One of our primary concerns is to deliver light of sufficient intensity to the display hologram, so all of our choices will reflect this concern.

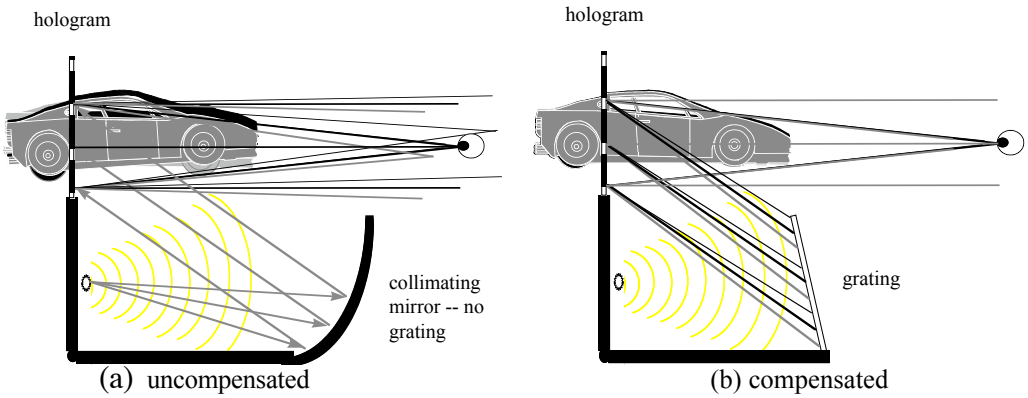

Figure 5.1: Uncompensated and compensated dispersion of a holographic image illuminated with a white light source. The images produced by three wavelengths are shown. In the uncompensated case (a), these images would appear as a continuous blur for broadband illumination. In the compensated case (b), these images are superimposed to form one sharp image.

5.1 The exposure wavelength

The choice of an exposure wavelength is actually an arbitrary one, so long as it is a wavelength the recording material (and our eye) is sensitive to, and one that the grating and hologram can reconstruct with high diffraction efficiency. Our initial experiments were performed with red, Helium-Neon lasers (632.8 nm) and a red, Krypton ion laser (647 nm, Coherent Innova 300). Final experiments and display holograms and gratings were exposed with a blue-green, Argon ion laser (514.5 nm, Coherent Innova 300). We chose the Argon ion laser because it could deliver sufficient power to relatively insensitive photopolymer materials and because its wavelength is close to the middle of the spectral luminous efficiency curve of the human eye (Chapter 1). Our display can be designed so that, for a single reconstruction geometry, it is suitable for playout at any visible wavelength. This allows us to overlap red, green, and blue color separations of the stereogram image for a full-color display.

Coupling of the different wavelengths through layers of recording materials and substrates of different indices of refraction may prove very difficult when the illumination angle is very steep (Please see the edgelit section at the beginning of the next chapter), but in general this should not pose a problem. The effects of scattering and absorption at the playout wavelength are sufficient to warrant care in choosing the recording material, however.

5.2 The holographic recording material

The two primary factors that influenced our choice of recording material are its thickness and diffraction efficiency. The number of fringes that may form through the volume of a recording material is proportional to the thickness of the recording material. As a reflection hologram is, in essence, a multitude of overlapping gratings in the form of interference filters, the thickness determines the degree to which wavelengths will be filtered, according to Equation (**5.1**): $\Delta\lambda \approx \frac{\lambda}{N}$ (Leith 1992)[28], where N is equal to the number of fringe planes. A very thick recording material that gives us a very restricted bandwidth enables the reconstruction of a very deep image, as the maximum acceptable image depth is dependent on the degree of dispersion, which is in turn dependent on the bandwidth. A broader bandwidth reflection hologram, on the other hand, offers the prospect of a brighter image. We have chosen a compromise of a reasonably broad bandwidth of 20 to 30 nm for the materials in our studies.

For the initial experiments and for the dispersion-compensated edgelit displays of the next chapter, red-sensitive silver halide emulsions (Agfa-Gevaert 8E75 HD NAH plates) were used. So that shrinkage of the emulsion would not introduce aberrations in the reconstruction geometry not in accordance with the viewstation design, the holograms

[28] Please refer to the section concerning bandwidth in Chapter 1.

and gratings were processed with minimum-shrinkage Ilford (Wood) developer and EDTA bleach (Bjelkhagen 1993). We found that a ratio of 75% to 25% for solutions A and B was preferable to the traditional 50%/50% ratio in minimizing shrinkage, attributable to increased tanning of the emulsion by pyrogallol in solution A:

Ilford Developer:

Solution A:		
pyrogallol	(C6H3(OH)3)	12.6g
ascorbic acid	(C6H8O6)	18g
distilled water		1 liter
Solution B:		
sodium carbonate	(anhydrous Na2CO3)	60g
distilled water		1 liter

EDTA rehalogenating bleach:

ferric sodium EDTA	(C10H12N2O8FeNa)	100g
potassium bromide	(KBr)	30g
distilled water		1 liter

The above processing was also used for blue/green-sensitive silver halide emulsions (Agfa-Gevaert 8E56 HD NAH and Ilford[29] plates) exposed with the Argon ion laser. After prototype displays were made using the silver halide plates, we used experimental DuPont photopolymer materials to attain higher diffraction efficiency for brighter images. These materials are rather insensitive, so exposures of about a minute or two were sometimes required at energies of about 50mJ at 514.5 nm. Use of these photopolymers has resulted in noticeably brighter gratings and holograms. More specific information about the photopolymers used will come in relevant sections of the chapter.

5.3 The exposure and reconstruction geometries

The geometry of the viewstation of this chapter, to be contrasted with those of the final chapter, is the traditional, plane-wave grating geometry for single view angle reconstruction. The only published account (as far as the author is aware) of the technique's use for the construction of a reflection grating/reflection hologram display is by Kubota (1989), although it is perfectly analogous to its transmission counterparts (Chapter 3). The author's display accommodates shrinkage of the recording material by allowing the grating to rotate orthogonal to the incident plane. Those wavelengths that play out off the Bragg angle do so with less efficiency. Although it is undesirable for a hologram to play out with lower efficiency, it is sometimes impossible to anticipate the reconstruction behavior of experimental materials such as photopolymers. If the grating or hologram is subjected to unanticipated shrinkage, the edge of the grating closer to the

[29] No longer manufactured

hologram is simply rotated toward the hologram until the new playout wavelengths illuminate it.

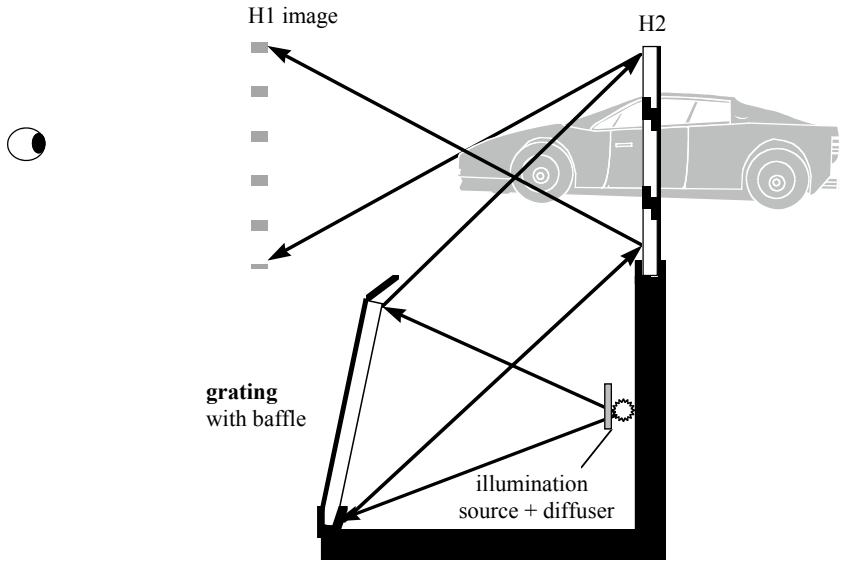

Figure 5.2: Schematic of the final viewstation with tipped grating

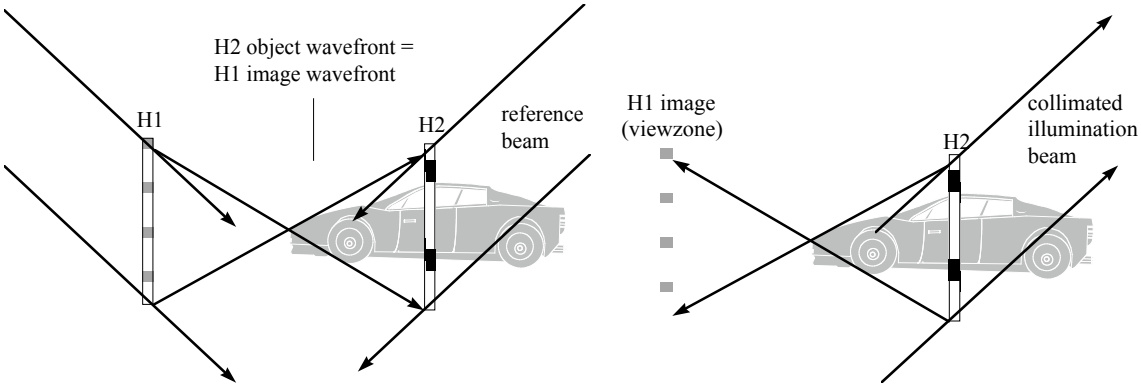

Figure 5.3: Schematic of the exposure (225°) and illumination (45°) geometries of the dispersion-compensated H2 (from Chapter 4)

To obtain the desired central wavelength output angle of 45° and on-axis illumination of 180°, the mastering holographic recording film (HRF) we used[30] required

[30] The mastering holographic recording film we used was HRF750-1x-179 on PVA (with the mylar removed). This film changes refractive index from 1.487 to 1.521. The 750 series film was chosen because it is not hazy after baking, it is on mylar (trirefringent) or PVA, and is of relatively narrow bandwidth (20 nm). The beams were approximately matched in intensity, and after an hour of settling time, the master grating was exposed for 100 seconds (50mJ, .5mW/cm^2), until the HRF contrast flicker spreads to its edges. Norland epoxy was used to index-match the master film (PVA side) to glass after exposure, UV-curing, and baking.

the exposure geometry pictured in Figures 5.5, table setup of Figure 5.6[31], with a corresponding contact copy exposure geometry of Figure 5.7 and table setup of Figure 5.8.

The primary goal in making a bright grating is that it should play out with a uniform, maximal diffraction efficiency at the desired wavelength and angle. Chapter 5 employs a perfect reconstruction geometry to approach a maximum attainable diffraction efficiency. Aside from the geometry and chemistry, obtaining high diffraction efficiency in a grating usually entails exposing the grating to object and reference beams with a one-to-one beam intensity ratio across the recording plate. The gaussian profile of the exposing beams makes uniform illumination from the center to the periphery of the plate rather difficult. To approach uniform light intensity across the plate, the beams are spread significantly by lenses with very short focal lengths. We used a highly diverging, 100X microscope objective[32] and ball lens[33].

The calculations for the geometries were made using an iterative TK Solver program[34] that takes into account the calculated shrinkage and index changes of the mastering and copying photopolymer films[35]:

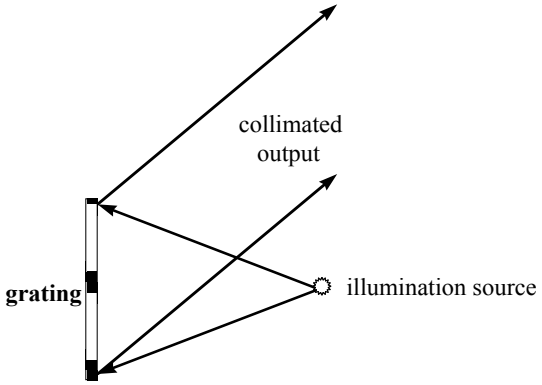

Figure 5.4: The desired grating playout (45°)

[31] The master and some of the transfer gratings were shot at E.I. du Pont de Nemours & Co.'s laboratories in Delaware by Steve Mackara. The laboratory had positive air flow with plastic wall curtains and a 10' x 16' x 2' pneumatically-supported, Newport table with plexiglas enclosure.

[32] Mitutoyo (Japan), ULWD Mplan Apo 100X, f=200μm (#378-806-1)

[33] Edmund Scientific (Barrington, NJ) BK-7 glass ball lenses with 2 mm focal length (#E32,744)

[34] Steve Mackara used a TK Solver program very much like the one in Appendix 4 to find this solution.

[35] The contact-copy transfer holographic recording film we used was HRF750-1x-193, on mylar. The exposure time for each copy was 60 to 90 seconds (0.8mW/cm^2, 20 mJ). This photopolymer film changes refractive index from 1.487 to 1.511. This type has a UV stabilizer to absorb ultra-violet wavelengths that would otherwise render the photopolymer chemically reactive, so it is cured at a higher wavelength (405 nm). UV curing also increases the bandwidth (and decreases the optical density) of these materials. After curing, it is baked for 2hours at 120°F for 99% efficiency.

The program uses the X - equation (Appendix 2):

$$\sin(\theta out) = m\frac{\lambda_2}{\lambda_1}\left(\sin(\theta obj) - \sin(\theta ref)\right) + \sin(\theta ill)$$

Contact - copied grating:

Desired reconstruction geometry: $\theta out = 45$; $\theta ill = 180$

$\lambda_2 = \lambda_1 = 514.5$ nm; $n_1 = 1.487$; $n_2 = 1.511$; $\frac{t_2}{t_1} = 3.9\%$

$0.7071 = \left(\sin(\theta obj) - \sin(\theta ref)\right)$

One possible geometry, the result of inputting the above data into the top (isolated) section of Appendix 4's program:

$\theta obj = 53.434$; $\theta ref = 174.488$

Master grating:

Desired reconstruction geometry: $\theta out = 53.434$; $\theta ill = 174.488$

$\lambda_2 = \lambda_1 = 514.5$ nm; $n_1 = 1.487$; $n_2 = 1.521$; $\frac{t_2}{t_1} = 3.4\%$

$0.7071 = \left(\sin(\theta obj) - \sin(\theta ref)\right)$

Again, one possible geometry is: $obj = 56.32$; $\theta ref = 172.817$

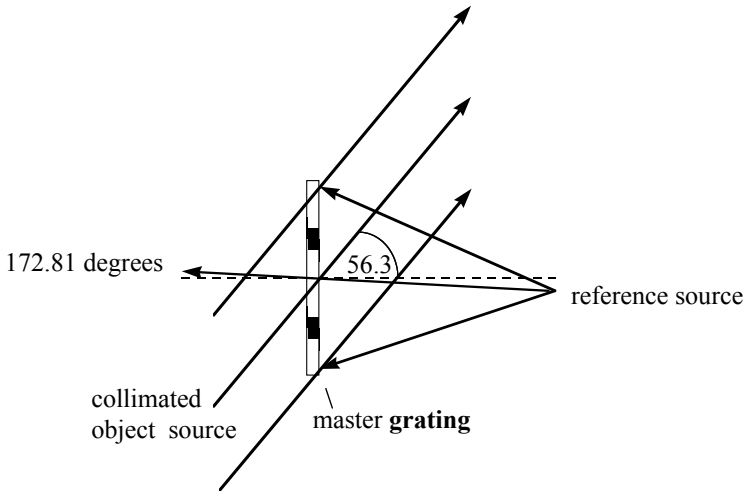

Figure 5.5: The required master grating exposure geometry (56.32° degrees, 514.5 nm), taking into account shrinkage of the photopolymer

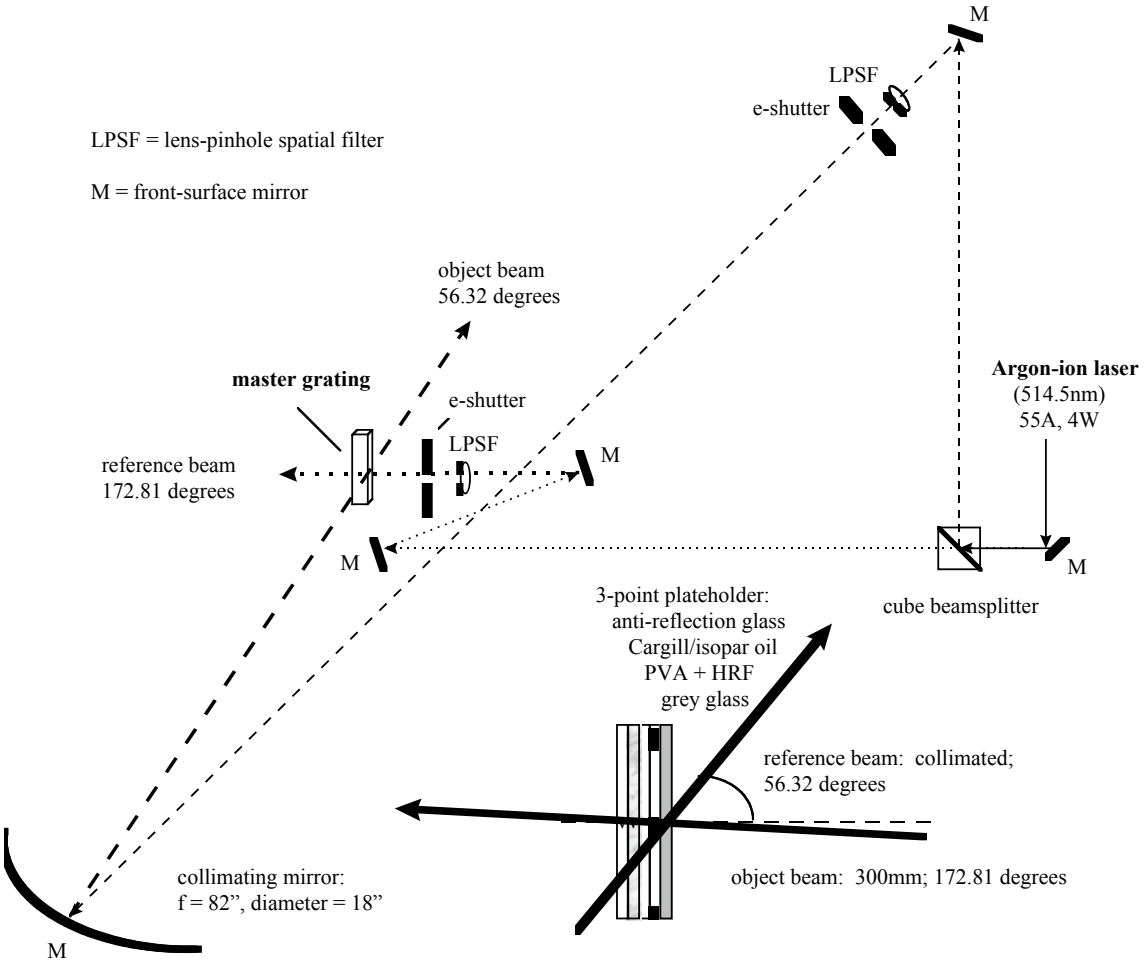

Figure 5.6: The master grating exposure holographic table setup

The contact-copying setup involves the use of multiple layers of anti-reflection glass, index-matching oil and epoxy, as well as the layers composing the holographic recording films[36]:

[36] The anti-reflection glass is used because light from the master grating would otherwise reflect at the mylar/air interface. Cargille/isopar oil is pressed between the plates and allowed to settle for at least an hour because the pressure deforms the photopolymer. The mylar is trirefringent. The Norland epoxy has an index of 1.51. The master grating had to be set slightly off the calculated Bragg angle.

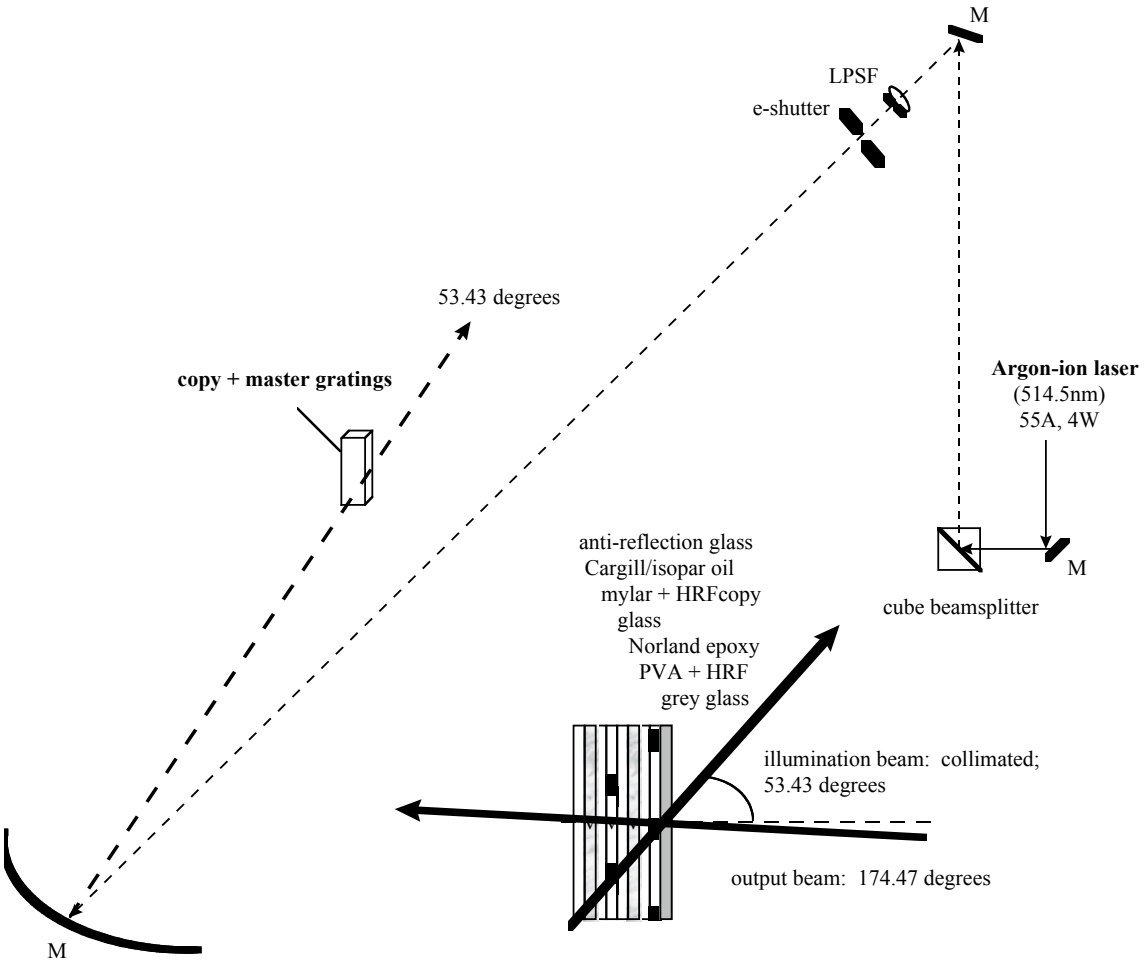

Figure 5.7: The transfer grating exposure holographic table setup

5.4 Selecting an illumination source

In the viewstation, the hologram is illuminated from below at 45° by a plane-wave, dispersion-compensation grating that is itself illuminated by a powerful light source set at a distance of 300 mm or so from the grating. This light has to be very intense, as it is passing light through the three successive "filters" of Chapter 1: (1) interference filters (the grating and hologram, with associated diffraction efficiency curves); (2) spread of the output wave front (viewzone magnification), and (3) the spectral luminous efficiency filter of the retina. In addition, the light source must also be extremely small to minimize source-size blur, particularly for small light source/grating distances.

Of the light sources we have evaluated so far, the best two were a Xenon arc lamp[37] coupled into multiple optical fibers, and a high wattage, bare tungsten-halogen bulb with a small filament. Both are broad band sources (good for later work in illuminating a full-color viewstation), and have very high lumen outputs. The arc lamp is significantly more expensive, but provides a very small source size, as its arc gap can be as small as a millimeter or so. Optional optical fibers, with their exposed ends placed at the focus of concave mirrors to couple in the arc lamp's light, and used to guide the light to multiple displays, may be of equally narrow width.

The tungsten-halogen bulb is a far less expensive option, and can deliver a significant amount of light to the grating if it is of high wattage and large size. As we hope to minimize the source size, an ideal tungsten source of a given size would consist of a solid piece of the material instead of a filament, for the highest possible luminous flux. Therefore, a small, coiled filament should be oriented with its most dense luminous area facing the grating.

For one of the viewstations, a 150W bulb[38] with a vertical coil is oriented with its tip facing the grating, at a slight angle. In this way, the center of the grating receives light from effectively a small, solid luminous area. Because tungsten-halogen bulbs are usually sealed at the tip, the uniformity of the beam is adversely affected in this orientation. Dense, "double filament (round core)[39]" bulbs with the filament oriented orthogonally to the tip are preferable:

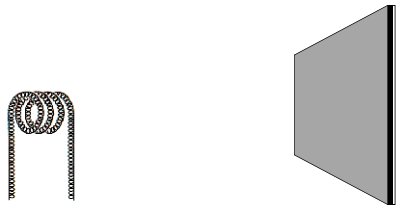

Figure 5.8: filament orientation

---

37 Manufactured by Color Ray, distributed by Laser Media, CA

38 JCD 120V 150WB with a TT61 socket

39 Osram Sylvania (1995)

A common misconception is that we could place multiple filaments adjacent to one another and collinear to the line of sight to a detector to deliver a higher lumen count than a single filament could provide. As each filament is a blackbody radiator, it will absorb frequencies that it emits, so such a scenario would not help matters unless the filaments have gaps through which otherwise occluded filaments may pass their light.

Another thing to be careful of when searching for a small, intense light source is the promise of a tight focus of high optical quality by the presence of a non-faceted, dichroic, ellipsoidal mirror behind the bulb. We evaluated several such mirrors only to find that the bare bulb was far preferable. The structure of the bulb and filament itself degrade the uniformity of the output, and the luminous area of the side of the bulb facing the mirror surface is usually considerably larger than the area from the top end of the bulb.

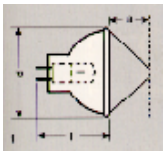

Figure 5.9: Bulb with an ellipsoidal, dichroic reflector

Two additional concerns arise when using a blackbody source such as a tungsten-halogen bulb: extraneous light and heat. The bulb is facing not only the grating in this geometry, but is also facing the viewer, so sufficient shielding of extraneous light must be taken into account when constructing the housing for the light. Shielding means added surface area collecting heat radiated by the bulb and restricted ventilation. For the viewstations with 150W bulbs, we installed a small fan, and sprayed close surfaces with flat matt black, high heat spray paint[40]. For a reflection grating/transmission hologram dispersion-compensated viewstation, we placed a heat mirror[41] in front of an interference filter used to restrict the bandwidth, resulting in a sharp image 300 mm in front of the hologram.

[40] Krylon BBQ and Stove Paint

[41] Edmund Scientific (Barrington, NJ) hot mirror to reflect infrared light and transmit visible light (#E43,452)

5.5 The resulting display

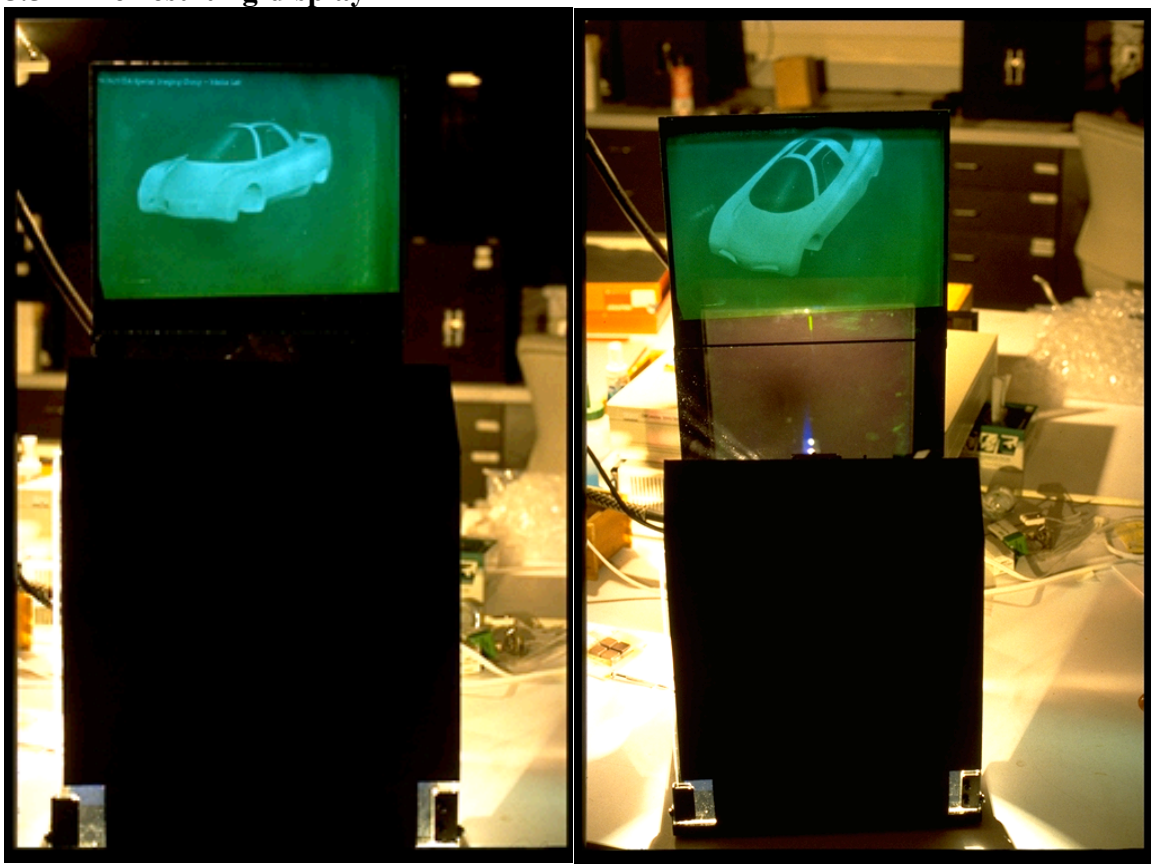

Figure 5.10: Plane-wave grating dispersion-compensation display (photos care of Michael Klug)

The results so far have been very promising. The dispersion compensation of one H2[42], made from an H1 of about 6,600 3 mm by 8 mm exposures, is so effective that the low perspective sampling in the vertical direction is all too apparent. When this H2 was replaced by another made with a 3 mm^2 aperture, astigmatism of the hologram became noticeable. If the viewer stands well in front of the H2, the horizontal and vertical lines comprising the grid of exposures focus to different depths. In fact, when illuminated with a small source like a fiber from the Xenon arc lamp, one can see images of scratches, bubbles in the xylene[43], and other blemishes on the H1, 300 mm in front of the H2. This was our first confirmation that we could compensate for the dispersion of image points at least that far in front of the hologram.

As gratifying as it is to find that the image depth can be sharp as far forward as the viewzone (300 mm), the dispersion-compensated image of the H1 grid is a distraction from the H2 image. In order to rid the viewstation of this artifact, we placed a diffuser in front of the Xenon arc lamp's fiber end to increase the apparent source size. The

---

[42] Repeated from Chapter 4.

[43] Excepting the edgelit holographic work of Chapter 6, all H1's, H2's, and transfer gratings shot at MIT were index-matched with xylene (n = 1.49).

resulting blur was sufficient to eradicate the grid image while retaining the image sharpness of image points closer to the H2 plane. By varying the size of the source in a continuous fashion, we are able to witness a slow degradation of image quality closer and closer to the H2 plane. The diffuser sacrifices light intensity considerably, however, so we turned to the range of filament sizes and shapes available in tungsten-halogen bulbs to provide sufficient blur. Increasing the filament size has the added advantage of providing more light.

The primary disadvantage of the viewstation design above is its size. If we attempt to take the present design and make it more compact while retaining the same hologram size, we encounter two limitations. First, if we try to simply place the grating at a closer distance to the hologram, at some proximity, the required output angle from the grating is not realizable, due to the high disparity between the indices of refraction of the recording material or substrate and air. The light will simply be subject to total internal reflection and not even escape the grating substrate. Second, it must be realized that to provide sufficient light coverage of the hologram, a plane-wave grating must be the same size as the hologram. Both of these problems are solved in the next and final chapter.

Chapter 6
Wave-front shapes, compact displays and designing gratings

As stated at the end of the previous chapter, the primary disadvantage of the Chapter 5's viewstation is its size. Although the viewstation displays holograms in a smaller space than would be required by an uncompensated hologram illuminated by a distant source, the uncompensated hologram still has the advantage that there is nothing lying between the light and hologram. It could be rationalized that for kiosk or showroom displays and table-top imaging systems, a single viewstation can display many alternate holograms, and is more compact than a designer's models or the objects themselves. However, because a plane-wave grating must be the same size as the display hologram, scaling up such a display significantly would result in a system not unlike a large-mirror, projection television.

To avoid this unsavory prospect, we will adopt two strategies for making a more compact display. The first will be to move the grating and hologram closer together and make a dispersion-compensated system in a variant of the edgelit format. The second will be to reduce the grating size and illuminate the hologram with a diverging wave front. This will carry us into an evaluation of wave front and field curvatures, and then development of an optimization program to compensate for dispersion in compact displays.

6.1 Sources of blur in edgelit holograms

The compact, self-illuminated edgelit display (Upatnieks 1992, Birner 1989, Henrion 1995) is a format where a hologram is exposed and illuminated from the edge of a glass block at a very steep angle. This steep angle ensures bright reconstruction by guiding the coupled light to the hologram with total internal reflection, and eliminates the source-size blurring effect of ambient light during reconstruction. However, source-size blur is instead exacerbated by multimodal reflections within the light guide from the widely diverging source. That is, light rays reflecting at different angles along the inside surface of the glass strike the hologram from many angles, although the hologram was exposed with a single reference wave front. Having the light situated so close to the hologram also introduces significant horizontal dispersion.

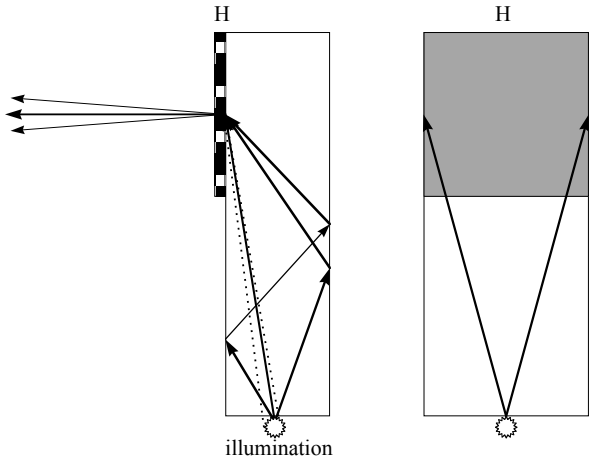

Figure 6.1: Non-chromatic blurring of the edgelit hologram. On the left is a diagram depicting mulitmodal reflections, and the dotted lines represent the angle subtended by the source. The diagram on the right shows the horizontal spread of light that creates horizontal dispersion.

To avoid these two sources of blur, the hologram could be illuminated through the glass from an apparent distance greater than the actual distance between the light source and the hologram. This is possible with two methods. One method is to illuminate the edgelit with a narrowly diverging illumination source and fold the beam path, to effectively increase the apparent distance of the source from the grating, as in Figure 6.2:

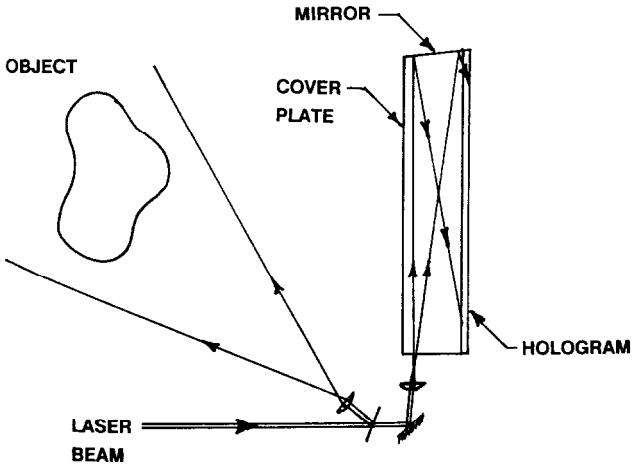

Figure 6.2: Exposure of an edgelit hologram illuminated with the same source distance and folded beam path (Upatnieks 1992)

A second method for increasing the apparent distance of the light source is not to illuminate the hologram from the edge of the glass block. To do this, an HOE (holographic optical element) grating could be placed on one side of the glass, and the hologram on the other (Figure 6.3). Illuminating a wave-front-reshaping grating along its normal, as opposed to illuminating the glass block from its edge, can eliminate not only multimodal reflections, but horizontal dispersion as well. Such a system is better termed a “steep angle” hologram (Birner 1989) rather than an “edgelit” hologram.

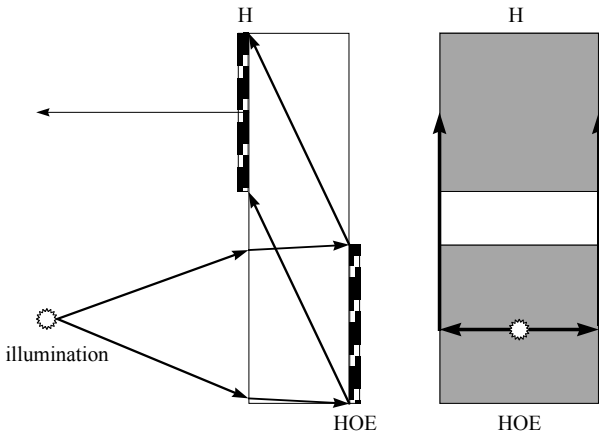

Figure 6.3: Reduction of chromatic and non-chromatic blurring of the edgelit hologram using a wave-front-shaping steep angle HOE

6.2 Pulling the grating and hologram closer together by using a light guide: the steep angle format

This HOE not only reduces the nonchromatic sources of blur mentioned above, but can also compensate for dispersion of the hologram (Birner 1989). This compensation is critical to obtain reasonable image depth. The bandwidth of a reflection steep angle hologram is quite high compared with a conventional reflection hologram, and with its high dispersive power, makes uncompensated chromatic aberration in this format a more formidable problem than in the conventional in-air geometries (Henrion 1995).

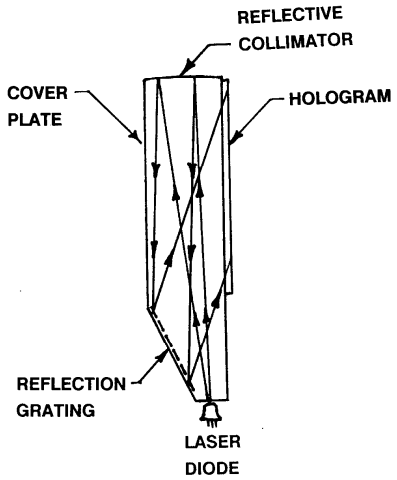

Figure 6.4: Upatnieks' achromatic edgelit hologram (1992)

Application of the dispersion-compensation technique to further reduce blur of deep image steep angle holograms is conceptually straightforward. The intervening air between the grating and hologram of Chapter 5's viewstation is replaced with a thin light guide of higher refractive index, such as glass or plastic, as in Figure 6.3 (or Kubota's

Figure 3.14 (b) may be compared with Figure 6.4). This light guide prevents light from being trapped in the grating due to total internal reflection for very steep angles at the interface between the recording material substrate and air.

Birner's display (Figures 6.3, 6.5), however, did not take best advantage of the potential compactness of the steep angle format, for the illumination source was quite distant (60 cm) from the (2 inch) thick glass block. The author has produced several steep angle reflection gratings and H2s with the grating illuminated from as little as 2 mm away from the Plexiglas block face. This was made possible by using a ball lens[44] of very short focal length for the grating reference beam. Unfortunately, however, Norland index-matching epoxy was used to mount one of the displays, and it was found to swell the grating and hologram. The expanded fringe structures play out at a slightly less obtuse angle, and as a result, the illumination source has to be placed farther from the grating (13 mm) and at an angle to reconstruct brightly and minimize distortion.

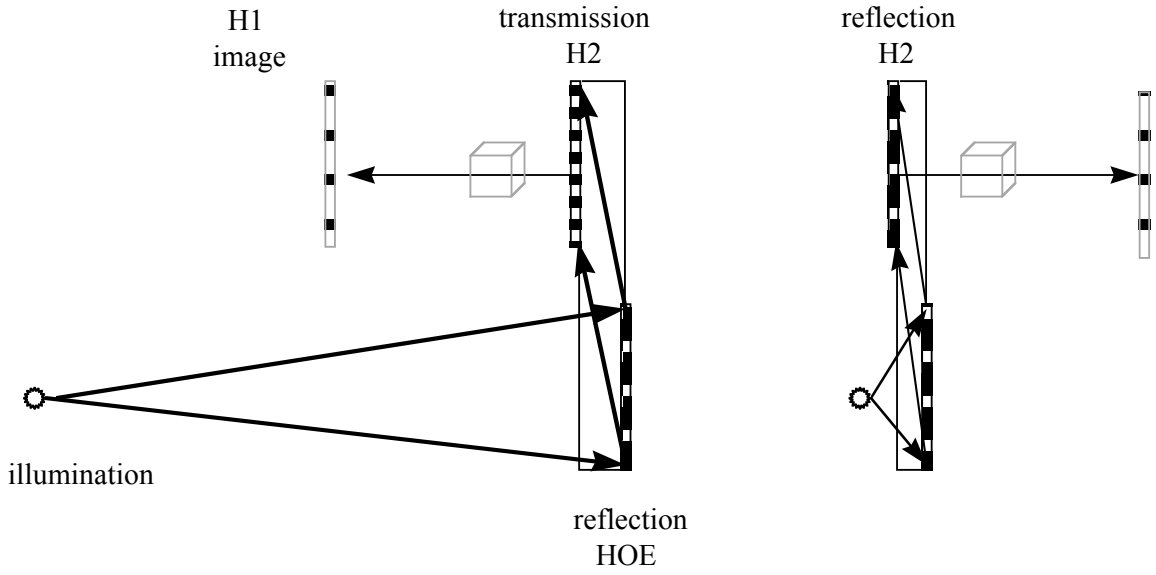

Figure 6.5: A comparison of Birner's reflection HOE/transmission steep angle H2 with the author's reflection/reflection displays. Birner's illumination distance is 60cm from a 2-inch thick block (Birner 1989), the author's, 1.2cm from a 1-inch thick block (after swelling due to epoxy).

The author also attempted to create steep angle gratings and H2s that reconstruct well using thinner (1/2 inch) light guides. Proper index matching becomes a barrier even with special index-matching oils[45] when one tries to illuminate through the block at an angle from the normal much greater than 80°. Other obstacles to dispersion compensation in the steep angle format are the high vertical dispersion and curved achromatic curves of edgelits (Henrion 1995). The latter problem may be circumvented in a full-color, steep angle display by having three narrow band reflection gratings. Each grating could provide dispersion compensation for its narrow band of the spectrum, and each could provide an ideal source angle and distance independent of the other colors, so that all three color

[44] Edmund Scientific (Barrington, NJ) BK-7 glass ball lenses with 2 mm focal length (#E32,744)
[45] Cargille Series A: n = 1.510 ± 0.0002, produced by Cargille Laboratories, Inc. (NJ)

separations of the hologram reconstruct corresponding average points in a superimposed fashion.

6.3 Compensation gratings with diverging wave fronts

The steep angle strategy for compressing the display's volume still does not take into account the grating's size as the display is scaled up. If the grating area is to be reduced in either the steep angle format above or in a revised viewstation, the hologram illumination distance for the central wavelength has to be closer than infinity. The smaller grating then acts as an aperture through which light illuminating the hologram diverges from a closely-spaced, blurred source reconstructed by the grating itself. The minimum size that this (tilted or untilted) grating can be, and still allow for light of the central wavelength to illuminate all parts of the hologram, is calculated in the program of Appendix 3. The grating height would of course have to be greater if every wavelength of a specified spectral band is to illuminate every part of the hologram. One advantage of using a diverging illumination source is that not only could the grating size be reduced in Chapter 5's viewstation, but the grating and light source could be placed relatively far from the hologram, taking advantage of dispersion compensation without having to construct a viewstation. The limitations of such a method will be described below.

The reason the hologram illumination source is situated (reconstructed with order m = +1) behind our grating, as opposed to being focused as a real image in front of the grating (m = -1), comes from our introductory discussion of dispersion in the first chapter. If a predispersing grating could play out a blurred real image of a point source with its dispersed wavelengths of the right orientation with respect to the hologram, then the grating could be placed farther from the hologram than would its m = +1 counterpart of equal size. However, the m = -1 image is blurred in the opposite sense as the m = +1 order image because the wavelengths are focused in front of the hologram, crossing through the focus point and appearing reversed in direction as a consequence (Figures 1.10 for the in-line geometry, 2.4 for the off-axis geometry). The author had therefore determined at the outset that an order m = -1 reconstruction from a predispersing grating would be unsuitable for most practical geometries and that we would reconstruct the m = +1 order instead for our displays.

6.4 Grating playout distances

Orientation of the grating's output blur involves not simply angles, as was assumed for the viewstation of Chapter 5, and is indeed universally assumed, but distances as well. Otherwise, red, green and blue wavelengths will reconstruct collinearly along the dispersion-compensated view angle, but will be staggered along that line of sight. A viewer looking off axis perceives this discrepancy as blur.

A viewer centered on axis has eyes straddling the axis, so the maximum acceptable perceived longitudinal blur length within the stereoacuity of the eye (Chapter 1) at the nearpoint distance from the image (250 mm) may be derived as follows:

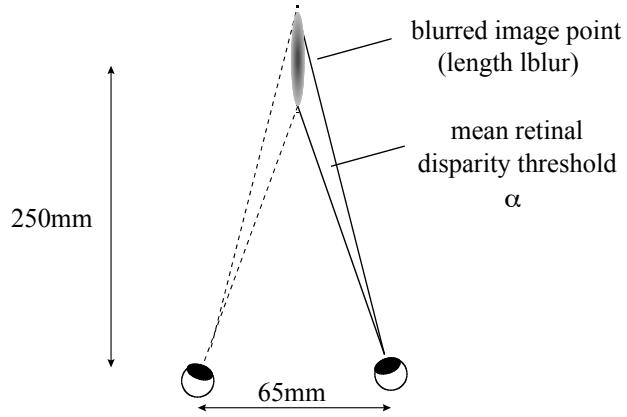

Figure 6.6: Maximum acceptable perceived longitudinal blur length

$$\frac{\text{lblur}/2}{\sin(\alpha/2)} = \frac{\sqrt{250^2 + \left(\frac{65}{2}\right)^2}}{\sin(90-\beta)}, \text{ with } \tan(\beta) = \frac{250}{65/2}$$

$$\therefore \text{ lblurl } = 4231.81\sin(\alpha/2)$$

For a stereoacuity of 30 arc seconds, the maximum acceptable perceived longitudinal blur would be:
lblurl = 0.31mm

In order to superimpose these collinear points, the grating must reconstruct output points at appropriate distances. Along the achromatic angle of Equation (2.25), a space defining where the different wavelengths focus vertically:

$$\tan\alpha = \frac{\sin(\theta\text{out}) - \sin(\theta\text{ill})}{\cos(\theta\text{out}) - \frac{\text{Rout}}{\cos\{\theta\text{out}\}} \cdot \frac{(\cos(\theta\text{ill}))^2}{\text{Rill}}}$$

With the vertical focus Equation (5.2), we have an alternative expression:

$$\frac{\cos(\theta ill)^2}{Rill} = \frac{\cos(\theta out)^2}{Rout} - m\cdot\frac{\lambda_2}{\lambda_1}\cdot\left[\frac{\left\{\cos\left\{\theta obj\right\}\right\}^2}{Robj} - \frac{\left\{\cos\left\{\theta ref\right\}\right\}^2}{Rref}\right]$$

Equation (**6.1**):
$$\tan\alpha = \frac{(\sin(\theta out) - \sin(\theta ill))\cdot\cos(\theta out)}{m\cdot\frac{\lambda_2}{\lambda_1}\cdot\left[\frac{\left\{\cos\left\{\theta obj\right\}\right\}^2}{Robj} - \frac{\left\{\cos\left\{\theta ref\right\}\right\}^2}{Rref}\right]\cdot Rout}$$

We can see from this expression that the angle is inversely proportional to Rout, so we should expect that as the playout distance increases to infinity, the achromatic angle approaches the hologram normal. Now, if we want to see how this angle is affected by wavelength spread, we will take the derivative of the tangent of this angle with respect to the spread in output angles at the extreme wavelengths:

$$\frac{\cos(\theta ill)^2}{Rill} = \frac{\cos(\theta out)^2}{Rout} - m\cdot\frac{\lambda_2}{\lambda_1}\cdot\left[\frac{\left\{\cos\left\{\theta obj\right\}\right\}^2}{Robj} - \frac{\left\{\cos\left\{\theta ref\right\}\right\}^2}{Rref}\right]$$

$$\frac{d}{d\theta out}\tan\alpha = \frac{-\sin(\theta out)\cdot d\theta out\cdot\cos(\theta out)\cdot d\theta out}{m\cdot\frac{\lambda_2}{\lambda_1}\cdot\left[\frac{\left\{\cos\left\{\theta obj\right\}\right\}^2}{Robj} - \frac{\left\{\cos\left\{\theta ref\right\}\right\}^2}{Rref}\right]\cdot Rout}$$

Equation (**6.2**):
$$\Delta\tan\alpha = \frac{-\sin(2\cdot\theta out)\cdot\Delta\theta out}{2\cdot m\cdot\frac{\lambda_2}{\lambda_1}\cdot\left[\frac{\left\{\cos\left\{\theta obj\right\}\right\}^2}{Robj} - \frac{\left\{\cos\left\{\theta ref\right\}\right\}^2}{Rref}\right]\cdot Rout}$$

Now it becomes apparent that a change in the spread of the output angles has a nonlinear effect on the achromatic angle. As it turns out, the achromatic angle, usually approximated as a line, is a curved surface (a surface if horizontal dispersion is also taken into account). For extreme angles, such as in the edgelit and steep angle holograms above, the dispersion is very high, and the achromatic surface is a curve curling back toward the hologram for extreme wavelengths and small output distances (Henrion 1995).

6.5 Dispersion compensation and grating output wave-front shapes

Although the edgelit hologram presents an extreme case of dispersion and corresponding distortion of output wave fronts, wave fronts distortion is not an unusual

occurrence. If the grating is not illuminated appropriately to present the appropriate blur orientation and length to the hologram, one should expect distortion and dispersion in the resulting holographic image. For any one-step hologram illuminated from the prescribed illumination source position, this does not pose a problem. However, when an H2 is to be illuminated to project an m = -1 image of its H1, it should be illuminated in a reverse-direction, phase-conjugate fashion. Illuminating an H2 with converging beam from a grating would defeat the purpose of the non-collimated technique, as the grating would then have to be larger than the hologram itself.

Indeed, there are distinct advantages to illuminating a stereogram transfer with an imperfect phase-conjugation beam, usually a diverging beam. We will refer to the imperfect phase-conjugate case where the reference and illumination sources are both diverging as a "diverging/diverging" geometry. The primary advantage to diverging/diverging reconstruction is ease of illumination: it is far easier to illuminate a large reflection hologram with a diverging source from the front than it is to illuminate the hologram with a large converging optic from behind. Diverging/diverging reconstruction is also a common technique for producing wide view zones when making an HPO HS; the diverging illumination wave front laterally and longitudinally magnifies the image of its master (H1) aperture plane. Of course, the component aperture windows are magnified as well, so sampling considerations have to be reevaluated in such an approach.

The author explored the effects of wave-front curvature on dispersion and made extensive calculations to compare the color blur of an H2 reconstructed in a phase-conjugate diverging or collimated fashion with the above-mentioned diverging/diverging geometry. If the H2 is illuminated with a grating that reconstructs at the ideal angles and distances for single view angle dispersion compensation for both geometries, a distinct advantage may be seen with the phase-conjugate case as expected, but there is also a compensation advantage conferred by the diverging/diverging geometry as well due to the asymmetry of the illumination angles across the recording material. We will treat both cases below.

6.6 The planar wave front case

The perfect phase-conjugate case is relatively straightforward. Assuming perfect reconstruction,[46] all the points reconstructed by the exposure wavelength will image where the original object points were. Image points lying along a preselected view direction will be color corrected (the single view angle dispersion compensation of Chapter 3). If the reference and illumination beams are collimated, then this compensation holds for every part of the plate, so that if the viewer looks directly ahead at any portion of the plate, points along this line of view and points within a small field of view about this line of view will appear sharp. As the view direction changes with respect to the plate normal, the central wavelength still forms an image in the right place, but shorter and longer wavelengths diffract at slightly different angles, so from these new view directions image points appear color-blurred if projected beyond a certain maximum acceptable image depth, marked along the lines of sight to the hologram in the following figures.[1]

We will define maximum image depth in this paper to be the maximum depth at which the color blur of a point reconstructed by a given spectral band equals the acuity of the human eye (1') at a given viewing distance in front of the hologram (500 mm). Using Benton's method (Figure 2.6), whose difference from the author's method is negligible for perfect reconstruction in the on-axis object/image geometries here, we have:

Equation (**6.3**): Maximum forward depth = $$\frac{D_{eye}\tan\left(\frac{\theta_{acuity}}{2}\right)}{\tan\left(\frac{\Delta\theta}{2}\right)+\tan\left(\frac{\theta_{acuity}}{2}\right)}$$

Equation (**6.4**): Maximum depth in back of the hologram = $$\frac{D_{eye}\tan\left(\frac{\theta_{acuity}}{2}\right)}{\tan\left(\frac{\Delta\theta}{2}\right)-\tan\left(\frac{\theta_{acuity}}{2}\right)}$$

[46] Again, perfect reconstruction is the case such that the fringe spacing is the same when illuminated as when recorded, and the wavelength and position of the illumination source/focus is equal to that of the reference source when recorded.

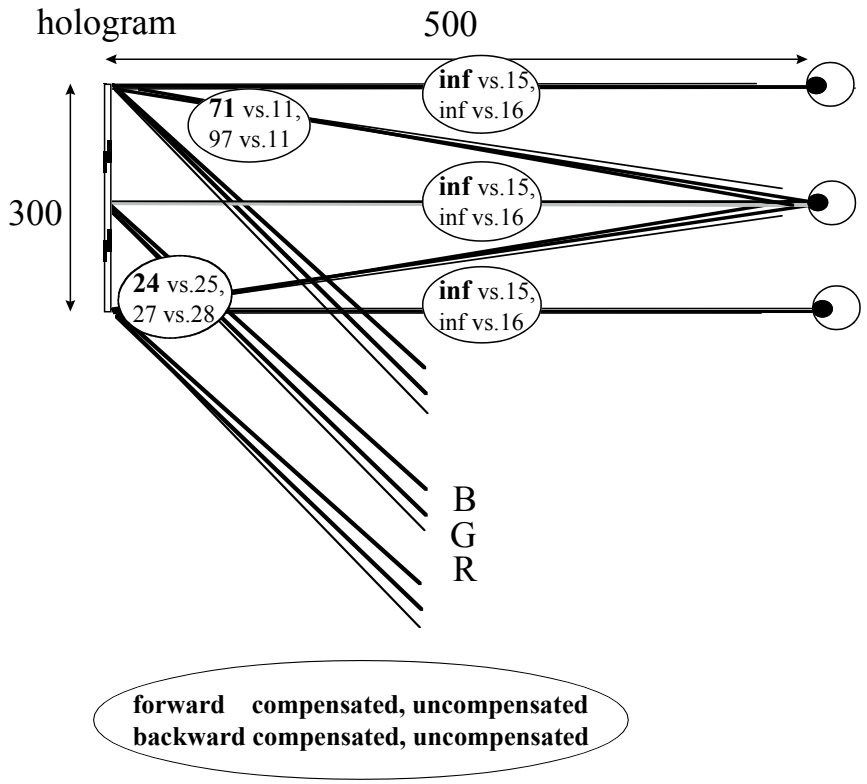

Figure 6.7: Collimated, phase-conjugate, single view angle dispersion-compensated hologram
The numbers in the balloons are maximum depths **(3 arc minutes of resolution)**; the numbers are ordered as in the balloon above this caption.

6.7 The diverging wave front case (phase-conjugate)

In the uncollimated, phase-conjugate case, it was found that the field of view from the central view direction containing relatively sharp image points is wider than in the collimated case, and its off-axis points may be much deeper, but that compensation degrades severely as the viewer moves away from this central position.

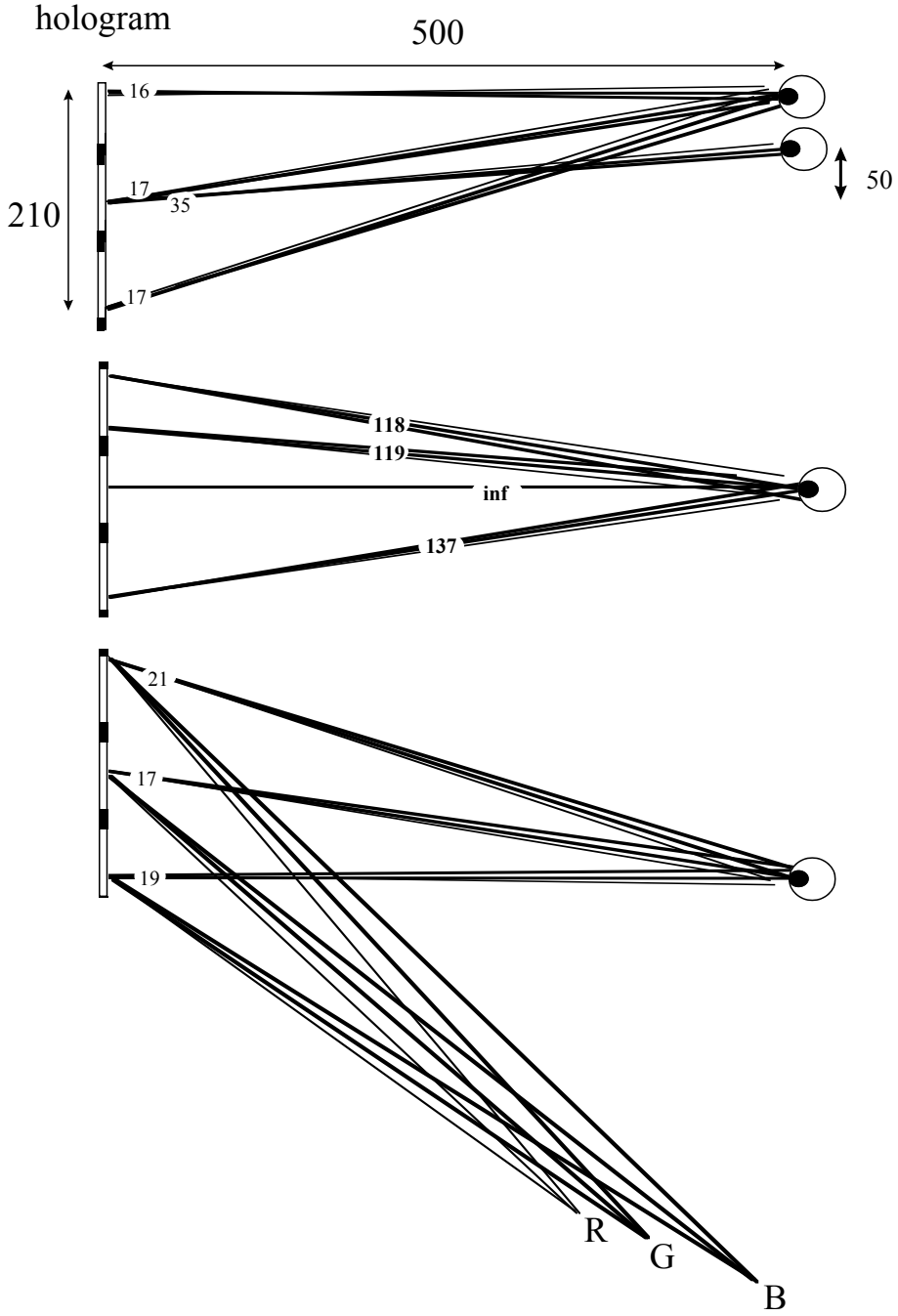

Figure 6.8: Uncollimated, phase-conjugate, single view angle dispersion-compensated hologram Maximum forward compensated depths **(1 arc minute of resolution):** top, middle, and bottom views

6.8 The diverging wave front case (non-phase-conjugate)

The diverging/diverging case in some ways presents a less desirable dispersion-compensation method than the above perfect phase-conjugate approach. In addition to astigmatism and serious image warping, it was found that the maximum acceptable image depth is inversely proportional to the holographic plate size. In addition, there is a more pronounced asymmetry in the maximum volume than in the perfect phase-conjugate cases above.

Both of these characteristics may be explained intuitively by the wave-front curvature difference between the diverging reference and diverging illumination beams striking opposite sides of the plate. In diverging/diverging illumination, ray bundles other than the central ray bundle composing these wave fronts strike the plate at angles non-supplementary to their reference counterparts. The reference and illumination angles on the side of the hologram farther from the predispersed illumination are closer to being supplementary than the corresponding angles on the side of the hologram closer to the illumination, so the side farther has a higher spatial frequency than the side closer to the illumination. There will likewise be greater color blurring on the side of the hologram farther away from the illumination. This increase in color blur is reflected in the figures by a lower maximum depth value.

It was noted in the comparison between the collimated and non-collimated perfect phase-conjugate cases above that the non-collimated case provided a central view with deeper maximum image points. Indeed, as the maximum depth from different viewpoints is further compromised in the present case of non-phase-conjugate illumination, there is also a further increase in the maximum depths of points viewed from the central viewpoint.

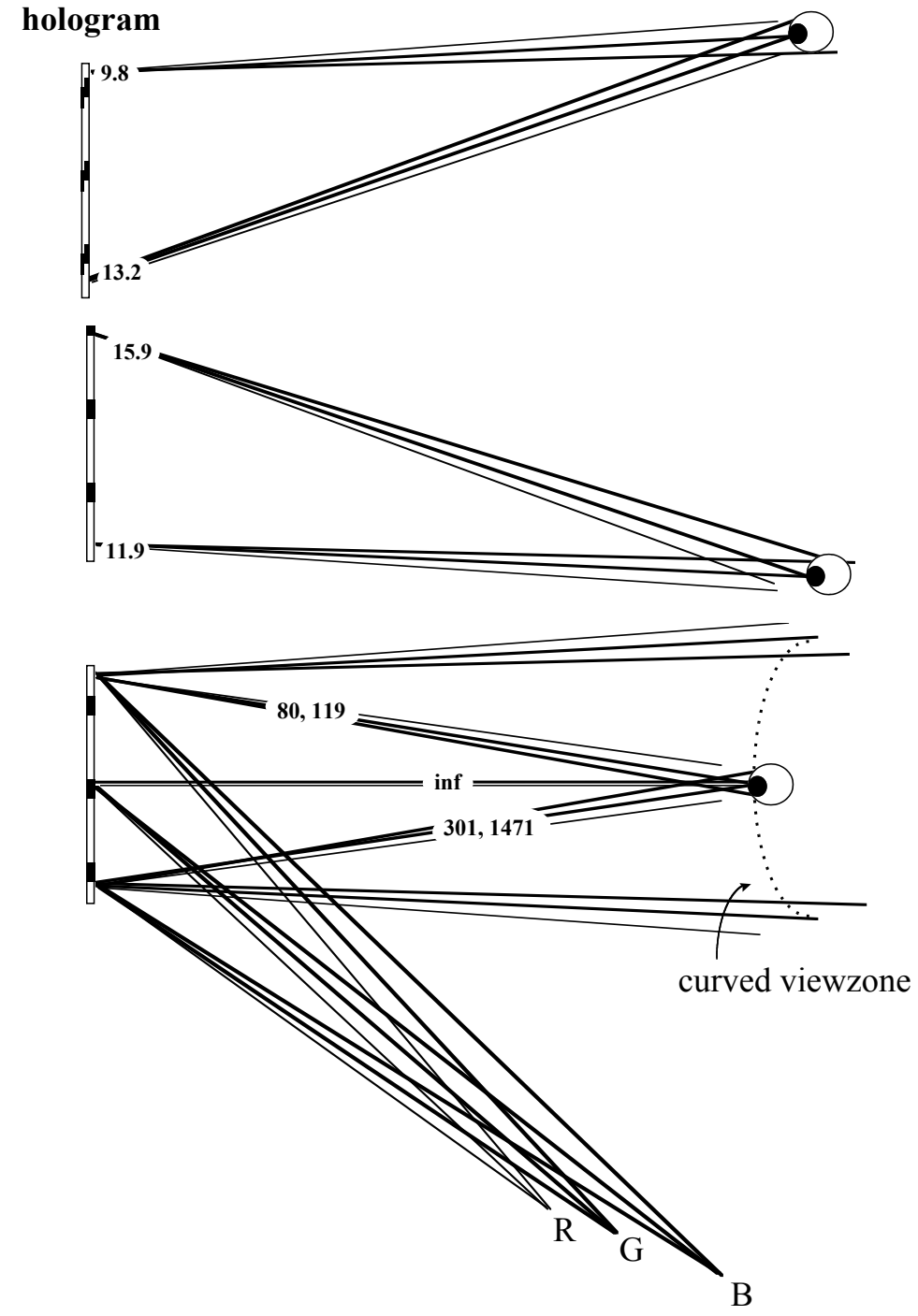

Figure 6.9: Uncollimated, non-phase-conjugate, single view angle dispersion-compensated hologram (diverging/diverging geometry) with extreme field curvature: The numbers in the figure represent the forward and backward maximum compensated depths **(1 arc minute of resolution)** for top, bottom, and middle views (the balloon above presents the order in which the maximum depths appear in the figure).

6.9 Consistent method for designing gratings

To outline a consistent technique for designing dispersion-compensation gratings, we need to work backwards from the illumination blur required of the hologram, to the appropriate output angles of the grating, and finally to the exposure geometry that would result in such playout angles.

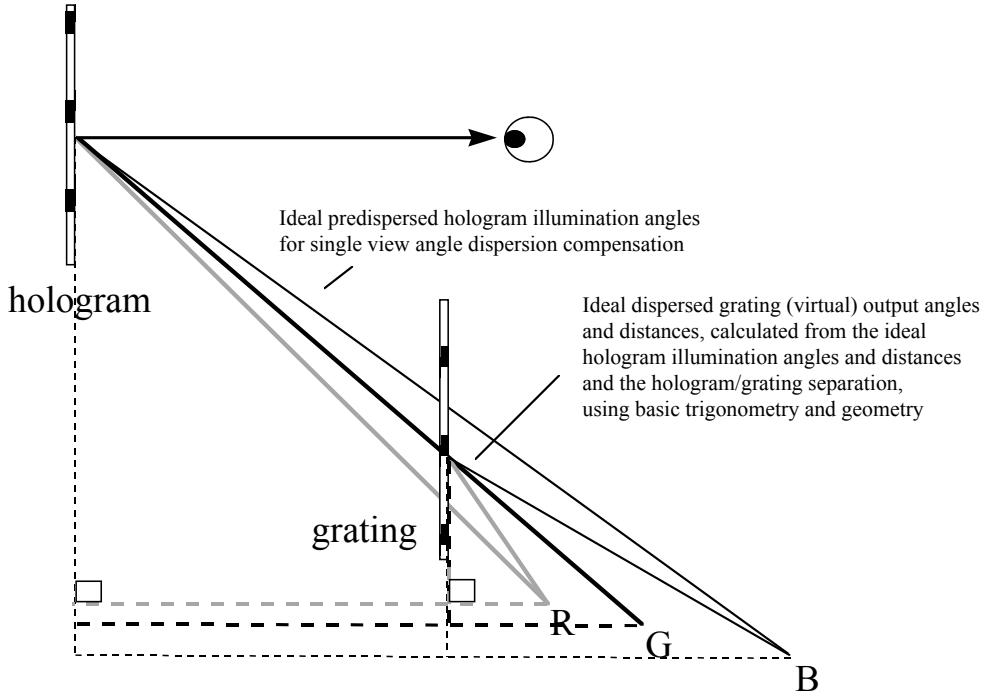

Figure 6.10: Ideal predispersed hologram illumination angles and distances should be equivalent to the ideal predispersed grating output angles.

For the plane-wave grating case, the playout distances for the extreme wavelengths are usually so large that compromising attainable ideal angular output for ideal output distances is unreasonable. However, as the output distance for the central wavelength nears the grating (and the hologram), taking into account the distances becomes more and more important. The author's attempt at optimizing the grating for ideal distances and angles has been implemented by computer programs written in C and Matlab (Appendix 4). The technique involves taking the pseudoinverse of two matrix equations (6.5 and 6.6), each composed of three linear equations to be outlined below.

The geometry and trigonometry for determining where the grating's output points should ideally be relative to the hologram is straightforward for single view angle dispersion compensation. In the diverging case, the ideal angles for individual wavelengths are not always attainable across the bandwidth. A compromise must be made between the ideal angular differences between the central wavelength and longer wavelength playout angles and between the central wavelength and shorter wavelength playout angles. A second compromise needs to be made between the ideal predispersed output angles and ideal output distances at different wavelengths (equal to the ideal illumination angles and distances for the hologram).

First, we will develop a technique to optimize grating playout angles by affecting the exposure and illumination geometries, and then we will apply this technique to optimize grating playout distances.

6.10 Solving for optimized angles

In order to solve for optimized angles, the X-equation[47] (for exposure and reconstruction angles) is solved for three different wavelengths and three ideal output angles:

$$\sin(\theta_{\text{outred}}) = m\frac{\lambda_{2\text{red}}}{\lambda_1}(\sin(\theta_{\text{obj}}) - \sin(\theta_{\text{ref}})) + \sin(\theta_{\text{ill}})$$

$$\sin(\theta_{\text{outgreen}}) = m\frac{\lambda_{2\text{green}}}{\lambda_1}(\sin(\theta_{\text{obj}}) - \sin(\theta_{\text{ref}})) + \sin(\theta_{\text{ill}})$$

$$\sin(\theta_{\text{outblue}}) = m\frac{\lambda_{2\text{blue}}}{\lambda_1}(\sin(\theta_{\text{obj}}) - \sin(\theta_{\text{ref}})) + \sin(\theta_{\text{ill}})$$

If a vector is made of the sines of the desired output angles, a matrix is made of the coefficients, and a vector is made of the sines of the unknown exposure angles, an expression can be formed, Equation (**6.5**):

$$\begin{bmatrix} \sin(\theta_{\text{outred}}) \\ \sin(\theta_{\text{outgreen}}) \\ \sin(\theta_{\text{outblue}}) \end{bmatrix} = \begin{bmatrix} \frac{\lambda_{2\text{red}}}{\lambda_1} & -\frac{\lambda_{2\text{red}}}{\lambda_1} & 1 \\ \frac{\lambda_{2\text{green}}}{\lambda_1} & -\frac{\lambda_{2\text{green}}}{\lambda_1} & 1 \\ \frac{\lambda_{2\text{blue}}}{\lambda_1} & -\frac{\lambda_{2\text{blue}}}{\lambda_1} & 1 \end{bmatrix} \times \begin{bmatrix} \sin(\theta_{\text{obj}}) \\ \sin(\theta_{\text{ref}}) \\ \sin(\theta_{\text{ill}}) \end{bmatrix}$$

However, because the first and second columns of the coefficient (middle) matrix are multiples of one another, a simple matrix equation with an inverse function will not work to solve for the unknown (object, reference, and illumination) angles. Instead, to simultaneously solve for an optimized solution for the three unknowns, we will perform a Moore-Penrose pseudoinverse[48] operation, Equation (**6.6**):

---

[47] The angle and distance equations are presented in Appendix 1.

[48] X = pinv(A) gives the Moore-Penrose pseudoinverse, a matrix of the same dimensions as A' satisfying the following four conditions: A*X*A = A
X*A*X = X
A*X and X*A are Hermitian

$$\begin{bmatrix} \sin(\theta_{obj}) \\ \sin(\theta_{ref}) \\ \sin(\theta_{ill}) \end{bmatrix} = \text{pinv} \begin{bmatrix} \frac{\lambda_{2red}}{\lambda_1} & -\frac{\lambda_{2red}}{\lambda_1} & 1 \\ \frac{\lambda_{2green}}{\lambda_1} & -\frac{\lambda_{2green}}{\lambda_1} & 1 \\ \frac{\lambda_{2blue}}{\lambda_1} & -\frac{\lambda_{2blue}}{\lambda_1} & 1 \end{bmatrix} \times \begin{bmatrix} \sin(\theta_{outred}) \\ \sin(\theta_{outgreen}) \\ \sin(\theta_{outblue}) \end{bmatrix}$$

If a range of central wavelength output angles are substituted into the above expression, a set of different optimized solutions for the unknowns may be found. These solutions correspond to different potential exposure and illumination geometries that provide the desired (ideal) blur from the predispersing grating.

Unfortunately, we can not obtain an exact solution for our matrix expression Ax=b representing [coefficients][sin(exposure angles)] = [sin(output angles)]. This may be proven by taking the original expression Ax = b and performing Gaussian elimination to form a zero submatrix in the modified A^*, and determining that A^*x can not equal b^*.

However, the pseudoinverse technique does provide an optimal solution $\tilde{x}$ to the least squares problem of Ax=b. This is verified by $\tilde{x}$ meeting the two conditions: (1) $\tilde{x}$ is in the row space of A, and (2) $A\tilde{x}$ must be a projection of b onto the column space of A. We will use this pseudoinverse technique to find optimized grating output distances and will work through several geometries to assess the degree of error in the optimization of both output angles and distances.

6.11 Solving for optimized distances

Solving for optimized distances requires the inclusion of a second set of three vertical focusing equations:

$$\frac{(\cos(\theta_{outred}))^2}{R_{outred}} = m\frac{\lambda_{2red}}{\lambda_1}\left(\frac{(\cos(\theta_{obj}))^2}{R_{obj}} - \frac{(\cos(\theta_{ref}))^2}{R_{ref}}\right) + \frac{(\cos(\theta_{ill}))^2}{R_{ill}}$$

$$\frac{(\cos(\theta_{outgreen}))^2}{R_{outgreen}} = m\frac{\lambda_{2green}}{\lambda_1}\left(\frac{(\cos(\theta_{obj}))^2}{R_{obj}} - \frac{(\cos(\theta_{ref}))^2}{R_{ref}}\right) + \frac{(\cos(\theta_{ill}))^2}{R_{ill}}$$

$$\frac{(\cos(\theta_{outblue}))^2}{R_{outblue}} = m\frac{\lambda_{2blue}}{\lambda_1}\left(\frac{(\cos(\theta_{obj}))^2}{R_{obj}} - \frac{(\cos(\theta_{ref}))^2}{R_{ref}}\right) + \frac{(\cos(\theta_{ill}))^2}{R_{ill}}$$

After we have substituted the most practical angles from the set of angle vector solutions into the distance matrix expression above, the remaining three unknowns are the object, reference, and illumination distances.

Equation (**6.7**) is a pseudoinverse expression solving for optimal exposure distances, given ideal output distances:

$$\begin{bmatrix} \frac{(\cos(\theta_{obj}))^2}{R_{obj}} \\ \frac{(\cos(\theta_{ref}))^2}{R_{ref}} \\ \frac{(\cos(\theta_{ill}))^2}{R_{ill}} \end{bmatrix} = \text{pinv} \begin{bmatrix} \frac{\lambda_{2red}}{\lambda_1} & -\frac{\lambda_{2red}}{\lambda_1} & 1 \\ \frac{\lambda_{2green}}{\lambda_1} & -\frac{\lambda_{2green}}{\lambda_1} & 1 \\ \frac{\lambda_{2blue}}{\lambda_1} & -\frac{\lambda_{2blue}}{\lambda_1} & 1 \end{bmatrix} \times \begin{bmatrix} \frac{(\cos(\theta_{outred}))^2}{R_{outred}} \\ \frac{(\cos(\theta_{outgreen}))^2}{R_{outgreen}} \\ \frac{(\cos(\theta_{outblue}))^2}{R_{outblue}} \end{bmatrix}$$

6.12 Designing a diverging wave-front grating for a compact display

Figure 6.9 is the model of the prototype diverging/diverging viewstation we made to evaluate the ease and effectiveness of non-phase-conjugate geometries for future reduced-size gratings. The standard procedure for the making of an HPO HS with a wide field of view was used for the first full-parallax trials. This procedure involves a 300 mm H1/H2 transfer separation and a 500 mm H1 image playout distance. The only compromise that the H2 underwent was to have a matching short reference and illumination distance of 750 mm, to limit warping of the H1 aperture image as well as satisfy the vertical focus equation. The vertical focus formula is much more sensitive to changes in distance than is the more familiar horizontal focus equation: a slight change in one distance could significantly alter the other distances used to expose and reconstruct the image.

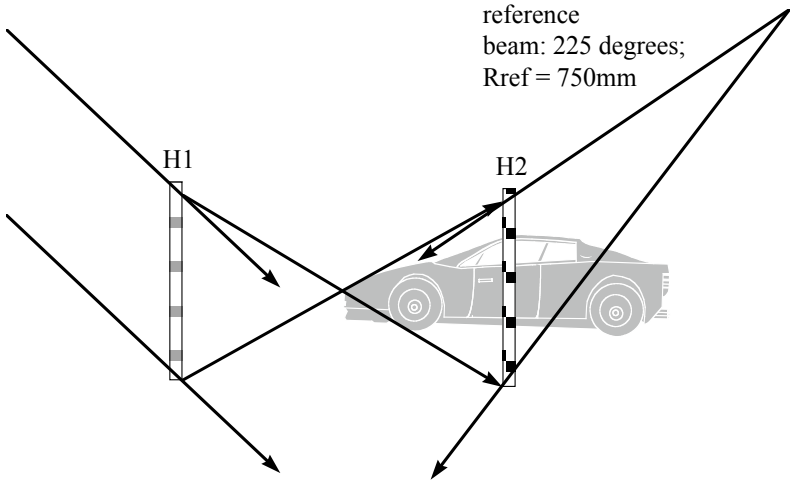

Figure 6.11: Exposure of the transfer (H2) hologram with a diverging reference source

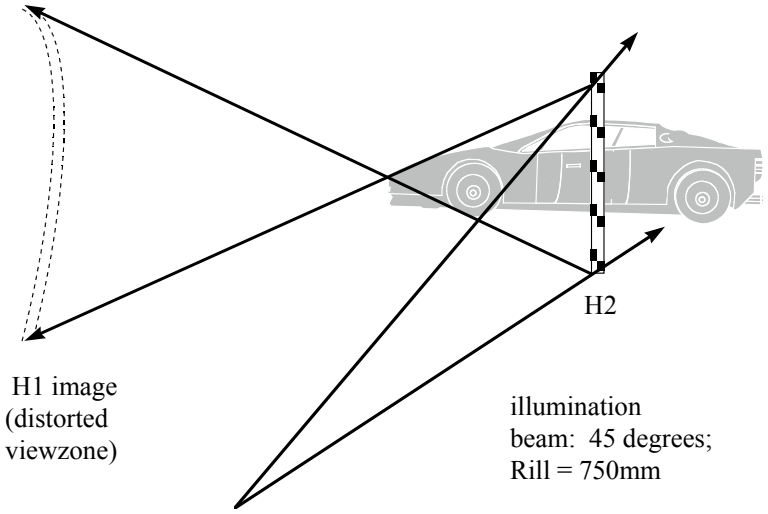

Figure 6.12: Reconstruction of the H2 with a diverging illumination source

The TK Solver+ program of Appendix 3 calculates with basic trigonometry that for a grating arbitrarily set 450 mm from the given 750 mm/750 mm 300 mm-high H2, its size may be reduced from the 300 mm required for a plane-wave grating to 130 mm. This reduced size is sufficient to illuminate all parts of the hologram with at least the central wavelength playing out of the grating. The size of the grating may be further reduced if its playout distance is smaller.

6.13 Designing a perfectly reconstructing diverging grating

The TK program also solves for an equivalent exposure and reconstruction geometry that will compensate for a given hologram's dispersion, based on a reverse raytrace of the blur extent required by the hologram, to the blur extent provided by the grating. This program has the constraint that the exposure and reconstruction angles are identical for the purpose of minimizing distortion. The grating and H2 were made without regard for the astigmatism that one obtains in such a diverging/diverging procedure, however. The resulting H2 in the present display has a vertical focus at the intended 500 mm, whereas its horizontal focus is thrown out to 1500 mm.

In the first step, the hologram's predispersed illumination angles had to be determined. These are the angles for their respective wavelengths (in nanometers) that all play out on the normal for single view angle dispersion compensation:

θ_{illred} = 43.874

$\Delta\theta illHredgreen$ = 1.126°

$\theta_{illgreen}$ = 45

$\Delta\theta illHbluegreen$ = 1.104°

$\theta_{illblue}$ = 46.104

The second step is to determine the playout angles of the grating. As mentioned earlier, the ideal angles for individual wavelengths are not always attainable across the bandwidth, and a compromise must be made between the ideal angular differences between the central wavelength and longer wavelength playout angles and between the central wavelength and shorter wavelength playout angles. The $\Delta\theta outIDEAL$'s are found through basic trigonometric calculations. In order to illuminate the grating close to the normal (an arbitrary choice), a tip angle is necessary during exposure if the same geometry is to be used during reconstruction. Following are three possible geometries, none of which are ideal:

$$\Delta\theta outG_{redgreenIDEAL} = 3.5°$$
$$\Delta\theta outG_{bluegreenIDEAL} = 2.4°$$

$\theta out_{green} = \theta obj = 65°$	$\theta obj = 66°$	$\theta obj = 67°$
$\Delta\theta outG_{redgreen} = 2.51°$	$\Delta\theta outG_{redgreen} = 2.64°$	$\Delta\theta outG_{redgreen} = 2.79°$
$\Delta\theta outG_{bluegreen} = 2.29°$	$\Delta\theta outG_{bluegreen} = 2.39°$	$\Delta\theta outG_{bluegreen} = 2.5°$

The exposure and central reconstruction wavelength is 514.5, a blue-green, so the center geometry was chosen as the closest approximation.

Please refer to Appendix 3; the TK Solver+ Variables menu contains the data derived here, as it was computed. With a grating/hologram separation of 450 mm, the grating perfectly reconstructs an image point 300 mm from its center, at an angle of 66° to its normal. The grating is therefore tipped 24° toward the H2 to illuminate the H2 at its 45° illumination angle. The tilt angle is simply to increase the blur of the grating required by the hologram at the close distance chosen. If the grating's playout distance were to be increased, then the grating would not have to be tipped as much and horizontal dispersion would be negligible. This would also, however, create a severe mismatch between the H2 reference and illumination distances and require a very short H2 reference beam, 375 mm in the limiting case of collimated illumination with the above procedure.

Of course, the tilt angle of the grating may be reduced, or sometimes eliminated, if it is illuminated for imperfect reconstruction (exposure angles different from the reconstruction angles), although this will lead to some distortion of the input blur to the hologram and will usually require an off-axis illumination source.

We made an exposure with the above geometry, and the final table setup is diagrammed below in Figure 6.13. The primary difficulty in the shooting of the grating was obtaining uniform intensities across its area. For the scale of the display, the proximity of the exposure sources were very small, and widely diverging lenses were required. A 100X objective (focal length of about 5 mm) and a ball lens of roughly the same focal length were used in the setup. To further increase the uniformity of the spread

of the beams, meniscus lenses were placed in the object and reference beam paths to shorten the diverging optics' apparent focal lengths.

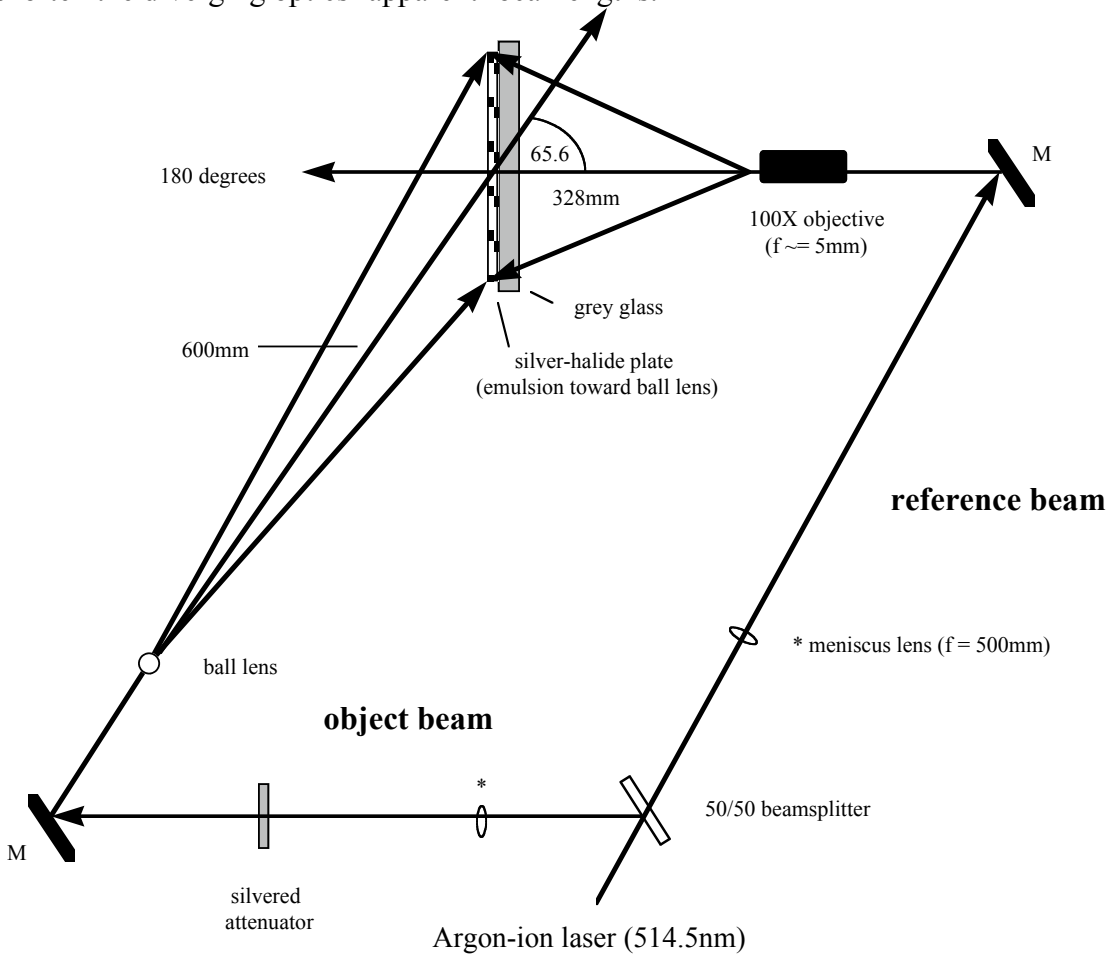

Figure 6.13: The final table setup for the 750/750 diverging/diverging geometry

6.14 Designing a diverging grating that plays out ideal angles and optimized distances

We used the resulting 24° tip angle in a prototype display to good effect. However, we were intent upon obtaining grating angles as close to the ideal angles as possible. If we follow the above pseudoinverse procedure, and input the desired grating output angles and distances into the Matlab program of Appendix 4, then we receive a list of potential geometries.

First, here is the list of input variables (Actually, the Matlab program of Appendix 4 calculates the grating's output angles and distances from hologram input variables.):

```
%%%
```

514.5	l1		nm	exposure wavelength (vacuum)
514.5	l2		nm	reconstruction wavelength (vacuum)
514.6	1 m			diffraction order: m=+1 for virtual
35.83	Øobj		degrees	between 0&90° object beam angle
215.83	Øref		degrees	between 90° and 270° reference angle
	Øout	62.10	degrees	between ±90° (for m =+1) output angle
196.68	Øill		degrees	between 90° and 270° (for m =+1) illum
	RoutR	217.400	mm	output distance -- Red
	RoutG	300.000	mm	output distance -- Green
	RoutB	300.000	mm	output distance -- Blue

The distances, however, are less precise and vary in precision in the Matlab program's output. Recalculated quantities are again set in boldface:

	outR = 49.909,	outG = 47.000,	outB = 44.327
	49.841	**47.123**	**44.271**
(1)	RoutRideal = 218.700,	RoutGideal = 300.000,	RoutBideal = 395.000
	RoutR = 257.400,	RoutG = 300.000,	RoutB = 320.000
	261.256	**291.717**	**324.146**
	outR = 64.909,	outG = 62.000,	outB = 59.327
(2)	**64.860**	**62.086**	**59.290**
	RoutRideal = 218.700,	RoutGideal = 300.000,	RoutBideal = 395.000
	RoutR = 217.400,	RoutG = 300.000,	RoutB = 300.000
	229.006	**270.884**	**313.414**
	outR = 72.909,	outG = 70.000,	outB = 67.327
(3)	**72.881**	**70.0466**	**67.3076**
	RoutRideal = 218.700,	RoutGideal = 300.000,	RoutBideal = 395.000
	RoutR = 237.400,	RoutG = 300.000,	RoutB = 360.000
	235.177	**305.546**	**376.597**

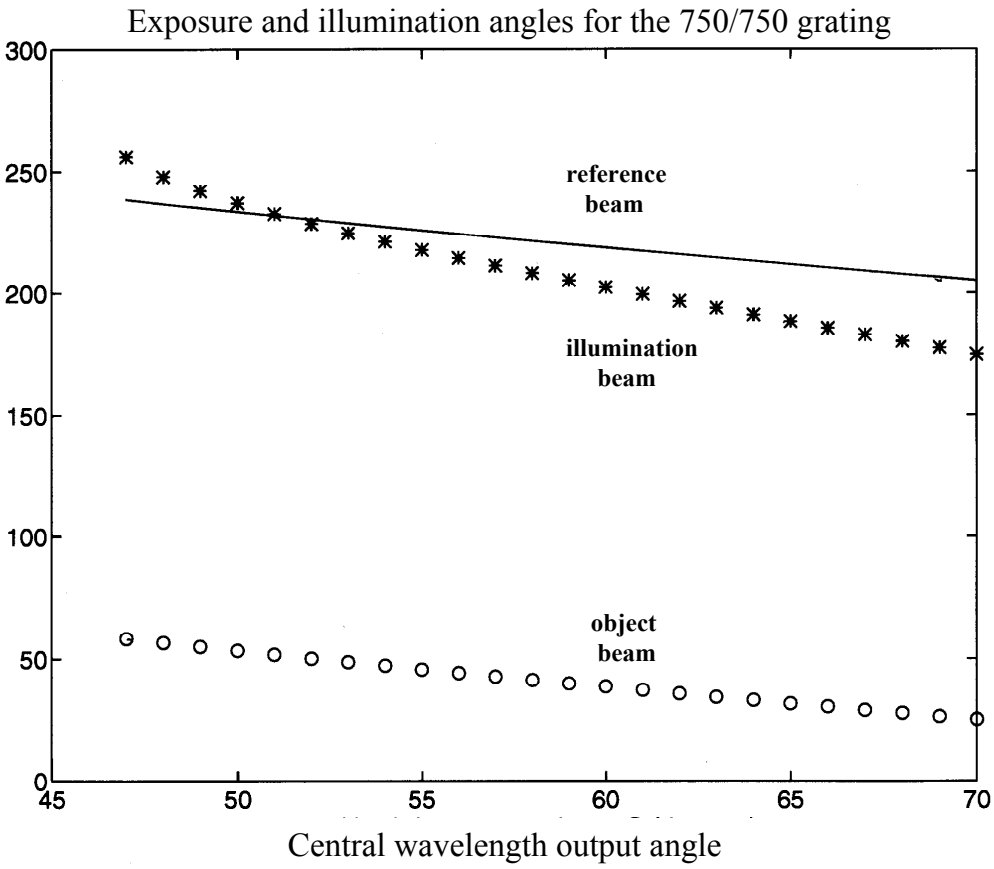

Figure 6.14: A graph of the exposure and illumination angles for a range of central output angles. This graph is the output from the Matlab plot command in the program of Appendix 4.

These reconstruction geometries are far closer to the ideal than is the case with the perfectly reconstructing angles in section 6.13. This improvement would suggest that perhaps the pseudoinverse function could improve dispersion compensation in the viewstations of Chapter 5 as well. At first this seems unlikely, because it is usually assumed that a plane-wave grating provides predispersed light from wavelength component points infinitely far away. However, this is not the case, as we shall see. We will follow the same procedure again, first computing the appropriate blur angle to illuminate the hologram with the TK Solver+ program variables of section 6.13. The grating/hologram separation will again be 450 mm:

	θillR	46.1247	degrees	H ill. angle for long (Red) l2
	θillG	45	degrees	H ill. angle for middle (Green) l2
	θillB	43.8969	degrees	H ill. angle for short (Blue) l2
	dθbluri	2.2278	degrees	blur angle illuminating H
450	sep		mm	dcGrating/H separation
	dθblur_	5.5658	degrees	necessary dcG blur angle

The above hologram illumination angles are used to find the necessary grating output angles. Below, the exposure and illumination distances are used to find the ideal grating output distances:

				dcG DISTANCES
	RobjBen	9E9	mm	(ideal: = RoutGvert_dcG)obj distance
300	RrefBen		mm	(ideal: = Rill_dcG) ref. distance
300	Rill_dc		mm	dcGrating illumination distance
	RoutRBe	-9354.555	mm	dcG playout distance: Red
	RoutGBe	9E9	mm	dcG playout distance: Green
	RoutBBe	8532.3305	mm	dcG playout distance: Blue
	RoutRve	-4372.711	mm	dcG vertical playout distance: Red
	RoutGve	9E9	mm	(=Rill-sep; ideal output =Robj_dcG)
	RoutBve	4560.6652	mm	dcG vertical playout distance: Blue

The ideal grating playout distances (Rout's) are all large compared with the dimensions of a normal hologram, but are not infinity. Now we will use the Matlab program of Appendix 4:

```
%%%
```

distances perfectly. The same imprecision for distances as above applies, so the recalculated values (boldface quantities) are included:

	outR = 49.909,	outG = 47.000,	outB = 44.327
	49.746	**47.029**	**44.179**
	obj = 58.479,	ref = 238.479,	ill = 256.704
(1)	Robj = 178.118,	Rref = -178.118,	Rill = -17.233
	RoutRideal = 6964.560,	RoutGideal = -9e9,	RoutBideal = -8464.580
	RoutR = 6964.560,	RoutG = -9e9,	RoutB = -8564.580
	7381.409	**-4.6e6**	**-8198.115**
	outR = 49.909,	outG = 47.000,	outB = 44.327
	49.746	**47.029**	**44.179**
	obj = 58.479,	ref = 238.479,	ill = 256.704
(2)	Robj = 177.070,	Rref = -177.070,	Rill = -17.130
	RoutRideal = 6964.560,	RoutGideal = -9e9,	RoutBideal = -8464.580
	RoutR = 6964.560,	RoutG = -9e9,	RoutB = -8464.580
	7375.484	**-1.2e6**	**-8112.68**
	outR = 49.909,	outG = 47.000,	outB = 44.327
	49.746	**47.029**	**44.179**
	obj = 58.479,	ref = 238.479,	ill = 256.704
(3)	Robj = 176.010,	Rref = -176.010,	Rill = -17.027
	RoutRideal = 6964.560,	RoutGideal = -9e9,	RoutBideal = -8464.580
	RoutR = 6964.560,	RoutG = -9e9,	RoutB = -8364.580
	7342.012	**-9.7e5**	**-8053.654**

We find that only in the case of a highly converging illumination beam can we attain the proper distances. However, the angles themselves are quite different from the simple perfect reconstruction geometry that is universally applied. This discrepancy suggests that in order to attain the proper distribution of wavelengths within the predispersed blur illuminating the hologram, a more careful approach such as the pseudoinverse function might prove advantageous, particularly for very deep images.

6.15 An attempt to design a pre- and post-dispersing compensation grating

The ultimate compact reflection dispersion-compensation display would consist not even of a small, unobtrusive grating at some distance from the hologram, but would ideally consist of a single material, or a double-layered film without an intervening wave guide or louver film of questionable optical quality. We will attempt here (and in the computer program of Appendix 5) to assess the viability of a pre&post-dispersing, compensation grating. We will again work backwards from the desired, dispersion-compensated condition where output angles = 0 through the grating (m = m1 in the 2nd pass), to the hologram, and back through the grating (m = +1 in the 1st pass). With the angle matrix above, we have:

Equation (**6.8**): 2nd pass through the grating (dc): $\sin(\theta_{out}) = 0$; m = m1

$$[\ \text{-dcILL2}\ ] = [\ \text{-dcCOEFF}\ ] \times [\ \text{dcUK}\ ]$$

$$-\begin{bmatrix}\sin(\theta 2_{\text{illdcred}})\\ \sin(\theta 2_{\text{illdcgreen}})\\ \sin(\theta 2_{\text{illdcblue}})\end{bmatrix} = \begin{bmatrix} m\frac{\lambda_{2\text{red}}}{\lambda_{1dc}} & \pm\frac{\lambda_{2\text{red}}}{\lambda_{1dc}}\\ m\frac{\lambda_{2\text{green}}}{\lambda_{1dc}} & \pm\frac{\lambda_{2\text{green}}}{\lambda_{1dc}}\\ m\frac{\lambda_{2\text{blue}}}{\lambda_{1dc}} & \pm\frac{\lambda_{2\text{blue}}}{\lambda_{1dc}}\end{bmatrix} \times \begin{bmatrix}(\sin\theta_{\text{objdc}})\\ \\ (\sin\theta_{\text{refdc}})\end{bmatrix}$$

Equation (**6.9**): hologram: $\sin(\theta_{outh}) = \sin(\theta 2_{illdc})$

$$[\ \text{dcILL2}\ ] = [\ \text{hCOEFF} + \text{hILL}\ ] \times [\ \text{hUK}\ ]$$

$$\begin{bmatrix}\sin(\theta 2_{\text{illdcred}})\\ \sin(\theta 2_{\text{illdcgreen}})\\ \sin(\theta 2_{\text{illdcblue}})\end{bmatrix} = \begin{bmatrix} m\frac{\lambda_{2\text{red}}}{\lambda_{1h}} & -m\frac{\lambda_{2\text{red}}}{\lambda_{1h}} & \sin(\theta_{\text{illredh}})\\ m\frac{\lambda_{2\text{green}}}{\lambda_{1h}} & -m\frac{\lambda_{2\text{green}}}{\lambda_{1h}} & \sin(\theta_{\text{illgreenh}})\\ m\frac{\lambda_{2\text{blue}}}{\lambda_{1h}} & -m\frac{\lambda_{2\text{blue}}}{\lambda_{1h}} & \sin(\theta_{\text{illblueh}})\end{bmatrix} \times \begin{bmatrix}\sin(\theta_{\text{objh}})\\ \sin(\theta_{\text{refh}})\\ 1\end{bmatrix}$$

Equation (**6.10**): 1st pass through the grating (dc): $\sin(\theta 1_{outdc}) = \sin(\theta_{illh})$; m = ± 1

$$[\ \text{hILL}\ ] = [\ \text{+dcCOEFF} + 1]\ \times [\ \text{dcUK}\ ]$$

$$\begin{bmatrix}\sin(\theta_{\text{illredh}})\\ \sin(\theta_{\text{illgreenh}})\\ \sin(\theta_{\text{illblueh}})\end{bmatrix} = \begin{bmatrix} \frac{\lambda_{2\text{red}}}{\lambda_{1dc}} & -\frac{\lambda_{2\text{red}}}{\lambda_{1dc}} & 1\\ \frac{\lambda_{2\text{green}}}{\lambda_{1dc}} & -\frac{\lambda_{2\text{green}}}{\lambda_{1dc}} & 1\\ \frac{\lambda_{2\text{blue}}}{\lambda_{1dc}} & -\frac{\lambda_{2\text{blue}}}{\lambda_{1dc}} & 1\end{bmatrix} \times \begin{bmatrix}\sin(\theta_{\text{objdc}})\\ \sin(\theta_{\text{refdc}})\\ \sin(\theta_{\text{illdc}})\end{bmatrix}$$

After substitutions, we have Equation (**6.11**):

$$-[-\text{dcCOEFF} \times \text{dcUK}] = [\ \pm\ \text{dcCOEFF} + ([\text{dcCOEFF}+1] \times \text{dcUK})] \times [\text{hUK}]$$

The values for the sines of the object and reference angles were incremented through a range of values in the example program of Appendix 5. However, it was consistently found to be the case that a single or double pre&post-dispersing transmission grating layer set in front of a reflection hologram cannot by itself compensate for its own dispersion as well as dispersion from the hologram. It has not yet been determined whether the introduction of very thin refractive optics between the layers could make this display viable.

In this final chapter, we have explored increasingly compact dispersion-compensation formats while evaluating their effectiveness. Two methods for HOE design have been developed here and in the accompanying appendices: (1) calculation of exposure and reconstruction angles based on a reverse-engineered analysis of perceived blur used for the grating /hologram dispersed focus, instead of the hologram/pupil dispersed focus, and (2) the Moore-Penrose pseudoinverse function for solving for a set of optimized geometries for ideal angles, with the further calculation of optimized distances as an option.

Conclusions and future work

"If the reader, in this spirit, recalls what has been stated by us throughout, generally and in detail, with regard to colour, he will himself pursue and unfold what has been here only lightly hinted at. He will augur well for science, technical processes, and art, if it should prove possible to rescue the attractive subject of the doctrine of colours from the atomic restriction and isolation in which it has been banished, in order to restore it to the general dynamic flow of life and action which the present age loves to recognise in nature. These considerations will press upon us more strongly when, in the historical portion, we shall have to speak of many an enterprising and intelligent man who failed to possess his contemporaries with his convictions."

-- Goethe, Theory of Colours (1810, 297-8)

This final section of the main body of the text will be kept very succinct to facilitate the reader's interpretation of the contents of the thesis. A brief mention will be made of the highlights and shortcomings of each chapter.

In **Chapter 1**, we found that for most illumination sources and reflection holograms with reasonably narrow bandwidth, the diffraction efficiency curve should be sufficient to determine the extent of blur an observer will perceive. Applying a modified form of Rayleigh's criterion, we defined the resolution of a holographic image, assuming uniform background noise. Both of these determinations rested on an approximation of the diffraction efficiency curve as a normalized distribution, with the absolute bandwidth constituting three standard deviations on either side of the curve, and the perceived bandwidth as two standard deviations on either side. The resulting perceived blur factor of 0.8165, to be multiplied by an absolute blur extent, needs to be verified with psychophysics experiments on human subjects.

In **Chapter 2**, our spectrophotometer data suggest that the absolute blur equation derived here measures favorably compared with Benton's blur equation for viewing distances in front of the image beyond the nearpoint of the eye. The difference between the two lies in the less mathematically intuitive, but more physically realistic, interpretation of the perception of blur in the author's equation. Although for on-axis object/image geometries the two equations render very close solutions, for less common geometries, their solutions deviate considerably. This equation gives absolute, raytraced blur extent, but until the perceived blur factor of Chapter 1 is verified or revised, perceived blur extent will not be fully characterized.

Chapter 3 is predominantly a brief history of the application of dispersion compensation to display holography, so some trends may be apparent to the reader. Certainly, the use of a predispersing, precompensating grating is much preferred over the original use of a post-compensating grating. An exception to this preference may be found in the compact geometry and narrow bandwidth conferred by reflection gratings relaying dispersion-compensated light in head-up displays. The incidence of the application of the technique to reflection holography has been extremely sparse, but recent, so its future is uncertain. However, a review of the literature gives one the

impression that there is a general desire to obtain full-color dispersion-compensated images. Reflection holography is well-suited to this task, as it provides sufficiently narrow bandwidth for deeper sharp images of higher hue saturation.

Chapter 4 provides the rationale for designing dispersion-compensation gratings for full-parallax, reflection holographic stereograms: The degree of improvement in image sharpness conferred by dispersion compensation relative to an uncompensated display is greater for full-parallax than for horizontal-parallax-only holographic stereograms because it can reduce blurring of vertical perspective views in the former.
It is recommended that care be taken when sampling perspective views in the making of a full-parallax holographic stereogram. Although coarse sampling in the vertical direction can reduce residual color blurring for a display with a vertically offset illumination source, the effect may sometimes be likened to a sporadic animation when the observer moves up and down.

As the device displaying the successive synthetic views is most likely going to have a resolution much coarser than the spacing of the just-resolvable blurred image points of Chapter 1, an expression accounting for object resolution should be incorporated into the perceived blur equation.

Chapter 5 presents an example of a viewstation with a plane-wave grating. Some of the advantages of a planar wave front for dispersion compensation will be mentioned in the Chapter 6 summary. The practical advantages in the display of a hologram illuminated by a plane-wave grating include the fact that the grating and hologram can be set at any unobtrusive distance from one another, and the resulting image can be made to exhibit no warping or astigmatism.

The single-most important factor when selecting a recording material, and deciding on exposure and reconstruction wavelengths and geometries, is how bright the final image will be. DuPont photopolymers were chosen because they reconstruct with very high diffraction efficiency. A high-wattage, bare tungsten-halogen lamp with its small filament oriented to present a solid, radiating area to the grating, can provide just enough source-size blur to a holographic stereogram so that its image may appear bright and sharp while the image of its master hologram is rendered an unnoticeable blur.
The grating edge farthest from the light source may be rotated toward the hologram for increased predispersing capability to compensate for shrinkage of the hologram. The grating may also be rotated if it itself has shrunk and is playing out at the wrong angles. The next step in plane-wave dispersion compensation is certainly to produce a bright, full-color viewstation.

Chapter 6 compares the effectiveness of compact dispersion-compensation displays that do and do not use a plane-wave grating. Phase-conjugate-illuminated plane-wave gratings provide the broadest range of viewer positions with perfect dispersion

compensation for a single view angle. Phase-conjugate-illuminated diverging wave-front gratings present a wider field of view with deeper peripheral points for an observer situated at the ideal viewer location and orientation. However, at non-ideal viewer positions, dispersion compensation degrades and the corresponding maximum image point distances reduce considerably. Non-phase-conjugate-illuminated diverging wave-front gratings present a wider field of view of even deeper off-axis image points in front of and behind the hologram, again when viewed from the ideal location. Maximum image point distances are more asymmetric about the ideal view axis than in the phase-conjugate cases above.

Although perfectly reconstructing gratings do not suffer from distortion, they do not necessarily approximate ideal predispersed angles or distances very closely. Imperfectly reconstructing gratings can be designed with optimized exposure and reconstruction angles and distances that are much better approximations of the ideal quantities.

The procedure the author has adopted to optimize grating playout angles and distances is a reverse-raytracing method using the Moore-Penrose pseudoinverse function of a matrix expression containing the grating and vertical focus equations. **Appendix 4**'s Matlab program is an implementation of the pseudoinverse method. Although the author has proven that there is no exact solution to the system of linear angle and distance equations, the pseudoinverse does provide an optimal solution. It is shown that the particular viewstation geometries of Chapters 5 and 6 are better approximated using this method. However, further experimental testing is required to validate the procedure's effectiveness.

A pre-and post-dispersing grating, set flush against the hologram, does not seem capable of compensating for the hologram's, in addition to its own, dispersion. (Appendix 5 is a trial Matlab program). It remains to be seen whether or not thin refractive optics might make such a display possible. The diverging wave-front grating has yet to be incorporated in the steep angle format; this could produce the next best approach toward very compact dispersion-compensated displays.

The main body of the thesis is a treatment of vertical dispersion and does not account for horizontal dispersion, even in the analysis of compact displays. A more rigorous vector analysis would provide a more complete picture of blur extent in three dimensions. This would also enable one to model a maximum image envelope, composed of image points at maximum distances in front of the hologram within the acuity of the eye, as the eye position and orientation changes.

I extend my sincere encouragement to my fellow researchers who further the work outlined in this thesis.

Appendix 1
Single-plane trigonometric raytracing formulas

A1.1 The X- and Z- raytracing equations

To begin to understand the significance of the complementary roles of the X- and Z-equations, imagine an infinitely thin recording material set between two sources of interfering light. The resulting grating would form an equivalent transmission hologram, and as such, would exhibit the same diffraction characteristics as its transmission counterpart.

If the recording material is thick, the surface grating structure alone still defines the diffraction pattern of light leaving the material, in terms of angular playout (not intensity) of any given wavelength. However, the fringe structure (the tip angle, spacing, and number of Bragg planes) will effectively act as a tipped interference filter that filters the diffracted light from the surface grating. The surface grating is governed by the X-equation, and the interference filter by the Z-equation. A simultaneous solution of the two equations means that one wavelength will constructively interfere at its primary output angle (as determined by the surface grating, or X-equation), and will therefore play out with the highest diffraction efficiency.

A1.2 The Welford and X-equations

Welford's Equation (**A1.1**) (1975) $\hat{n} \times (\hat{s}_{out} - \hat{s}_{ill}) = m \frac{\lambda_2 n'_1}{\lambda_1 n'_2} \hat{n} \times (\hat{s}_{obj} - \hat{s}_{ref})$

reduces to the trigonometric

X-Equation (**A1.2**) (Benton 1994) $\sin\theta_{out} - \sin\theta_{ill} = m \frac{\lambda_2 \cdot n_1}{\lambda_1 \cdot n_2} (\sin\theta_{obj} - \sin\theta_{ref})$

A1.3 The Z-equation

Z-Equation (**A1.3**) (Benton 1994) $\cos\theta'_{out} - \cos\theta'_{ill} = m \frac{t_1 \lambda_2 n'_1}{t_2 \lambda_1 n'_2} (\cos\theta'_{obj} - \cos\theta'_{ref})$

This filtering equation will have some degree of uncertainty in its filtering capability. A final term reflecting this uncertainty in off-Bragg reconstruction may be added. The following term, Equation (A1.4), is a simplified form of Goodman's blurred K- (grating) vector analysis (Goodman 1996) and defines the spread of the angular and bandwidth playout:

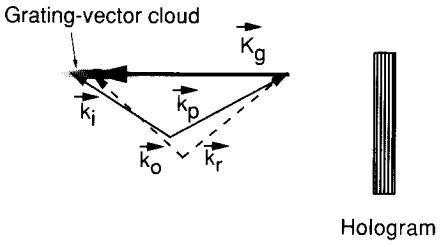

Equation (**A1.4**) $$\pm \frac{\lambda_2}{t_2 n'_2}$$

Figure A1.1: Grating vector cloud (Goodman, 1996)

For our analyses, however, we will assume, calculate, or measure a spectral bandwidth and perform calculations for primary (on-Bragg) playout angles.

A1.4 Spectrophotometer data

The author evaluated a grating exposed to two source points with a Krypton laser at 647 nm on Agfa-Gevaert's 8E75 silver halide emulsion. The grating was illuminated with white light focused 600 mm from the film, at 45°, so that it would play out a chromatically blurred real image of the object point on axis. The exposed fiber end of an Oriel spectrophotometer was carefully translated along this spectral line, and recordings were made of the playout wavelengths and corresponding angles.

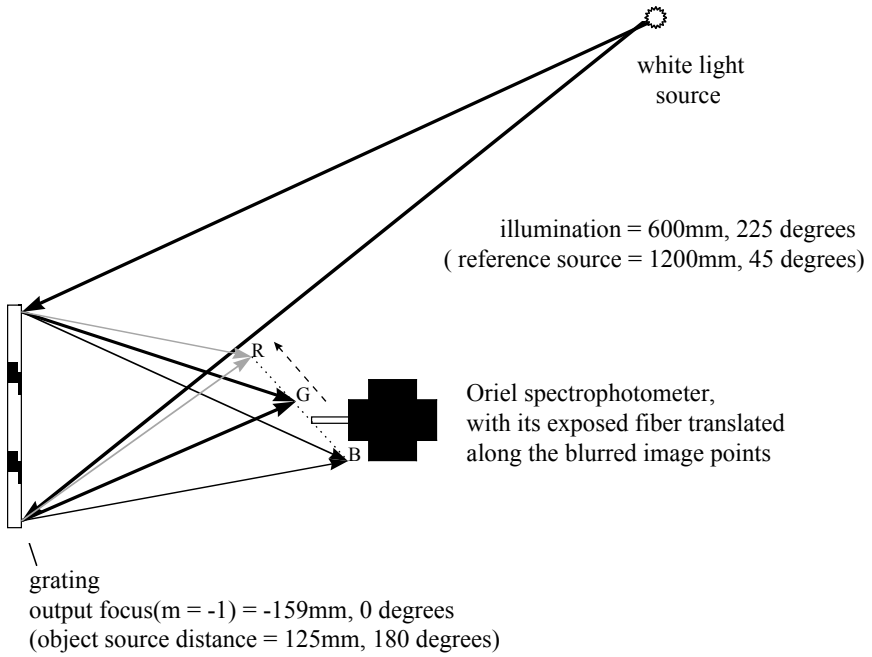

Figure A1.2: Dispersion measurements with an Oriel spectrophotometer translated along the blur (achromatic) angle while oriented parallel to the hologram normal

In Table A1.1, the first column lists the recorded wavelengths, and in the adjacent column, measured angles. From the wavelength measured along the normal, a shrinkage of 8.66% was calculated (assuming negligible change in index of refraction).

Wavelength (nm)	Measured ∠ (degrees)	∠: X-equation
680.2	186.1	182.1
670		181.4
660	185.1	180.8
650	184.1	180.2
647	183.8	180
640	183.2	179.6
632.8	182.6	179.1
630	182.4	178.9
619.9	181.6	178.3
610	181.1	177.7
599.9	180.2	177.1
590.1	180	176.4
580.1	179.9	175.8
570.1	178.8	175.2
560	178.5	174.6
550	177.5	173.9
543.1	176.3	173.5

Table A1.1: Measurements of dispersion with an Oriel spectrophotometer

A1.5 The horizontal and vertical focus equations

Two additional equations that we will be using throughout the text are distance, or focusing equations, the "1/R," or horizontal focus equation and the "$\cos^2\theta$," or vertical focus equation.

The horizontal focus Equation (**A1.5**) is: $$\frac{1}{R_{out1}} - \frac{1}{R_{ill1}} = m\frac{\lambda_2}{\lambda_1}\left(\frac{1}{R_{obj1}} - \frac{1}{R_{ref1}}\right)$$

We will conclude this appendix with Benton's trigonometric derivation for the vertical focus equation. This equation is essentially a derivation for the horizontal focus equation as well, but takes into account the effect of wave-front curvature on relative phase.

Figure A1.3: (Benton, 1994)

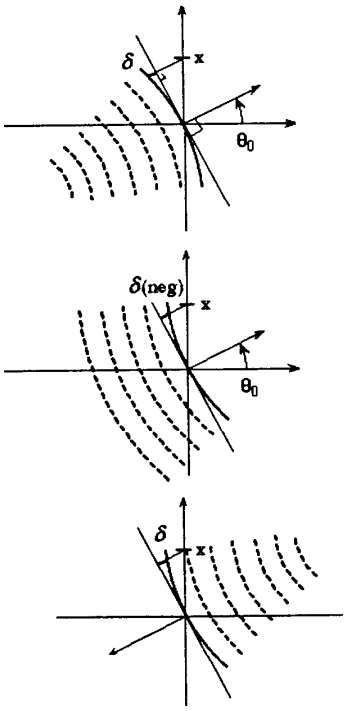

$$R_{out1}\,\$_{out2} + \frac{(h\cos(\theta_1))^2}{R_{out1}}\,\$_{out2} = R_{out1}\,\$_{out1} + h\cos(\theta_1)\,\$_{out1+90°}$$

$$\$_{out2} = \frac{(R_{out1})^2\,\$_{out1} + R_{out1}h\cos(\theta_1)\,\$_{out1+90°}}{(R_{out1})^2 + (h\cos(\theta_1))^2}$$

$$= \frac{(R_{out1})^2 \sin(\theta_1)}{(R_{out1})^2 + (h\cos(\theta_1))^2} + \frac{R_{out1}(h)^2\cos(\theta_1)}{(R_{out1})^2 + (h\cos(\theta_1))^2}$$

$$= \sin(\theta_1) + \frac{h(\cos(\theta_1))^2}{R_{out1}}$$

Equation (**A1.6**) $$\frac{(\cos(\theta_{out1}))^2}{R_{out1}} - \frac{(\cos(\theta_{ill1}))^2}{R_{ill1}} = m\frac{\lambda_2}{\lambda_1}\left(\frac{(\cos(\theta_{obj1}))^2}{R_{obj1}} - \frac{(\cos(\theta_{ref1}))^2}{R_{ref1}}\right)$$

Appendix 2

Derivation of a vector blur equation and its reduction to the single-plane, trigonometric blur equation of Chapter 2

A2.1 Color blur equation derivation

In this appendix, we will raytrace multiple wavelengths about a hologram so as to derive a vector blur equation. We will compare the result with the trigonometric result of Chapter 2. The key to the following derivation is the same as that of the trigonometric analysis: Position (1) values are in terms of the central wavelength, whereas position (2) values are in terms of an extreme wavelength for a given spectral bandwidth.

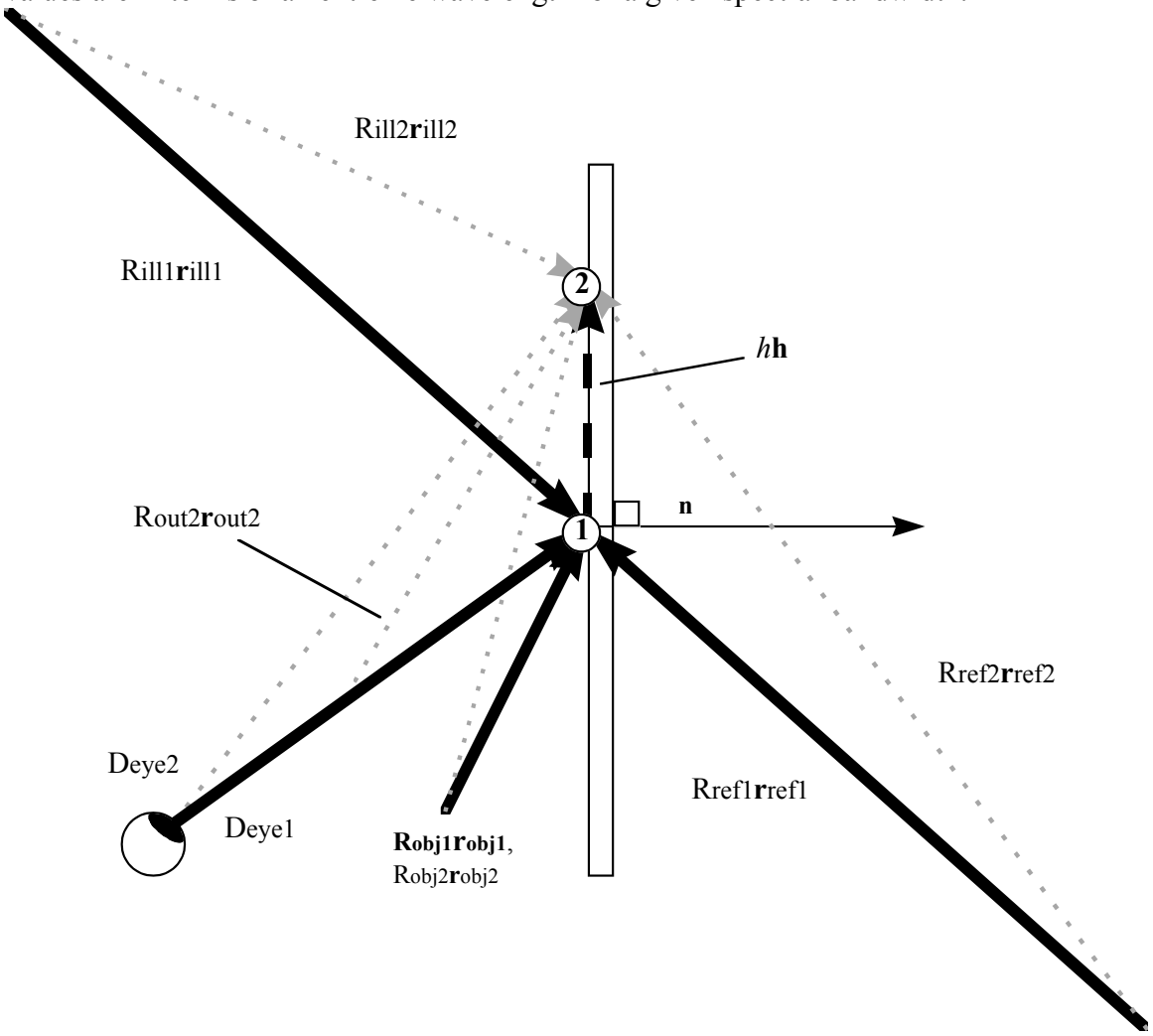

Figure A2.1: Magnitudes and directions for the vector derivation of a blur equation

We will substitute the following variables into a raytracing equation just as we did in the trigonometric version in Chapter 2. As we hope to compare the result with the result from the trigonometric analysis of the x,z-plane geometry, we will begin with Welford's Equation (A1.1):

$$n'\times(\mathbf{s}'_{out}-\mathbf{s}'_{ill})=m\frac{\lambda_2}{\lambda_1}n\times(\mathbf{s}_{obj}-\mathbf{s}_{ref})$$

Equations (**A2.1**):

$$D_{eye2}\mathbf{s}'_{out2}=D_{eye1}\mathbf{s}'_{out1}+h\mathbf{n}' \quad\Rightarrow\quad \mathbf{s}'_{out2}=\frac{D_{eye1}\mathbf{s}'_{out1}+h\mathbf{n}'}{D_{eye2}}$$

$$R_{ill2}\mathbf{s}'_{ill2}=R_{ill1}\mathbf{s}'_{ill1}+h\mathbf{n}' \quad\Rightarrow\quad \mathbf{s}'_{ill2}=\frac{R_{ill1}\mathbf{s}'_{ill1}+h\mathbf{n}'}{R_{ill2}}$$

$$R_{obj2}\mathbf{s}_{obj2}=R_{obj1}\mathbf{s}_{obj1}+h\mathbf{n} \quad\Rightarrow\quad \mathbf{s}_{obj2}=\frac{R_{obj1}\mathbf{s}_{obj1}+h\mathbf{n}}{R_{obj2}}$$

$$R_{ref2}\mathbf{s}_{ref2}=R_{ref1}\mathbf{s}_{ref1}+h\mathbf{n} \quad\Rightarrow\quad \mathbf{s}_{ref2}=\frac{R_{ref1}\mathbf{s}_{ref1}+h\mathbf{n}}{R_{ref2}}$$

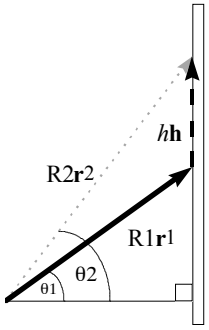

Figure A2.2

The result of the substitutions of Equations (A2.1) into (A1.1) is Equation (**A2.2**):

$$n'\times\left(\frac{D_{eye1}\mathbf{s}'_{out1}+h\mathbf{n}'}{D_{eye2}}-\frac{R_{ill1}\mathbf{s}'_{ill1}+h\mathbf{n}'}{R_{ill2}}\right)=m\frac{\lambda_2}{\lambda_1}n\times\left(\frac{R_{obj1}\mathbf{s}_{obj1}+h\mathbf{n}}{R_{obj2}}-\frac{R_{ref1}\mathbf{s}_{ref1}+h\mathbf{n}}{R_{ref2}}\right)$$

==========

===A2.2 Approximation proof

We will now prove that the denominators with the subscript 2 may be approximated as their counterparts of subscript 1. Then we will proceed with our derivation.

$$\sin\left(\theta_2\right) := \frac{R_1 \cdot \sin\left(\theta_1\right) + h}{R_2} \lambda_{red}$$

For small h, R_1 is approximately equal to R_2 $\sin\left(\theta_{2approx}\right) := \frac{R_1 \cdot \sin\left(\theta_1\right) + h}{R_1} \lambda_{red}$

In order to determine how reasonable an approximation the above equation is, one needs to know the maximum discrepancies between the two angles and the two hypotenuses.The difference between the angle and its approximation must lie within the acuity of the eye:

$$\Delta\theta_{2max} := \theta_{2approx} - \theta_2 = \frac{1}{60} \text{ degree}$$

This difference would then give us a maximum difference between the two hypotenuses:

$$\delta_{max} := D_2 - D_1$$

The determination is made using trigonometric identities:

$$\sin\theta_{2approx} - \sin\theta_2 = 2 \cdot \sin\left\{\frac{\theta_{2approx} - \theta_2}{2}\right\} \cdot \cos\left\{\frac{\theta_{2approx} + \theta_2}{2}\right\}$$

$$= 2 \cdot \sin\left\{\frac{1}{120}\right\} \cdot \cos\left\{\frac{2 \cdot \theta_2 + \frac{1}{60}}{2}\right\} = 2.91 \cdot 10^{-4} \cdot \left\{\cos\left(\theta_2\right) - 1.45 \cdot 10^{-4} \cdot \sin\left(\theta_2\right)\right\}$$

$$\cos\left(\theta_2\right) := \frac{D_1 \cdot \cos\left(\theta_1\right)}{D_2}$$

$$\sin\theta_{2approx} - \sin\theta_2 = 2.91 \cdot 10^{-4} \cdot \frac{D_1 \cdot \cos\left(\theta_1\right)}{D_2}$$

Equating this quantity with the difference between the two sines results in:

$$\sin\theta_{2approx} - \sin\theta_2 = \left(D_1\cdot\sin\left(\theta_1\right) + h\right)\cdot\left\{\frac{1}{D_1} - \frac{1}{D_2}\right\} = \frac{-\left(D_1\cdot\sin\left(\theta_1\right) + h\right)}{D_1 + \delta_{max}} + \sin\left(\theta_1\right) + \frac{h}{D_1}$$

$$\frac{2.91\cdot10^{-4}\cdot D_1\cdot\cos\left(\theta_1\right)}{D_1 + \delta_{max}} = \left(D_1\cdot\sin\left(\theta_1\right) + h\right)\cdot\left\{\frac{1}{D_1} - \frac{1}{D_1 + \delta_{max}}\right\}$$

$$\delta_{max} := \frac{2.91\cdot10^{-4}\cdot D_1\cdot\cos\left(\theta_1\right)}{\frac{h}{D_1} + \sin\left(\theta_1\right)} = \frac{D_1\cdot\cos\left(\theta_1\right)}{3436\cdot\sin\left(\theta_1\right)}$$

An extreme viewing condition testing the approximation is a viewing angle of 45 degrees and viewing distance at the near point (200 mm):

$$\delta_{max} := \frac{200\cdot\cos(45)}{3436\cdot\sin(45)} = 0.0582 \text{ mm}$$

$$\cos\left(\theta_2\right) := \frac{D_1\cdot\cos\left(\theta_1\right)}{D_1 + \delta_{max}} = \frac{200\cdot\cos(45)}{200 + 0.0582} = 0.7069 \qquad \theta_2 := 45.017 \text{ degrees}$$

$$\sin\left(\theta_2\right) := \frac{D_1\cdot\sin\left(\theta_1\right) + h_{max}}{D_2} \qquad h_{max} := 0.085 \text{ mm}$$

$$\sin\left(\theta_{2approx}\right) := \frac{D_1\cdot\sin\left(\theta_1\right) + h_{max}}{D_1} \qquad \theta_{2approx} := 45.034 \text{ degrees}$$

The difference is then seen to be within the acuity of the eye for this extreme viewing condition, so the approximation is a reasonable one to make for the derivation of the blur equation:

$$\theta_{2approx} - \theta_2 = \frac{1}{60} \text{ degree}$$

To resume the derivation, if we ascribe a central wavelength λ_{2green} to position (1) different from that of position (2), then we may reduce the vector expression to the single-plane condition, Equation (**A2.3**):

$$\sin(\theta_{out1(\,2green)}) + \frac{h_{red}}{D_{eye1}} - \sin(\theta_{ill1}) - \frac{h_{red}}{R_{ill1}} = m\frac{\lambda_{2red}}{\lambda_1}\left(\sin(\theta_{obj1}) + \frac{h_{red}}{R_{obj1}} - \sin(\theta_{ref1}) - \frac{h_{red}}{R_{ref1}}\right)$$

$$h_{red}\left[\frac{1}{D_{eye1}} - \frac{1}{R_{ill1}} - m\frac{\lambda_{2red}}{\lambda_1}\left(\frac{1}{R_{obj1}} - \frac{1}{R_{ref1}}\right)\right] = -\sin(\theta_{out1(\lambda_{2green})}) + \sin(\theta_{ill1}) + m\frac{\lambda_{2red}}{\lambda_1}\left(\sin(\theta_{obj1}) - \sin(\theta_{ref1})\right)$$

$$\therefore\ h_{red} = \left|\frac{m\dfrac{(\lambda_{2red} - \lambda_{2green})}{\lambda_1}\left(\sin(\theta_{obj1}) - \sin(\theta_{ref1})\right)}{\dfrac{1}{D_{eye1}} - \dfrac{1}{R_{out1HORIZred}}}\right|$$

The above Equation (A2.3) exactly matches the trigonometric color blur Equation (2.8) of Chapter 2, with a negative value for Rout1HORIZred. Our final derivation will add the source-size component to image blur.

A2.3 Source-size blur derivation

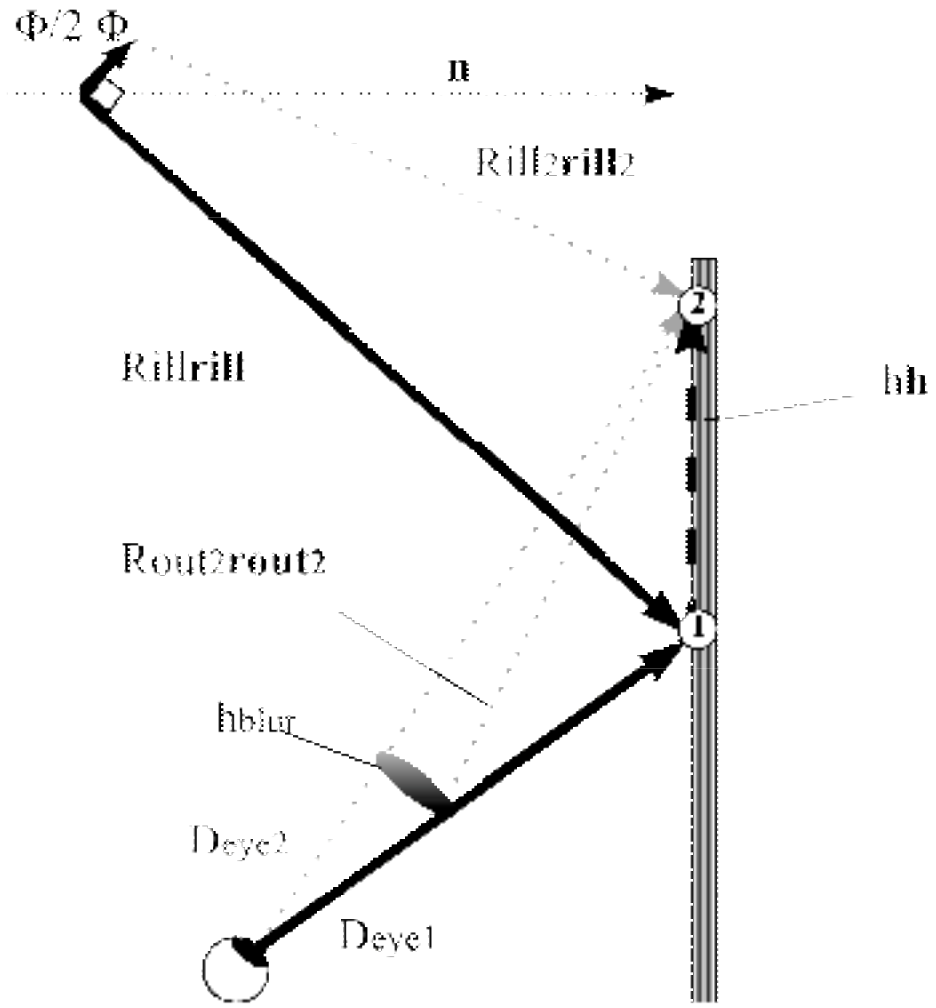

Figure A2.3: A dispersed focus at the pupil creating the perception of blur height

$$R_{ill2}\hat{s}_{ill2} = -\frac{\Phi}{2}\hat{\Phi} + h\hat{n} + R_{ill1}\hat{s}_{ill1}$$

$$(\vec{\Phi} \times \vec{r}_{ill1}) \times \vec{h} = (\vec{r}_{ill1} \times \vec{h}) \times \vec{h}$$

$$(\vec{h} \cdot \vec{\Phi})\hat{s}_{ill1} - (\vec{r}_{ill1} \cdot \vec{h})\hat{\Phi} = (\vec{h} \cdot \vec{r}_{ill1})\hat{n} - (\vec{h} \cdot \vec{h})\vec{r}_{ill1}$$

$$\hat{\Phi} = \frac{-(\vec{h} \cdot \vec{r}_{ill1})\hat{n} + (\vec{h} \cdot \vec{h})\vec{r}_{ill1} + (\vec{h} \cdot \vec{\Phi})\vec{r}_{ill1}}{(\vec{r}_{ill1} \cdot \vec{h})}$$

$$(\vec{h} \cdot \vec{\Phi}) = h\frac{\Phi}{2}\cos(\theta_{ill1})$$

$$\hat{\Phi} = \frac{-(\vec{h} \cdot \vec{r}_{ill1})\hat{n} + (\vec{h} \cdot \vec{h})\vec{r}_{ill1} + \left(h\frac{\Phi}{2}\cos(\theta_{ill1})\right)\vec{r}_{ill1}}{(\vec{r}_{ill1} \cdot \vec{h})} = -\hat{n} + \frac{\left(h + \frac{\Phi}{2}\cos(\theta_{ill1})\right)\vec{r}_{ill1}}{R_{ill1}\cos(\theta_{ill})}$$

$$R_{ill2}\hat{s}_{ill2} = -\frac{\Phi}{2}\left(-\hat{n} + \frac{\left(h + \frac{\Phi}{2}\cos(\theta_{ill1})\right)\hat{s}_{ill}}{R_{ill1}\cos(\theta_{ill1})}\right) + h\hat{n} + R_{ill1}\vec{r}_{ill1}$$

$$\hat{s}_{ill2} = \frac{\left(\frac{\Phi}{2} + h\right)}{R_{ill2}}\hat{n} + \left(\frac{-\frac{\Phi}{2}\left(h + \frac{\Phi}{2}\cos(\theta_{ill1})\right)}{R_{ill2}R_{ill1}\cos(\theta_{ill1})} + \frac{R_{ill1}}{R_{ill2}}\right)\vec{r}_{ill1} \approx \left(\frac{\Phi}{2R_{ill2}} + \frac{h}{R_{ill2}}\right)\hat{n} + \vec{r}_{ill1}$$

$$\approx \frac{\Phi}{2R_{ill\lambda}}\hat{n} + \hat{s}_{ill\lambda}$$

Substituting the revised $\mathbf{r}_{ill2}$ again into Equation (A1.1),

$\hat{n} \times (\hat{s}_{out1} - \hat{s}_{ill1}) = m\frac{\lambda_2}{\lambda_1}\hat{n} \times (\hat{s}_{obj1} - \hat{s}_{ref11})$, leads us to our final single-plane vector blur Equation (**A2.4**):

$$h_{blur} = \frac{(\hat{n} \times (\hat{s}_{out1red} - \hat{s}_{out1green}))R_{out1HORIZred}D_{eye1}}{R_{out1HORIZred} - D_{eye1}} + \frac{\left(\frac{\Phi_{ill}}{2R_{ill1}} + (\hat{n} \times \hat{s}_{ill1})\right)R_{out1HORIZred}D_{eye1}}{R_{out1HORIZred} - D_{eye1}}$$

If D_{eye1} is made a positive number indicating distance of the viewer from the hologram position (1), then the form of the Equation (A2.4) closely matches that of the trigonometric result, Equation (2.13), further demonstrating that the methods are compatible, and that the vector approach generates a more general form for the trigonometric expressions commonly used in display holography.

Appendix 3
TK Solver+ and Matlab programs applying the derived equations

- solves for blur in uncompensated holograms
- calculates the maximum front and back image depth
- calculates the minimum grating size required
- solves for a dispersion compensation grating whose exposure and illumination geometries are the same (perfect reconstruction)

St	Input Name	Output	Unit	Comment	HOLOGRAM (H) INPUT
					==========
7	t1			microns	emulsion thickness -- exposure
7	t2			microns	emulsion thickness -- reconstruction
	shrink	0		%	percent physical shrinkage
1.63	n1				emulsion refr. index -- exposure
1.63	n2				emulsion thickness -- reconstruction
514.5	l1			nm	exposure wavelength (vacuum)
514.5	l2			nm	reconstruction wavelength (vacuum)
-1	m				diffraction order: m=+1 for virtual
0	Øobj			degrees	between 0&90° object beam angle
225	Øref			degrees	between 90° and 270° reference angle
	Øout	180		degrees	between ±90° (for m =+1) output
45	Øill			degrees	between 90° and 270° (for m =+1)
					UNCOMPENSATED DISPERSION
					==========
0	ssize			mm	illumination source size (diameter)
34.59	bandwid			nm	spectral bandwidth (min. for H, dcG)
531	l2R			nm	long (Red) reconstruction wavelength
	l2G	514.5		nm	central (Green) wavelength (= l2)
	l2B	496.41		nm	short (Blue) reconstruction lambda
	ØoutR	181.29		degrees	dispersed playout (no dcG) -- Red
	ØoutG	180		degrees	dispersed playout (no dcG) -- Blue
	ØoutB	178.57		degrees	dispersed playout (no dcG) -- Green
	dØout	2.7240		degrees	dispersed playout (no dcG)
300	Robj			mm	H object source distance
9E9	Rref			mm	H reference distance
9E9	Rill			mm	H illumination distance
	RoutRve	-290.5285		mm	H vertical output distance -- Red
	RoutGve	-300		mm	H vertical output distance -- Green
	RoutBve	-310.7403		mm	H vertical output distance -- Blue
	Lblur	14.358136		mm	blur Length
	dØblur	1.1752294		degrees	blur angle at eye
	dØBento	2.723785		degrees	color blur angle -- Benton
	dØBento	0		degrees	source size blur angle -- Benton
	dØBento	2.723785		degrees	blur angle -- Benton
	LblurBe	14.261705		mm	blur Length -- Benton
	dØblurB	1.1673365		degrees	blur angle at eye -- Benton
1000	Deye			mm	viewer distance

.0167	dØacuit		degrees	(1) Set maximum acceptable blur at eye (resolving power = 1/60 deg.)
				(2) Guess the Robjmax's, and solve
	Robjmax	6.0560283	mm	max. object distance => plays out w/
	Robjmax	6.1306821	mm	acceptable blur -- front and back
	Routfro	-6.056028	mm	maximum output distance with
	Routbac	6.1306821	mm	specified acceptable blur -- front and back
	RoutBen	-6.080584	mm	max. output (front) -- Benton
	RoutBen	6.1554416	mm	max. output (back) -- Benton
				==========
				DISPERSION COMPENSATION GRATING (dcG) INPUT
				(necessary input from above: everything up through "bandwidth,"&"Rill"&"Deye")
7	t1_dcG		microns	H `\\\||//' || ||
7	t2_dcG		microns	@=Ø||> <--------- || ||
	shrink_	0	%	[< . || ||
1.63	n1_dcG			Deye .
1.63	n2_dcG			.
514.5	l1_dcG		nm	// // .
				// //<----------*
				// // Rill_dcG
				dcG
				* B
				* RoutGvert_dcG (m=+1)
				* R
	ØillR	46.868262	degrees	H ill. angle for long (Red) l2
	ØillG	45	degrees	H ill. angle for middle (Green) l2
	ØillB	43.019299	degrees	H ill. angle for short (Blue) l2
	dØbluri	3.8489632	degrees	blur angle illuminating H
450	sep		mm	dcGrating/H separation
	dØblur_	3.8489634	degrees	necessary dcG blur angle
				dcG ANGLES

				Perfect reconstruction
				Input ØoutG_dcG, Guess Øill_dcG

	ØobjBen	45	degrees	dcG object angle (between ±90°)
	ØrefBen	179.96792	degrees	dcG reference angle (90° to 270°)
	ØillBen	179.96792	degrees	dcG illumination angle
	ØoutRBe	46.866757	degrees	dcG output angle
45	ØoutGBe		degrees	dcG output angle (=Øill if perfect=0)
	ØoutBBe	43.020841		dcG output angle
	ØtiltBe 0	degrees		dcG tilt angle
				dcG DISTANCES
	RobjBen	9E9	mm	(ideal: = RoutGvert_dcG)obj distance
300	RrefBen		mm	(ideal: = Rill_dcG) ref. distance
300	Rill_dc		mm	dcGrating illumination distance
	RoutRBe	-9354.555	mm	dcG playout distance: Red
	RoutGBe	9E9	mm	dcG playout distance: Green
	RoutBBe	8532.3305	mm	dcG playout distance: Blue
	RoutRve	-4372.711	mm	dcG vertical playout distance: Red

	RoutGve	9E9	mm	(=Rill-sep; ideal output =Robj_dcG)
	RoutBve	4560.6652	mm	dcG vertical playout distance: Blue
				MINIMUM dcG SIZE
300	Lholo		mm	vertical Length of the hologram
	LdcGBen	299.99999	mm	min. recom. vertical Length -- Benton

```
"dispersion compensation                                                    © Arno K
''''''
```

```
"  This block calculates blur according to A.A.Ward's diagram."
"Horizontal focus playout distances -- Rout_ calculations"
1/RoutR = m*l2R/l1*(1/Robj - 1/Rref) + 1/Rill
1/RoutG = m*l2G/l1*(1/Robj - 1/Rref) + 1/Rill
1/RoutB = m*l2B/l1*(1/Robj - 1/Rref) + 1/Rill
Lholo_Bcolor = abs((m*l2G/l1-m*l2B/l1)*(sind(Øobj)-sind(Øref))*
        Deye*RoutB/(Deye+RoutB))
Lholo_Rcolor = abs((m*l2R/l1-m*l2G/l1)*(sind(Øobj)-sind(Øref))*
        Deye*RoutR/(Deye+RoutR))
Lholo_Bssize = abs(ssize*cosd(Øill)*Deye*RoutB/(2*Rill*(Deye+RoutB)))
Lholo_Rssize = abs(ssize*cosd(Øill)*Deye*RoutR/(2*Rill*(Deye+RoutR)))
Lholo_blur = Lholo_Bcolor+Lholo_Bssize+Lholo_Rcolor+Lholo_Rssize
Lblur = Lholo_blur*abs(cosd(ØoutG))*(Deye+RoutGvert)/Deye
dØblur*pi()/180 =  Lblur/(Deye+RoutGvert)

"  Maximum depth (front and back):  Øblur = Øacuity"
"  USAGE:  Type 'G' for 'Guess' in the 'St' field on the left.
"          Then type a small value in the Input field and Solve."
dØacuity*pi()/180 =  Lholo_blurmaxfront*abs(cosd(ØoutG))/Deye
dØacuity*pi()/180 =  Lholo_blurmaxback*abs(cosd(ØoutG))/Deye
Lholo_blurmaxfront =
        Lholo_Bcolormaxfront+Lholo_Bssizemaxfront+Lholo_Rcolormaxfront+Lholo_Rssizemaxfront
Lholo_blurmaxback =
        Lholo_Bcolormaxback+Lholo_Bssizemaxback+Lholo_Rcolormaxback+Lholo_Rssizemaxback
Lholo_Bcolormaxfront = abs((l2G/l1-l2B/l1)*
        (sind(Øobj)-sind(Øref))*Deye*RoutBmaxfront/(Deye+RoutBmaxfront))
Lholo_Rcolormaxfront = abs((l2R/l1-l2G/l1)*
        (sind(Øobj)-sind(Øref))*Deye*RoutRmaxfront/(Deye+RoutRmaxfront))
Lholo_Bcolormaxback = abs((l2G/l1-l2B/l1)*
        (sind(Øobj)-sind(Øref))*Deye*RoutBmaxback/(Deye+RoutBmaxback))
Lholo_Rcolormaxback = abs((l2R/l1-l2G/l1)*
        (sind(Øobj)-sind(Øref))*Deye*RoutRmaxback/(Deye+RoutRmaxback))
Lholo_Bssizemaxfront = abs(ssize*cosd(Øill)*Deye*RoutBmaxfront/(2*Rill*(Deye+RoutBmaxfront)))
Lholo_Rssizemaxfront = abs(ssize*cosd(Øill)*Deye*RoutRmaxfront/(2*Rill*(Deye+RoutRmaxfront)))
Lholo_Bssizemaxback = abs(ssize*cosd(Øill)*Deye*RoutBmaxback/(2*Rill*(Deye+RoutBmaxback)))
Lholo_Rssizemaxback = abs(ssize*cosd(Øill)*Deye*RoutRmaxback/(2*Rill*(Deye+RoutRmaxback)))
1/RoutRmaxfront = -l2R/l1*(1/Robjmaxfront - 1/Rref) + 1/Rill
1/RoutBmaxfront = -l2B/l1*(1/Robjmaxfront - 1/Rref) + 1/Rill
1/RoutRmaxback = l2R/l1*(1/Robjmaxback - 1/Rref) + 1/Rill
1/RoutBmaxback = l2B/l1*(1/Robjmaxback - 1/Rref) + 1/Rill
-abs(cosd(ØoutG))^2/Routfront =
        abs(-l2G/l1*((cosd(Øobj))^2/Robjmaxfront - (cosd(Øref))^2/Rref) + abs(cosd(Øill))^2/Rill)
abs(cosd(ØoutG))^2/Routback =
        abs(l2G/l1*((cosd(Øobj))^2/Robjmaxback - (cosd(Øref))^2/Rref) + abs(cosd(Øill))^2/Rill)

"  This block calculates blur according to S.A.Benton's diagram."
dØBenton_color = 180/pi()*(bandwidth/l2G)*abs((sind(ØoutG)-sind(Øill))/cosd(ØoutG))
dØBenton_ssize = 180/pi()*ssize*abs(cosd(Øill)/(Rill*cosd(ØoutG)))
dØBenton^2 = dØBenton_color^2 + dØBenton_ssize^2
LblurBenton =  abs(RoutGvert*dØBenton*pi()/180)
dØblurBenton*pi()/180 = LblurBenton/(RoutGvert+Deye)
```

```
"  Maximum depth (front and back) -- Benton:"
RoutBentonfront = -Deye*tand(dØacuity/2)/(tand(dØBenton/2)+tand(dØacuity/2))
RoutBentonback = Deye*tand(dØacuity/2)/(tand(dØBenton/2)-tand(dØacuity/2))

"""""""
```

```
(cosd(ØoutB_dcG))^2/RoutBvert_dcG = l2B/l1_dcG*((cosd(Øobj_dcG))^2/Robj_dcG -
        (cosd(Øref_dcG))^2/Rref_dcG) + (cosd(Øill_dcG))^2/Rill_dcG

"  The ANGLES for the different wavelengths playing out of the
"  dcG are all the result of a constant illumination angle (Øill_dcG).
sind(ØoutR_dcG )-sind(180-Øill_dcG ) = Rratio*(sind(Øobj_dcG ) - sind(180-Øref_dcG ))
sind(ØoutG_dcG )-sind(180-Øill_dcG ) = Gratio*(sind(Øobj_dcG ) - sind(180-Øref_dcG ))
sind(ØoutB_dcG )-sind(180-Øill_dcG ) = Bratio*(sind(Øobj_dcG ) - sind(180-Øref_dcG ))

"  This block calculates angles from blur according to S.A.Benton's diagram."
dØblur_dcG^2 = dØblurBenton_color^2 + dØblurBenton_ssize^2
dØblurBenton_color = 180/pi()*(bandwidth/l2G)*abs((sind(ØoutGBenton_dcG)-
        sind(ØillBenton_dcG))/cosd(ØoutGBenton_dcG))
dØblurBenton_ssize = 180/pi()*ssize*abs(cosd(ØillBenton_dcG)/(Rill_dcG*cosd(ØoutGBenton_dcG)))
RillBenton_dcG = Rill_dcG
1/RoutRBenton_dcG =  l2R/l1_dcG*(1/RobjBenton_dcG - 1/RrefBenton_dcG) + 1/Rill_dcG
1/RoutGBenton_dcG = l2G/l1_dcG*(1/RobjBenton_dcG - 1/RrefBenton_dcG) + 1/Rill_dcG
1/RoutBBenton_dcG = l2B/l1_dcG*(1/RobjBenton_dcG - 1/RrefBenton_dcG) + 1/Rill_dcG
 (cosd(ØoutRBenton_dcG))^2/RoutRvertBenton_dcG =
        l2R/l1_dcG*((cosd(ØobjBenton_dcG))^2/RobjBenton_dcG -
        (cosd(ØrefBenton_dcG))^2/RrefBenton_dcG) + (cosd(ØillBenton_dcG))^2/Rill_dcG
RoutGvertBenton_dcG = RoutGvert_dcG
 (cosd(ØoutGBenton_dcG))^2/RoutGvertBenton_dcG =
        l2G/l1_dcG*((cosd(ØobjBenton_dcG))^2/RobjBenton_dcG -
        (cosd(ØrefBenton_dcG))^2/RrefBenton_dcG) + (cosd(ØillBenton_dcG))^2/Rill_dcG
 (cosd(ØoutBBenton_dcG))^2/RoutBvertBenton_dcG =
        l2B/l1_dcG*((cosd(ØobjBenton_dcG))^2/RobjBenton_dcG -
        (cosd(ØrefBenton_dcG))^2/RrefBenton_dcG) + (cosd(ØillBenton_dcG))^2/Rill_dcG
sind(ØoutRBenton_dcG) =
        Rratio*(sind(ØobjBenton_dcG) - sind(180-ØrefBenton_dcG)) + sind(180-ØillBenton_dcG)
sind(ØoutGBenton_dcG) =
        Gratio*(sind(ØobjBenton_dcG) - sind(ØrefBenton_dcG)) + sind(ØillBenton_dcG)
sind(ØoutBBenton_dcG) =
        Bratio*(sind(ØobjBenton_dcG) - sind(180-ØrefBenton_dcG)) + sind(180-ØillBenton_dcG)

"  For the case of perfect reconstruction of the dcG (reconstruction angles =
"    exposure angles), the dcG will be tilted with respect to H
"    so that the dcG creates sufficient blur.
"  This tilt angle will be the illumination angle of the dcG, so that the l2G
"    output angle of the dcG will equal the central illumination angle of H."
Input Øout_dcG or Øill_dcG, Guess the other.

Øtilt_dcG = Øill - (m*90+90) - ØoutG_dcG
Øref_dcG = Øill_dcG
Øobj_dcG = ØoutG_dcG
ØtiltBenton_dcG =  Øill - (m*90+90) - ØoutGBenton_dcG
ØrefBenton_dcG = ØillBenton_dcG
ØobjBenton_dcG = ØoutGBenton_dcG


" MINIMUM dcG SIZE
"  Because the dcG acts as a window through which H is illuminated,
"  we will determine a reasonable minimum dcG size based on previous
"  calculations.  The size could be smaller, depending on the blur length,
"  but this calculation assumes that we want the whole H area to be
"  illuminated by at least the central wavelength.
"  Lholo = length of the hologram; LdcG = length of the dcGrating
tand(Ølow) = (Rill*sind(ØillG)-Lholo/2)/(Rill*cosd(ØillG))
tand(Øhigh) = (Rill*sind(ØillG)+Lholo/2)/(Rill*cosd(ØillG))
```

```
dØspread = Øhigh-Ølow
LdcG = abs(dØspread*pi()/180 * RoutGvert_dcG/(cosd(ØillG)*cosd(Øtilt_dcG)))
LdcGBenton = abs(dØspread*pi()/180 * RoutGvertBenton_dcG/(cosd(ØillG)*cosd(ØtiltBenton_dcG)))
```

Alternative Matlab program

```
%  WARDvsSABblur.m color blur
%  MATLAB program to compare color blur values for Benton's and Ward's diagrams

clg
clear

fid = fopen('WARD.dat', 'w');

HBLURWARD = [ ];
HBLURSAB = [ ];
DVIEWER = [ ];
HTOTALWARD = [ ];
BLURANGLEWARD = [ ];
BLURANGLESAB = [ ];
ROBJG = [ ];
ROUTGVERT = [ ];

        objG  = 68.179171;
        refG  = 180.02732;
        illG  = 180.02732;
        RobjG = 9E9;
        RrefG = 9E9;
        RillG = 9E9;
        ssize = 0;

        lambda1 = 647;
        lambdaR = 657;
        lambdaG = 647;
        lambdaB = 637;
        m = 1;

ROBJG = [ROBJG RobjG];

lambdaRratio = m*lambdaR/lambda1;
lambdaGratio = m*lambdaG/lambda1;
lambdaBratio = m*lambdaB/lambda1;

sinobjG = sin(objG*pi/180);
cosobjG = cos(objG*pi/180);
sinrefG = sin(refG*pi/180);
cosrefG = cos(refG*pi/180);
sinillG = sin(illG*pi/180);
cosillG = cos(illG*pi/180);

sinoutG = lambdaGratio*(sinobjG - sinrefG) + sinillG;
outG = asin(sinoutG)*180/pi;

if abs(objG) > 90 & m >= 1
        outG = 180 - outG;
end

cosoutG = cos(outG*pi/180);
RoutRhorz = 1/(lambdaRratio*(1/RobjG - 1/RrefG) + 1/RillG);
RoutGhorz = 1/(lambdaGratio*(1/RobjG - 1/RrefG) + 1/RillG);
RoutBhorz = 1/(lambdaBratio*(1/RobjG - 1/RrefG) + 1/RillG);
```

```
RoutGvert = cosoutG*cosoutG/(lambdaGratio*(cosobjG*cosobjG/RobjG - cosrefG*cosrefG/RrefG) +
cosillG*cosillG/RillG);
ROUTGVERT = [ROUTGVERT RoutGvert];


fprintf(fid, 'objG = %4.3f,       refG = %4.3f,       illG = %4.3f\noutG = %4.3f\nRrefG = %4.3f,       RillG
= %4.3f\nRoutRhorz = %4.3f,       RoutBhorz = %4.3f\nlambdaGratio = %4.3f/%4.3f\n',
objG,refG,illG,outG,RrefG,RillG,RoutRhorz,RoutBhorz,lambdaG,lambda1);

DMIN = 200;
if m == -1
        DMIN = -RoutBhorz + 200;
end

for D = DMIN : 10 : 1000;

    hRcolorWARD = (lambdaRratio-lambdaGratio)*(sinobjG-sinrefG)*D*RoutRhorz/(D + RoutRhorz);
    hBcolorWARD = (lambdaBratio-lambdaGratio)*(sinobjG-sinrefG)*D*RoutBhorz/(D + RoutBhorz);
     hRssizeWARD = ssize*cosillG*D*RoutRhorz/(2*RillG*(D + RoutRhorz));
     hBssizeWARD = ssize*cosillG*D*RoutBhorz/(2*RillG*(D + RoutBhorz));
    htotalWARD  = abs(hRcolorWARD+hRssizeWARD) + abs(hBcolorWARD+hBssizeWARD);
    hblurWARD   = htotalWARD*abs(D+RoutGvert)*abs(cosoutG)/D;
     blurangleWARD = hblurWARD/(D+RoutGvert) * 180/pi;

        DVIEWER = [DVIEWER D];
        HTOTALWARD = [HTOTALWARD htotalWARD];
        HBLURWARD = [HBLURWARD hblurWARD];
        BLURANGLEWARD = [BLURANGLEWARD blurangleWARD];


        hcolorSAB = ((lambdaR-lambdaB)/lambdaG)*(sinoutG-sinillG)/cosoutG;
        hssizeSAB = ssize*cosillG/(RillG*cosoutG);
        hblurSAB = abs(RoutGvert*sqrt(hcolorSAB*hcolorSAB + hssizeSAB*hssizeSAB));
        blurangleSAB2 = sqrt(hcolorSAB*hcolorSAB + hssizeSAB*hssizeSAB) * 180/pi;
        blurangleSAB = hblurSAB/(D+RoutGvert) * 180/pi;

        HBLURSAB = [HBLURSAB hblurSAB];
        BLURANGLESAB = [BLURANGLESAB blurangleSAB];

fprintf(fid, 'RobjG = %4.3f,       RoutGvert = %4.3f,       D = %4.3f\nhblurWARD = %4.3f,
hblurSAB = %4.3f\nblurangleWARD = %4.4f,    blurangleSAB = %4.4f\n\n',
RobjG,RoutGvert,D,hblurWARD,hblurSAB,blurangleWARD,blurangleSAB);

end
end
end

fclose(fid)


subplot (3,1,1), plot (ROUTGVERT, HBLURWARD, 'go');
title ('perceived blur height with image output distance');
hold on
plot (ROUTGVERT, HBLURSAB, 'y*');
xlabel('Image output distance (mm)');
ylabel('perceived blur height (mm)');

subplot (3,1,2), plot (ROUTGVERT, BLURANGLEWARD, 'go');
title ('perceived blur angle with image output distance');
```

```
hold on
plot (ROUTGVERT,BLURANGLESAB, 'y*');
xlabel('image output distance (mm)');
ylabel('perceived blur angle (degrees)');

subplot (3,1,3), plot (ROUTGVERT, HTOTALWARD, 'g-');
title ('Height of hologram region contributing to blur');
xlabel('image output distance (mm)');
ylabel('hologram height -- blurWARD');
hold off
```

Appendix 4
A Matlab program for the design of dispersion-compensation gratings (Chapter 6)

```
% gratingdesigner.m
%       This program first calculates the angles and distances required for three different wavelengths to %
reconstruct a holographic image (H2) along a viewer axis.  Illumination of the hologram from these
% calculated positions compensates for chromatic dispersion that would have occurred had a single,
% broadband point source of light illuminated the hologram.
%       Then the program takes the specified separation between this hologram and a dispersion
% compensation grating (H1), and calculates what the playout angles and distances for the three different %
wavelengths would have to be from H1 to compensate for dispersion of H2.
%       Finally, the program outputs a list of potential exposure and reconstruction geometries into the
% file: "gratingdesigner.dat".
clear
fid = fopen('gratingdesigner.dat', 'w');
OBJ = [];
REF = [];
ILL = [];
OUTG = [];

%%%
```

```
lambdaGratio = lambdaG/lambda1;
lambdaBratio = lambdaB/lambda1;

H2illR = asin(sin(H2out) - lambdaRratio*mH2*(sin(H2obj)-sin(H2ref)));
H2illG = asin(sin(H2out) - lambdaGratio*mH2*(sin(H2obj)-sin(H2ref)));
H2illB = asin(sin(H2out) - lambdaBratio*mH2*(sin(H2obj)-sin(H2ref)));

RH2G = abs(H2illR - H2illG);       % angular H2 illumination (green-red)
BH2G = abs(H2illG - H2illB);       % angular H2 illumination (green-blue)

%%%%%%%%%%%%%%%%%%%%%%%%%%%%%%%%%%%%%%%%%%%%%%%%%%%%%%%%%%%%%%%%%%%%%%%%%%%%
%                                H2 DISTANCES
%
%%%%%%%%%%%%%%%%%%%%%%%%%%%%%%%%%%%%%%%%%%%%%%%%%%%%%%%%%%%%%%%%%%%%%%%%%%%%
% ideal H2 illumination distances -- Red, Green, and Blue
RH2 = cos(H2illR)^2/(cos(H2out)^2/H2Rout - lambdaRratio*mH2*(cos(H2obj)^2/H2Robj -
cos(H2ref)^2/H2Rref));
GH2 = cos(H2illG)^2/(cos(H2out)^2/H2Rout - lambdaGratio*mH2*(cos(H2obj)^2/H2Robj -
cos(H2ref)^2/H2Rref));
BH2 = cos(H2illB)^2/(cos(H2out)^2/H2Rout - lambdaBratio*mH2*(cos(H2obj)^2/H2Robj -
cos(H2ref)^2/H2Rref));

%%%%%%%%%%%%%%%%%%%%%%%%%%%%%%%%%%%%%%%%%%%%%%%%%%%%%%%%%%%%%%%%%%%%%%%%%%%%
%                                H1 DISTANCES
%
%%%%%%%%%%%%%%%%%%%%%%%%%%%%%%%%%%%%%%%%%%%%%%%%%%%%%%%%%%%%%%%%%%%%%%%%%%%%
% H1 ideal playout (Green)
H1G = GH2 - H1H2separation;
% H1 ideal playout (Blue, Red) (cosine law)
H1Bideal = sqrt(BH2^2 + H1H2separation^2 - 2*BH2*H1H2separation*cos(BH2G));
H1Rideal = sqrt(RH2^2 + H1H2separation^2 - 2*RH2*H1H2separation*cos(RH2G));

%%%%%%%%%%%%%%%%%%%%%%%%%%%%%%%%%%%%%%%%%%%%%%%%%%%%%%%%%%%%%%%%%%%%%%%%%%%%
%                             H1 EXPOSURE ANGLES
%
%%%%%%%%%%%%%%%%%%%%%%%%%%%%%%%%%%%%%%%%%%%%%%%%%%%%%%%%%%%%%%%%%%%%%%%%%%%%
coeff1 = [lambdaRratio*mH1  -lambdaRratio*mH1  1
          lambdaGratio*mH1  -lambdaGratio*mH1  1
          lambdaBratio*mH1  -lambdaBratio*mH1  1];

% H1 playout angles: sin(H2H1Bideal)/BH2 = sin(BH2G)/H1Bideal (sine law)
H2H1B = pi - asin(BH2*sin(BH2G)/H1Bideal);
BH1G  = pi - H2H1B;
H2H1R = pi - asin(RH2*sin(RH2G)/H1Rideal);
RH1G  = pi - H2H1R;

outG = H1outGmin;
for outG = H1outGmin : 1*pi/180 : H1outGmax
  outR = outG + RH1G;
  outB = outG - BH1G;
  sinoutR = sin(outR);
  sinoutG = sin(outG);
  sinoutB = sin(outB);
  sinout = [sinoutR; sinoutG; sinoutB];

  sinobjrefill = pinv(coeff1)*sinout;
  sinobj = sinobjrefill(1);
  sinref = sinobjrefill(2);
  sinill = sinobjrefill(3);
```

```
  if sinobj<1 & sinref<1 & sinill<1 & sinobj>-1 & sinref>-1 & sinill>-1
            obj = asin(sinobj);
            ref = pi-asin(sinref);
            ill = pi-asin(sinill);
            OBJ = [OBJ obj*180/pi];
            REF = [REF ref*180/pi];
            ILL = [ILL ill*180/pi];
            OUTG = [OUTG outG*180/pi];

%%%%%%%%%%%%%%%%%%%%%%%%%%%%%%%%%%%%%%%%%%%%%%%%%%%%%%%%%%%%%%%%%%%%%%%%%%%%%%%%
%                              H1 EXPOSURE DISTANCES
%
%%%%%%%%%%%%%%%%%%%%%%%%%%%%%%%%%%%%%%%%%%%%%%%%%%%%%%%%%%%%%%%%%%%%%%%%%%%%%%%%
coeff2 = [lambdaRratio*mH1*cos(obj*pi/180)^2  -lambdaRratio*mH1*cos(ref*pi/180)^2  cos(ill)^2
             lambdaGratio*mH1*cos(obj*pi/180)^2  -lambdaGratio*mH1*cos(ref*pi/180)^2  cos(ill)^2
             lambdaBratio*mH1*cos(obj*pi/180)^2  -lambdaBratio*mH1*cos(ref*pi/180)^2  cos(ill)^2];

% Non-ideal H1 output distances may be required to satisfy the vertical focus equations.
% H1R = H1Rideal;
% H1B = H1Bideal;
for H1R = H1Rideal - deltaH1Rout/2 : 1 : H1Rideal + deltaH1Rout/2
for H1B = H1Bideal - deltaH1Rout/2 : 1 : H1Bideal + deltaH1Rout/2
               cossqoverH1R = cos(outR)^2/H1R;
               cossqoverH1G = cos(outG)^2/H1G;
               cossqoverH1B = cos(outB)^2/H1B;
               cossqoverH1out = [cossqoverH1R; cossqoverH1G; cossqoverH1B];

               oneoverRobjrefill = pinv(coeff2)*cossqoverH1out;
               Robj = 1/oneoverRobjrefill(1);
               Rref = 1/oneoverRobjrefill(2);
               Rill = 1/oneoverRobjrefill(3);
%  if (Robj<-1000 | Robj>0) & (Rref<-1000 | Rref>0) & Rill>0 & Rill <= H1Rillmax
fprintf(fid, 'outR = %4.3f,          outG = %4.3f,          outB = %4.3f\nobj  = %4.3f,          ref  = %4.3f,
ill  = %4.3f\nRobj = %4.3f,         Rref = %4.3f,        Rill = %4.3f\nRH2 = %4.3f,          GH2 = %4.3f,
BH2 = %4.3f\nH1Rideal = %4.3f,   H1Gideal = %4.3f,   H1Bideal = %4.3f\nH1R = %4.3f,         H1G =
%4.3f,         H1B = %4.3f\n\n', outR*180/pi, outG*180/pi, outB*180/pi, obj*180/pi, ref*180/pi,
ill*180/pi, Robj, Rref, Rill, RH2, GH2, BH2, H1Rideal, H1G, H1Bideal, H1R, H1G, H1B);
%          end
end
end
end
end
plot (OUTG, OBJ, 'go');
hold on;
title ('Exposure and Illumination Angles for the Diverging Grating: 750/750');
plot (OUTG, REF, 'g-');
plot (OUTG, ILL, 'y*');
xlabel('central lambda output angle, outG (degrees)');
ylabel('obj(o), ref(-), and ill(*) angles (degrees)');
```

Appendix 5
A Matlab program attempting to solve for a pre- and post-dispersing grating set flush against a hologram (Chapter 6)

```
% Hologram/grating sandwich
%-----------------------------------------------------------------------------------------------
%  fdcg = abs(sinobjdcg - sinrefdcg)/lambda1;
%  fH = abs(sinobjH - sinrefH)/lambda1;
%-----------------------------------------------------------------------------------------------
% 1st pass through the dcg
%-----------------------------------------------------------------------------------------------
%  sinout1dcg = sinill1dcg + m1dcg*lambda2*fdcg;
%-----------------------------------------------------------------------------------------------
% Reflection hologram
%-----------------------------------------------------------------------------------------------
%  sinoutH = sinout1dcg + mH*lambda2*fH;
%  sinoutH = sinill1dcg + m1dcg*lambda2*fdcg + mH*lambda2*fH;
%-----------------------------------------------------------------------------------------------
% 2nd pass through the dcg
%-----------------------------------------------------------------------------------------------
%  sinout2dcg = 0 = sinoutH + m2dcg*lambda2*fdcg;
%  0 = sinill1dcg + m1dcg*lambda2*fdcg + mH*lambda2*fH + m2dcg*lambda2*fdcg;
%-----------------------------------------------------------------------------------------------
% Substitution:
%-----------------------------------------------------------------------------------------------
%  sinill1dcg = -m1dcg*lambda2*fdcg - mH*lambda2*fH - m2dcg*lambda2*fdcg;
%
%  fdcg = (sinobjdcg - sinrefdcg)/lambda1;
%  refdcg = illdcg
%  sinill1dcg = (-(m1dcg*lambda2 + m2dcg*lambda2)*objdcg-
%                    mH*lambda1*lambda2*fH)
%                     /(lambda1 - m1dcg*lambda2 - m2dcg*lambda2)
%-----------------------------------------------------------------------------------------------
fid = fopen('bumsteadDcgH.dat','w');
fid2 = fopen('bumsteadDcgH.dat','a');
fprintf(fid,'\n');

lambda1G = .000000514;
lambda2R = .000000524;
lambda2G = .000000514;
lambda2B = .000000504;

for m1dcg = -1 : 2 : 1
for m2dcg = -1 : 2 : 1
for mH    = -1 : 2 : 1
  for objdcg = 110 : 10 : 180
    for objH = -70 : 10 : 250
      for refH = -70 : 10 : 250

sinobjdcg = sin(pi/180*objdcg);

fH = abs(sin(objH*pi/180) - sin(refH*pi/180))/lambda1G;

numG = (-(m1dcg*lambda2G + m2dcg*lambda2G)*sinobjdcg - mH*lambda1G*lambda2G*fH);
numR = (-(m1dcg*lambda2R + m2dcg*lambda2R)*sinobjdcg - mH*lambda1G*lambda2R*fH);
numB = (-(m1dcg*lambda2B + m2dcg*lambda2B)*sinobjdcg - mH*lambda1G*lambda2B*fH);
denomG = (lambda1G - m1dcg*lambda2G - m2dcg*lambda2G);
```

```
denomR = (lambda1G - m1dcg*lambda2R - m2dcg*lambda2R);
denomB = (lambda1G - m1dcg*lambda2B - m2dcg*lambda2B);
sinill1dcgG = numG/denomG;
sinill1dcgR = numR/denomR;
sinill1dcgB = numB/denomB;

illdcg = 180 - 180/pi*asin(sinill1dcgG);

% just to make sure that the zero order does not strike the viewer: outH>30 or outH<30deg
fdcg = abs(sinobjdcg - sinill1dcgG)/lambda1G;
sinout1dcg = sinill1dcgG + m1dcg*lambda2G*fdcg;
sinoutH = sinout1dcg + mH*lambda2G*fH;
outH = 180/pi*asin(sinoutH);
if outH>30 | outH<-30
 if sinill1dcgG >-1 & sinill1dcgG <1
  if illdcg>100 & illdcg<260
   if sinill1dcgR == sinill1dcgG
    if sinill1dcgB == sinill1dcgG
     if (objH>-70 & objH<70 & refH>110 & refH<250) | (objH>110 & objH<250 & refH>-70 & refH<70)

            fprintf(fid2,'m1dcg = %4.5f, m2dcg = %4.5f, mH = %4.5f\n', m1dcg,m2dcg,mH);
             fprintf(fid2,'refdcg = %4.5f, or %4.5f\n', illdcg, -180 - illdcg);
            fprintf(fid2,'objdcg = %4.5f, refdcg = %4.5f, or %4.5f\n', objdcg,illdcg,-180-illdcg);
            fprintf(fid2,'objH = %4.5f, refH = %4.5f\n\n', objH, refH);

                  end
                end
              end
            end
          end
      end
   end
end
        end
      end
   end
end
fclose(fid)
```

References

Abramson, Nils. 1981. Chapter 1: Interference. In *The making and evaluation of holograms.* New York: Academic Press, Inc.

Bazargan, Kaveh. 1985. A practical, portable system for white-light display of transmission holograms using dispersion compensation. *SPIE* 523 Applications of Holography: 24-5.

_____. Techniques in Display Holography. 1986. Ph.D. diss., Imperial College of Science and Technology (U.K.).

Belendez, A., I. Pascual, and A. Fimia. 1991. Effective holographic grating model to analyze thick holograms. *SPIE.* 1507 Holographic Optics III: Principles and Applications: 268-76.

Benton, Stephen A. 1972. Method for making reduced bandwidth holograms. United States Patent No. 3,633,989.

_____. 1975. Holographic Displays--A Review. *Optical Engineering* 14 (September-October): 402-7.

_____. 1977. White-light transmission/reflection holographic imaging. In *Applications of holography and optical data processing*. Edited by E. Marom and A.A. Friesem. Oxford and New York: Pergamon Press. 401-9.

_____. 1983. Photographic holography. *SPIE.* 391 Optics in Entertainment: 2-9.

_____. 1985. Method and apparatus for making achromatic holograms. United States Patent No. 4,498,729.

_____. July 1988. The Principles of Reflection Holographic Stereograms. *Proc. Third Int'l Symp. on Display Holography*. Lake Forest College.

_____. 1994. Holographic Imaging class lecture notes.

_____. 1996. Notes for the SPIE Short course on practical holography.

Birner, Sabrina M. 1989. Steep Reference Angle Holography: Analysis and Applications. Master's thesis, MIT.

Bjelkhagen, Hans I. 1993. *Silver-halide recording materials for holography and their processing*. New York: Springer-Verlag.

Boj, P.G, M. Pardo, M., and J.A. Quintana. 1986. *Applied Optics.* 25: 4146-9.

Borowski, E.J., and J.M. Borwein. 1991. *The Harper Collins dictionary of mathematics.* New York: Harper Collins Publishers.

Burckhardt, Christoph B. December 1966. Display of holograms in white light. *B.S.T.J. Briefs*: 1841-4.

Caulfield, H.J., ed. 1979. Estimation of image brightness. In *Handbook of optical holography*. New York: Academic Press, Inc. 6.3: 235-7.

Charman, W.N. 1995. Chapter 24: Optics of the eye. In *Handbook of optics: Volume I, 2nd ed.* New York: McGraw-Hill.

Collier, Robert J., Christoph B. Burckhardt, and Lawrence H. Lin. 1971. *Optical holography.* San Diego, California: Academic Press, Inc.

DeBitetto, Dominic J. December 1966. White-light viewing of surface holograms by simple dispersion compensation. *Applied Physics Letters.* 9: 417-8.

_____. 1969. Holographic panoramic stereograms synthesized from white light recordings. *Applied Optics.* 8: 1740-1.

Faklis, Dean, and G. Michael Morris. 1988. Broadband imaging with combinations of holographic and conventional lenses. *SPIE* 883 Holographic Optics: Design and Applications.

Ferwerda, Jac. G. 1982. *The world of 3-D: a practical guide to stereo photography.* Netherlands Society for Stereo Photography.

French, A.P. 1971. Chapter 8: Boundary effects and interference. In *Vibrations and waves.* New York: W.W. Norton and Co.

Gabor, Dennis. 1948. A new microscopic principle. *Nature.* 161: 777.

Geisler, Wilson S., and Martin S. Banks. 1995. Chapter 7.25: Visual performance. In *Handbook of optics: Volume I, 2nd ed.* New York: McGraw-Hill.

George, Nicholas, and J.T. McCrickerd. 1969. Holography and stereoscopy: the holographic stereogram. *Photographic Science and Engineering.* 13: 342-50.

Geothe. [1810] 1967. Relation to general physics. In *Theory of colours.* London: Frank Cass and Co. Ltd. Translated by Charles Lock Eastlake.

Greivenkamp, John E. Jr. 1995. Chapter 2.3: Interference. In *Handbook of optics: Volume I, 2nd ed.* New York: McGraw-Hill.

Goodman, Joseph W. 1971. An introduction to the principles and applications of holography. *Proc. IEEE*. 59: 1292-1304.
_____. 1996. Chapter 9: Holography. In *Introduction to Fourier optics, 2nd edition*. New York: McGraw-Hill.
Halle, Michael. W. 1991. The generalized holographic stereogram. Master's thesis, MIT.
Hardy. 1936. *Handbook of colorimetry.* Cambridge: Technology Press.
Henrion, Michele. 1995. Diffraction and exposure characteristics of the edgelit hologram. Master's thesis, MIT.
Holloway, H.W., and R.A. Ferrante. 1981. Computer analysis of holographic systems by means of vector ray tracing. *Applied Optics* 20: 2081-4.-
Horn, Berthold Klaus Paul. 1986. Appendix 2: Manipulation of vectors. In *Robot vision*. Cambridge: MIT Press.
Jeong, Tung H. 1980. The principles of holography. *The Optical Industry and Systems Purchasing Directory.* B-337 - B-355.
Katyl, Robert H. 1972. Compensating optical systems. Part1: broadband holographic reconstruction. *Applied Optics* 11: 1241-7.
King, M.C., A.M. Noll, and D.H. Berry. 1970. A new approach to computer-generated holography. *Applied Optics.* 9: 471-5.
Kogelnik, Herwig. 1967. Reconstructing response and efficiency of hologram gratings. Presented at the Symposium on Modern Optics at the Polytechnic Institute of Brooklyn.
_____. 1969. Coupled wave theory for thick hologram gratings. *Bell System Technical Journal.* 48: 2909-47.
Kubota, Toshihiro. 1989. Image sharpening of Lippmann hologram by compensation of wavelength dispersion. *SPIE* 1051 Practical Holography III: 12-7.
Latta, John L. March 1971. Computer-based analysis of hologram imagery and aberrations II: aberrations induced by a wavelength shift. *Applied Optics.* 10: 609-18.
_____. December 1971. Computer-based analysis of holography using ray tracing. *Applied Optics.* 10: 2698-710.
_____. 1972. Analysis of multiple hologram optical elements with low dispersion and low aberrations. *Applied Optics.* 11: 1686-96.
Leith, Emmett N. May 22, 1956. Willow Run Laboratories memorandum. 26-8, 36-8.
_____. 1979. Introduction to *Handbook of Optical Holography*. H.J. Caulfield, ed. 1979. New York: Academic Press.
_____. 1992. Optics class lecture notes.
Leith, Emmett N., and Juris Upatnieks. 1962. Reconstructed wavefronts and communication theory. *J. Opt. Soc. Amer.* 52:
MIT. Color Measurement Laboratory. 1936. *Handbook of Colorimetry.* Cambridge: The Technology Press.
McCrickerd, J.T., and Nicholas George. 1967. Holographic stereogram from sequential component photographs. *Applied Physics Letters.* 12: 10-2.
McFadden, S.A. 1987. The binocular depth stereoacuity of the pigeon and its relation to the anatomical resolving power of the eye. *Vision Research.* 27: 1967-79.
McPherson, Glen. 1990. *Statistics in scientific investigation.* New York: Springer-Verlag.
Osram Sylvania. 1996 catalogs.
Paques, Henri. 1966. Achromatization of holograms. *Proc. IEEE* 54: 1195-6.
Redman, J.D. 1968. The three dimensional reconstruction of people and outdoor scenes using holographic multiplexing. *SPIE.* 15: 117-22.
Riggs, Lorrin A. 1965. Chapter 11: Visual acuity. In *Vision and visual perception.* Edited by Clarence H. Graham. New York: John Wiley and Sons.
Roberts, Martin D., et al. 1995. Lateral and longitudinal chromatic dispersion correction in display systems employing non-conformal reflection holograms. Patent number 5,396,349.
Saxby,Graham. 1988 and 1994 (2nd ed.). *Practical holography.* New York: Prentice Hall.
Smith, Warren J. 1990. Chapter 5: The Eye; Chapter 8: Radiometry and Photometry. In *Modern optical engineering, 2nd edition.* New York: McGraw-Hill.
Strang, Gilbert. 1993. *Introduction to linear algebra*. Wellesley, MA: Wellesley-Cambridge Press.
Syms, R.R.A. 1990. Chapter 2: Coupled wave theory; Chapter 10: Pictorial holography. In *Practical volume holography.* Oxford: Clarendon Press.
University of Chicago Press. 1993. *The Chicago manual of style*: 14th ed. Chicago: University of Chicago Press.

Upatnieks, Juris. 1992. Edge-illuminated holograms. *Applied Optics* 31: 1048-52.
Ward, A. A., J. C. W. Newell and L. Solymar. 1985. Image blurring in display holograms and in holographic optical elements. *SPIE* 600 Progress in Holographic Applications: 57-65.
Ward, A. A., and L. Solymar. 1986. Image distortions in display holograms. *J. Photographic Science* 34: 62-76.
Welford, W.T. 1975. A vector raytracing equation for hologram lenses of arbitrary shape. *Optics Communications.* 14: 322-3.
Wyszecki, Gunter, and W.S. Stiles. 1967. *Color science*. New York: John Wiley and Sons.